In compliance with the
Canadian Privacy Legislation
some supporting forms
may have been removed from
this dissertation.

While these forms may be included
in the document page count,
their removal does not represent
any loss of content from the dissertation.

University of Alberta

The Influence of Residual Stress on the Initiation and Propagation of Trans-granular Stress Corrosion Cracking in High Pressure Natural Gas Transmission Pipelines.

by

Gregory John Van Boven

©

A thesis submitted to the Faculty of Graduate Studies and Research in partial fulfillment of the
requirements for the degree of *Master of Science*

in

Materials Engineering

Department of *Chemical and Materials Engineering*

Edmonton, Alberta

Fall 2003

National Library
of Canada

Acquisitions and
Bibliographic Services

395 Wellington Street
Ottawa ON K1A 0N4
Canada

Bibliothèque nationale
du Canada

Acquisisitons et
services bibliographiques

395, rue Wellington
Ottawa ON K1A 0N4
Canada

Your file Votre référence
ISBN: 0-612-87902-X
Our file Notre référence
ISBN: 0-612-87902-X

The author has granted a non-exclusive licence allowing the National Library of Canada to reproduce, loan, distribute or sell copies of this thesis in microform, paper or electronic formats.

The author retains ownership of the copyright in this thesis. Neither the thesis nor substantial extracts from it may be printed or otherwise reproduced without the author's permission.

L'auteur a accordé une licence non exclusive permettant à la Bibliothèque nationale du Canada de reproduire, prêter, distribuer ou vendre des copies de cette thèse sous la forme de microfiche/film, de reproduction sur papier ou sur format électronique.

L'auteur conserve la propriété du droit d'auteur qui protège cette thèse. Ni la thèse ni des extraits substantiels de celle-ci ne doivent être imprimés ou aturement reproduits sans son autorisation.

Canada

University of Alberta

Library Release Form

Name of Author: *Gregory John Van Boven*

Title of Thesis: The Influence of Residual Stress on the Initiation and Propagation of Trans-granular Stress Corrosion Cracking in High Pressure Natural Gas Transmission Pipelines.

Degree: *Master of Science*

Year this Degree Granted: *2003*

Permission is hereby granted to the University of Alberta Library to reproduce single copies of this thesis and to lend or sell such copies for private, scholarly or scientific research purposes only.

The author reserves all other publication and other rights in association with the copyright in the thesis, and except as herein before provided, neither the thesis nor any substantial portion thereof may be printed or otherwise reproduced in any material form whatever without the author's prior written permission.

_____

Sept 30, 2003

University of Alberta

Faculty of Graduate Studies and Research

The undersigned certify that they have read, and recommend to the Faculty of Graduate Studies and Research for acceptance, a thesis titled;

"The Influence of Residual Stress on the Initiation and Propagation of trans-granular Stress Corrosion Cracking in High Pressure Natural Gas Transmission Pipelines."

submitted by **Gregory John Van Boven** in partial fulfillment of the requirements for the degree of **Master of Science** in Materials Engineering.

SEPT 30 /2003.
Date Thesis Approved

ABSTRACT

Trans-granular stress corrosion cracking is a phenomenon that occurs on the exterior surfaces of buried high-pressure steel pipelines that transport gas and other liquid hydrocarbons. Trans-granular stress corrosion cracking has been recognized as a significant contributor to the total leaks and ruptures experienced by the massive infrastructure of buried pipelines in North America. Currently, the exact mechanism of trans-granular stress corrosion cracking initiation and growth on pipelines surfaces, although theorized, is not well defined. Empirical evidence supports the action of an aqueous environment, a failed surface coating, a susceptible material and stress as necessary components for the initiation and growth of trans-granular stress corrosion cracking. Residual stress may be one source of stress that plays a role in the initiation and early stage growth of trans-granular stress corrosion cracking. This thesis will investigate the relationship between levels of residual stress and the location of trans-granular stress corrosion cracking initiation, early stage crack growth and cracking velocity.

ACKNOWLEDGEMENTS

I would like to acknowledge the support of the National Research Council of Canada for the use of the Chalk River facility operated by the Steacie Institute of Molecular Science of Ottawa, Canada in conducting residual stress measurements.

I would also like to thank TransCanada Pipelines for financial support and NOVA Research and Technology, a division of NOVA Chemicals, for facility and financial support.

TABLE OF CONTENTS

1.0 **INTRODUCTION** 1

2.0 **LITERATURE REVIEW** 5

2.1 Characteristics of trans-granular stress corrosion cracking 5

2.2 Residual stress 7

2.2.1 Nature of residual stresses in pipeline steels 7

2.2.2 The influence of residual stress on trans-granular SCC 10

2.3 Measurement of residual stress 12

2.3.1 Neutron diffraction 12

2.3.2 X-Ray diffraction 14

2.3.3 Hole drilling 14

2.4 Methods for laboratory testing for SCC susceptibility 16

2.4.1 Cyclic loading 16

2.4.2 Slow strain rate testing 17

2.5 Proposed mechanisms for the initiation and growth of trans-granular SCC 20

2.5.1 Hydrogen embrittlement 20

2.5.2 Surface mobility 22

2.5.3 Stress sorption 23

2.5.4 Slip dissolution 24

2.5.5 Fast film fracture 25

2.6 Literature review summary 27

3.0 **METHODS & MATERIALS** 29

3.1 Experimental design overview 29

3.2 Material selection 29

3.3 Fabrication of test specimens and test apparatus 30

3.3.1 Residual stress plates and tensile specimens 30

3.3.2 Environmental chamber design 31

3.4 Pre-conditioning test specimen 32
3.5 Neutron diffraction analysis of test specimens at Chalk River Laboratories 32
3.6 Cyclic load testing for SCC 35
3.7 Modified slow strain rate testing for SCC 36
3.8 Metallurgical Examination for SCC 36

4.0 RESULTS 38
4.1 Residual stress analysis of test specimens 38
4.2 Cyclic loading experiments 39
4.3 Modified slow strain rate experiments 40

5.0 DISCUSSION 43
5.1 Stress analysis of tensile specimens 43
5.2 Occurrence of corrosion 44
5.3 Residual stress versus crack initiation 45
5.3.1 Crack initiation under cyclic loading conditions 45
5.3.2 Crack initiation under SSRT conditions 46
5.4 Crack growth 49
5.5 Proposed mechanism 54

6.0 CONCLUSIONS 56
7.0 REFERENCES 60
8.0 TABLES 64
9.0 FIGURES 72
10.0 APPENDICES 125
Appendix A Tensile specimen schematic. 126
Appendix B: Environmental chamber schematic. 127
Appendix C: Tensile grips schematic. 129
Appendix D: Tensile specimen mounting jig schematic. 130

LIST OF TABLES

Table 1: Experimental methodology flowchart.

Table 2: Chemical composition of X65 pipeline steel.

Table 3: Electrolyte solution composition.

Table 4: List of tensile specimens and testing performed.

Table 5: Frequency of corrosion pitting versus measured surface residual stress in a four month cyclical loading tests on tensile specimens 13, 21, 22,31.

Table 6: Location, depth and measured residual stress of blunt cracks formed on tensile specimens subject to cyclic loading in an electrolyte.

Table 7: Location, depth and measured residual stress of sharp cracks formed on tensile specimens subject to modified SSRT in an electrolyte.

Table 8: Rate of change of surface residual stress at cracking locations and rate of change as a percentage of the largest rate of change found on the corresponding tensile specimen.

LIST OF FIGURES

Figure 1: Stress - strain curve performed on a residual stress tensile specimen.

Figure 2: Orientation of the residual stress test plate when removed from the pipeline (**a**) and the residual stress test plate dimensions before three point bending. (**b**)

Figure 3: Deforming of test steel into a high residual stress test plate by three point bending.

Figure 4: Applied load versus displacement in three point bending of a residual stress plate.

Figure 5 : Predicted stress profile during and after bending.

Figure 6: Illustration of tensile specimen orientation after machining from residual stress plate.

Figure 7: Orientation of the tensile specimen with respect to residual stress plate and maximum expected residual stress field.

Figure 8: Environmental chamber with tensile specimen mounted in grips.

Figure 9: Load pattern used in pre-conditioning of tensile specimen. A total of 8000 cycles were applied.

Figure 10: Neutron spectrometer used to measure residual stresses in tensile specimens.

Figure 11: Positioning of tensile specimen on the specimen table in the neutron spectrometer.

Figure 12: Schematic of neutron scattering to measure inter-planar distance.

Figure 13: Example of magnitude versus scattering angle Gaussian curve collected by the neutron spectrometer.

Figure 14: Gauge volume of material measured by neutron diffraction.

Figure 15: Cyclic loading experiment for tSCC after test completion.

Figure 16: Load pattern used in cyclic loading experiment (2631 hrs – 518 cycles).

Figure 17: Stress – strain curve recorded during a modified slow strain rate experiment.

Figure 18: Axial (gauge length) residual stresses measured on tensile specimen 13.

Figure 19: Axial (gauge length) residual stresses measured on tensile specimen 21.

Figure 20: Axial (gauge length) residual stresses measured on the pre-conditioned tensile specimen 32.
Figure 21: Axial (gauge length) residual stresses measured on tensile specimen 33.
Figure 22: Axial (gauge length) residual stresses measured on tensile specimen 41.
Figure 23: Axial (gauge length) strain measured on tensile specimen 21.
Figure 24: Number of corrosion pits versus residual stress level observed on the four tensile specimens after four months of testing in the cyclical loading experiment.
Figure 25: Crack formed in tensile specimen 13 during a four-month cyclic loading test in an aqueous environment. (2.1 mm from gauge length center location).
Figure 26: Crack formed in tensile specimen 13 during a four-month cyclic loading test in an aqueous environment. (2.0 mm from gauge length center location).
Figure 27: Two cracks formed in tensile specimen 13 during a four-month cyclic loading test in an aqueous environment. (-1.5 mm and – 3.7 mm from the gauge length center location).
Figure 28: Crack formed in tensile specimen 13 during a four-month cyclic loading test in an aqueous environment. (-4.2 mm from the gauge length center location).
Figure 29: Crack formed in tensile specimen 13 during a four-month cyclic loading test in an aqueous environment. (-2.2 mm from the gauge length center location).
Figure 30: Crack formed in tensile specimen 21 during a four-month cyclic loading test in an aqueous environment. (-3.4 mm from the gauge length center location).
Figure 31: Two cracks formed in tensile specimen 21 during a four-month cyclic loading test in an aqueous environment. (-4.2 mm and –3.9 mm from the gauge length center location).
Figure 32: Crack formed in tensile specimen 21 during a four-month cyclic loading test in an aqueous environment. (-4.0 mm from the gauge length center location).

Figure 33: Crack formed in tensile specimen 21 during a four-month cyclic loading test in an aqueous environment. (4.3 mm from the gauge length center location).
Figure 34: Crack formed in tensile specimen 22 during a four-month cyclic loading test in an aqueous environment. (4.8 mm from the gauge length center location).
Figure 35: Crack formed in tensile specimen 31 during a four-month cyclic loading test in an aqueous environment. (14.1 mm from the gauge length center location).
Figure 36: Crack formed in tensile specimen 31 during a four-month cyclic loading test in an aqueous environment. (14.2 mm from gauge length center location).
Figure 37: Crack formed in tensile specimen 22 during a four-month cyclic loading test in an aqueous environment. (5.0 mm from the gauge length center location).
Figure 38: Crack formed in tensile specimen 22 during a four-month cyclic loading test in an aqueous environment. (0.9 mm from the gauge length center location).
Figure 39: Crack formed in tensile specimen 22 during a four-month cyclic loading test in an aqueous environment. (6.8 mm from the gauge length center location).
Figure 40: Crack formed in tensile specimen 22 during a four-month cyclic loading test in an aqueous environment. (6.7 mm from gauge length center location).
Figure 41: Crack formed in tensile specimen 22 during a four-month cyclic loading test in an aqueous environment. (-3.1 mm from the gauge length center location).
Figure 42: Measured surface residual stress versus frequency of cracking of four tensile specimens after a four-month cyclical loading experiment.
Figure 43: Electron micrograph of cracking in pre-conditioned tensile specimen 32
Figure 44: Electron micrograph of cracking in tensile specimen 41.
Figure 45: Electron micrograph of cracking in tensile specimen 42.

Figure 46: Electron micrograph of cracking in tensile specimen 43.

Figure 47: Optical micrograph of compressive residual stress surface area (**a**) and tensile residual stress surface area (**b**) after a twelve day exposure in a modified SSRT experiment.

Figure 48: Measured surface residual stress versus frequency of cracking on six tensile specimens tested in the twelve day modified slow strain rate experiment.

Figure 49: Measured surface residual stress versus normalized frequency of cracking for all cracks detected.

Figure 50: Frequency of the absolute rate of change of residual stress at each cracking location as a percentage of the maximum rate of change of residual stress measured for each tensile specimen.

Figure 51: Stress and stress intensity for a theoretical crack propagating through the center of the gauge section on tensile specimen 13.

Figure 52: The change in stress intensity (ΔK) experienced by a crack propagating through the center of the gauge section on tensile specimen 13 when calculated from the experimental cyclic stress and measured residual stress.

SYMBOLS, NOMENCLATURE and ABBREVIATIONS

Coupon	Metal test specimen
CTOD	Crack tip opening displacement
EDM	Electrical discharge machining
EDX	Energy dispersive X-ray
iSCC	Inter-granular stress corrosion cracking
K	Crack stress intensity factor
Haz	Heat affected zone
ΔK	Change in crack stress intensity factor
MPa	Mega-Pascal (1×10^6 Pascal)
PM	Pseudo-macrostress
RA	Reduction in area
R-ratio	Minimum pressure / maximum pressure
SCC	Stress corrosion cracking.
SEM	Scanning electron microscope
SMYS	Specified minimum yield stress
SSRT	Slow strain rate test
TEM	Transmission electron microscope
tSCC	Trans-granular stress corrosion cracking

1.0 INTRODUCTION

Stress corrosion cracking (SCC) can be defined as the interaction of a tensile stress and an aqueous environment acting on a metallic surface to initiate and propagate cracks. The formation of SCC occurs below the yield strength of the bulk material and typically below the design stress and fatigue limit of an engineered structure. Since the first discovery of SCC on the exterior surface of a buried, high pressure, natural gas transmission pipeline in 1965, SCC has continued to make a significant contribution to the number of leaks and ruptures experienced by the massive North American and world infrastructure of buried pipelines.

Two forms of SCC can exist on mild steel buried pipelines. The first discovered form of SCC propagates inter–granularly and is associated with a concentrated alkaline electrolyte in contact with the steel surface. The mechanism of crack growth is reasonably well understood and control of this type of cracking is possible by reducing pipe temperature and controlling the pipe electrochemical potential range. A second form of SCC was discovered in Canada in the early 1980's. This form of SCC propagates trans-granularly and is associated with a dilute, neutral pH electrolyte in contact with the steel surface. It is this form of SCC, designated trans-granular SCC (tSCC) that will be the focus of this study.

TSCC failures have occurred unpredictably across the Canadian pipeline system. As such tSCC research has focused, to a large extent, on attempting to identify critical environmental conditions such as electrolyte, pH and potential by analysis of large amounts of empirical data derived from field excavations of pipelines susceptible to tSCC. This research methodology resulted from the immediate need to identify susceptible tSCC locations on the pipeline and thereby create a means to control a relatively new and poorly understood integrity threat to pipelines. Concurrent laboratory investigations supported this need by investigating parameters necessary for tSCC management such as cracking velocity.

Current laboratory and field data support the following tSCC characteristics;

I. Occurrence beneath a failed high impedance coating. The failed coating is capable of partially shielding the steel surface from cathodic current while allowing the ingress and trapping of an electrolyte against the pipe surface.

II. A tendency to form large colonies containing many shallow cracks (<10% of pipe wall). The vast majority of the cracks have a very slow or non-detectable cracking velocity. Failures are typically composed of several coalesced cracks.

III. Capable of forming in the absence of general corrosion, but may initiate at the bottom of slowing or dormant corrosion, or the bottom of corrosion pits.

IV. Alignment perpendicular to a tensile stress, typically the hoop stress induced by internal pressure. Many cracks are associated with welds or defects, which may induce other tensile stresses.

V. Trans-granular crack propagation.

VI. Low corrosion rates of the crack wall and crack tip but also no evidence of a passive film, such as a calcium carbonate, forming on the walls of the crack.

Currently the exact mechanism of tSCC, although theorized, is not well defined or completely supported by scientific studies to date. Current mechanistic theories are typically a derivation of past theories of cracking on systems other than pipelines that exhibit similar crack characteristics. Some theorized mechanistic features of tSCC include the following;

I. A role for mono-atomic hydrogen in the embrittlement of the crack tip.

II. The generation of hydrogen by interaction of a cathodic bulk surface and an anodic crack wall surface.

III. A possible synergistic growth by fatigue for deeper cracks.

IV. Discontinuous propagation of the crack from a location beyond the crack tip back to the crack tip.

Although stress is a necessary parameter for tSCC, little research has focused on defining the role of stresses in crack initiation and growth. Present research that does incorporate pipe stresses are focused on the fatigue aspect of tSCC growth.

Residual stresses have been measured at tSCC colonies and have been found to be substantially higher than those residual stresses measured in adjacent tSCC free material. The pipe property of residual stress exhibits a strong correlation with the incidence of tSCC. Aside from the empirical correlation of residual stress and tSCC, little research has been performed to understand the basis for this correlation.

Residual stresses measured on pipe surfaces are typically created as a result of pipe manufacturing techniques such as cold expansion. *Residual stresses arise as a result of non-homogeneous plastic deformation of a pipeline, where one area becomes plastically deformed and an adjacent area is elastically deformed.* Residual stresses can arise between adjacent grains, which can react elastically or plastically depending on their orientation, size and properties. Alternatively, residual stresses can arise between different metallic phases that yield at different stress values. Finally, macro-residual stresses occur due to a difference in applied load across discrete locations on the structure. For example, a difference in applied load can be expected between the interior and exterior pipe surfaces, at welds, or at a change in pipe wall thickness.

This research project will study the relationship between residual stresses in pipeline steels and the initiation and growth of tSCC. A hypothesis is proposed

where:

Surface residual stresses provide anodic or "high energy" sites that focus initial grain dissolution and lead to stress intensification, a pre-cursor to cracking. Below surface residual stresses provide a tensile load necessary to keep small cracks open and allow growth. Therefore, propagation of a crack into a compressive residual stress field will create dormancy, while a tensile residual stress will allow growth to continue.

Underlying this work is a proposed environmental mechanism for SCC growth that is in some manner reliant on an increased crack tip stress to focus the build up of diffusible (mono-atomic) hydrogen in the area of the crack tip in order to propagate the crack. The source of this stress, for initiation and growth of a crack in the very early stages of its life, may be the residual stresses commonly found in a pipe. Further growth may be propagated by external stresses introduced by the pressure in the pipeline.

To test the above hypothesis, tensile specimens were fabricated in such a manner to contain a large residual stress gradient along the gauge length and through the specimen depth. Preferential cracking at increased residual stress levels in otherwise identical conditions may support a role of residual stress in crack initiation. The stresses in these tensile specimens were measured non-destructively along the gauge length direction and through the thickness using neutron diffraction. Testing of the tensile specimens for crack initiation and growth is performed by slow strain rate and cyclic loading techniques. An environment was generated around the coupon during testing to support the proposed hydrogen growth mechanism. The tensile specimens were examined after testing to identify the type of failure and location of the failure, and conclusions were formulated on the basis of these results.

2.0 LITERATURE REVIEW

This literature review will focus on work related to the proposed and alternative initiation and growth mechanisms for trans-granular SCC. A review will be performed on the methodology of the measurement techniques for quantifying residual stresses. The work performed to correlate residual stress with SCC will be reviewed. Pertinent literature related to the testing techniques used in this study will also be examined.

2.1 Characteristics of stress corrosion cracking

Two forms of stress corrosion cracking have been found on the exterior surface of pipelines since the 1960's. The two forms of SCC share a similar attribute in that the cracks form as a result of a degraded coating that allows an electrolyte to penetrate to the surface of the pipe. Cracks then initiate in an aqueous environment well below the yield point of the material and continue to grow and coalesce in an orientation perpendicular to the applied hoop stress. Some of the cracks, when properly aligned, will reach a critical length and depth and cause the pipe to fail by leak or more typically by rupture. [1,2,3]

The earlier form of cracking was labeled high pH SCC due to the high pH bicarbonate/carbonate electrolyte in contact with the crack colonies. This type of cracking was characterized by inter-granular growth through the pipe wall. The mechanism for this type of cracking has been well studied and draws analogies in mechanism from cracking in other materials such as brass and stainless steels. A high pH inter-granular cracking mechanism relies on stress focused anodic dissolution wherein the highly stressed grain boundaries at the leading edge of a crack become sites for preferred anodic attack. The crack wall is quickly passivated by the solution and becomes cathodic in relation to the crack tip. This process of galvanic action is supported by the lack of crack wall dissolution and the increasing crack growth response to increasing temperature. [3,4]

The later form of cracking, near neutral pH SCC, is relatively new and was first detected in the mid 1980's on Canadian pipelines and has now been identified in several countries around the world. Several key differences distinguish this form of cracking from the high pH form of cracking. These differences include a dilute bicarbonate electrolyte with small amounts of chloride, an electrolyte pH of approximately 7 pH units, trans-granular crack propagation and a mechanism that is different from that of high pH SCC. The trans-granular SCC mechanism, although not well understood, is purported to involve a role of diffusible hydrogen in weakening the material at the crack tip to the point where the material may locally yield. The result is a fracture surface often defined as "quasi-cleavage" in that evidence of micro-plasticity is found on the fracture surface. [2,3,5,6]

Indirect evidence of the effects of hydrogen supports the theory that hydrogen may be involved in the trans-granular SCC mechanism. It was found that hydrogen can be discharged in these low pH solutions well below the over-potential of water as indicated by internal cracks in the steel that were clearly caused by diffusible hydrogen. [7] Birnbaum has shown that static dislocations start to move in the presence of hydrogen and stop when the hydrogen is removed. [8] Beachem showed that the flow stress of mild steel was reduced by the presence of hydrogen during torsion testing. [9] Cracknell and Petch showed that hydrogen eliminates the upper yield point and lowered the yield strength in a wide range of carbon steels. [10] Oriani and Josephic showed that introducing low fugacity hydrogen above a lower limit resulted in a rapid increase in creep rate followed by increased strain hardening. [11] The summation of all this work provides evidence that it is possible and probable that hydrogen will allow for micro-plastic deformation at a crack tip at stresses well below the overall yield strength for pipeline steels.

Other recent research into trans-granular SCC provides several observations that may be useful to the present research on the conditions that favor trans-granular SCC.

Parkins states that when pipelines are placed in the ground it is assumed that the conditions for SCC do not exist. As a result of this observation Parkins concludes

that a period of incubation must exist in which the proper conditions of coating degeneration and electrolyte penetration occur. [2]

The absence of any significant amount of impressed cathodic current will allow the pipe to remain at a low pH. The pH will then be directly controlled by the partial pressure of CO_2 in the soil adjacent to the pipeline. [2]

Crack growth rate does not decrease as a function of increasingly electronegative applied potentials. Such a correlation would exist if anodic dissolution played a role in crack growth. Instead, the trend of quasi-cleavage indications increase as potential decreases, pointing to a role of hydrogen in the embrittlement of the crack tip. [3,12]

Cyclic loading acts to reduce the threshold stress for SCC below the normal applied load. This can allow for crack initiation with an elastic applied load, which provides the basis for the use of cyclic loading in laboratory testing. [4]

2.2 Residual stresses

2.2.1 Nature of residual stresses in pipeline steels.

"*Residual stresses occur when there has been an non homogeneous plastic deformation of the specimen wherein one part of the specimen has been plastically deformed and other locations have been elastically deformed.*" *(Holden, Root, Rogge, Clarke)* [13]

Residual stresses can occur on a microscale of grains where grains of different orientation may either elastically or plastically deform depending on their alignment in the applied stress field. This is particularly common in anisotropic materials. More commonly for steels with little anisotropy are macro-stresses wherein the material experiences different levels of residual stresses across a region, such as high tensile stresses near a bent surface, little or no stresses near a neutral axis and perhaps compressive stresses on the inside of the bend. [14]

Physically, residual stress is exhibited as a change in the normal interplanar spacing between atomic planes of atoms, resulting in either an increase or decrease in this spacing. An external stress applied in the same direction as a tensile residual stress will add to the residual stress and can result in local areas of stress which exceed the yield point for the material. These areas favor crack initiation and propagation. Conversely, compressive residual stresses will reduce the effect of applied external tensile stresses and may halt crack propagation. Therefore, it is possible that crack propagation starting in the high tensile residual stress region near the pipe surface can become dormant as the crack propagates through the pipe wall and into a compressive residual stress region. [13-16]

Residual stresses can be produced as a result of both manufacturing and in service use of pipelines. Sources of residual stress in manufacturing can include heat treatments including welding and rolling processes. Upon cooling, differential rates of cooling between the surface and the interior of the steel can induce plastic flow or permanent yielding. The differential heat can be quantified by Young's modulus and the coefficient of expansion for steels wherein a stress of 3.5 MPa is created per °C in temperature difference between surface and inner steels. Typically the surface ends up with compressive forces relative to the steel interior due to the more rapid cooling experienced on the surface. [6,15]

Welding of the long seam weld can produce residual stresses through differential heating and cooling of adjacent material. In this case the heat affected zone will have tensile residual stresses in relation to the material adjacent to the HAZ. [6,15]

Heat treatments that create an austenitic phase transformation in steels can create different patterns of residual stresses than expected by differential cooling rates. In the case where martensite is formed from austenite, the low strength austenite will plastically deform to accommodate the expansion of the initially formed adjacent martensitic structure. The higher strength martensite will resist this expansion creating tensile stresses across the martensitic structure. Often these martensitic structures will form at the surface where the rate of heating and cooling is higher,

thereby creating areas of tensile residual stresses at the surface. This is the opposite residual stress condition than that caused by differential cooling rates alone. [13]

In-service residual stresses can be caused by the yielding of the material in and around dents or rock impingements. The surface near mechanically damaged areas can form a complex pattern of compressive and tensile stresses.

A definition of residual stresses provided by Mura defines residual stresses as the *"self-equilibrating internal stresses existing in a free body which has no external forces or constraints acting on its boundary."* [17]

It was earlier stated that macroscopic stresses are homogeneous over large surfaces, usually larger than a grain size whereas microscopic stresses are micro sized, such as at the grain boundary of two phases with differing inelastic properties. Micro-residual stresses may be more important in crack initiation as they more accurately reflect the local conditions at the crack tip. Micro-stresses are not homogeneous across any macro-sampling of the material. In reality, residual stresses induced by plastic deformation contain both macro-stresses and micro-stresses. The macro-stresses are created as a result of differential applied strains acting on adjacent material, whereas the micro-stresses are formed from differential yield points of adjacent phases or grain orientation subject to equivalent load conditions. Upon measuring residual stresses by diffraction methods, an average representative volume is sampled which can be more closely defined as the average micro-stress for that volume of sampled material. This measurement of stress is sometimes referred to as pseudo-macro (PM) residual stresses. PM stresses are not representative of the micro-stress for any particular phase but provide an average stress for a continuous matrix and discrete phases and precipitates as long as there is a statistically representative specimen of each in the volume of specimen measured. [19]

PM residual stresses obey the average equation of equilibrium in that the net force

acting on any volume of material must be zero. [19]

$$\sigma_{(ij)} = 0$$

For multiphase materials such as steels containing both precipitates and a matrix, a derivation of stresses yields; [19]

$$\sum_{i=1}^{N} f_i \bullet \langle \sigma_{ij} \rangle_i = 0$$

where N is the number of phases, f_i is the volume fraction of the I^{th} phase, which has the average stress $\langle \sigma_{ij} \rangle_i$. This equation is used as a basis to support the use of linear elastic theory in analyzing measured strains and converting them to appropriate values of stress.

2.2.2 The influence of residual stresses on tSCC

The most recent relevant work on material factors that influence SCC was conducted by Beavers and Johnson. [18] These researchers focused on pipe metallurgical factors including residual stress, surface roughness, chemical composition, inclusion properties, cyclic stress-strain behavior and micro-hardness.

The test methodology was developed to quantify each of these parameters using standard techniques on tensile specimens containing pre-existing SCC and no SCC. Fourteen pipe specimens were examined with grades ranging from X52 to X70 and vintages from the 1950's to the 1970's.

Residual stresses were measured at various locations in and around the SCC colony and the control area on the intact pipe using the hole drilling technique. Holes were drilled to seven depths and the average residual stress for each layer

was calculated using the method outlined in the ASTM standard E 837-94a. The maximum depth studied was 2.0 mm or 20% of the total wall thickness. Residual stresses were shown to increase twofold in the area of the SCC colony to an average value of 216 +/- 104 MPa in comparison to an average value of 108 +/- 66 MPa in non-SCC areas. Statistical evaluation of the data showing a difference in residual stress levels in the SCC and non-SCC areas revealed a confidence level of 99.98% that the SCC and non-SCC areas differ in terms of residual stresses. The depth profile for residual stress in pipeline steels revealed that in many cases the surface of the coupon was in compressive stress and quickly became tensile reaching a plateau value of between 75 and 210 MPa at the 1.5 mm depth (15% of wall thickness)

Surface roughness measurements revealed slightly higher surface roughness values for areas with SCC as opposed to areas with no SCC, but this difference failed to meet a standard confidence level of 95%, suggesting that this difference may have occurred coincidentally.

Micro-hardness values for SCC and non-SCC areas revealed that surfaces with SCC had average values of 210 Knoop Hardness (KHN) compared to 202 for non-SCC surfaces. Again, a statistical confidence level of 93% was not great enough to confirm this correlation.

No other significant correlations were found between areas of SCC and inclusion properties, local galvanic behaviour, cyclic stress-strain behaviour, chemical composition or tensile properties.

The work of Beavers and Johnson [18] indicated a strong correlation of SCC with residual stresses and a weaker correlation with micro-hardness at the SCC colony. The sources of residual stresses were suggested to originate from fabrication processes, welding, mechanical damage and surface preparation.

2.3 Measurement of residual stresses

2.3.1 Neutron diffraction

Neutron diffraction was first used in studies of inelastic scattering by Canadian Nobel Laureate B.N. Brockhouse at the Chalk River Laboratory near Ottawa, Ontario and was routinely used for measurements of residual stresses in the early 1980's. The principal advantages of this technique are the high degree of precision in the technique and the penetrating ability of neutrons, allowing for measurements through the specimen to be made without destruction of the specimen. The disadvantage of the technique is the need for a neutron source, such as a nuclear reactor, and the radioactivity associated with this. As well, the neutron diffraction technique is a time consuming process, as much attention must be paid to the alignment of the beam in three directions. A high degree of automation is necessary to make multiple measurements on a specimen to maximize use of the reactor and minimize operator error. [14,15]

Neutron diffraction relies on a high intensity thermal neutron source, such as from a nuclear reactor or spallation of radioactive material to interact with a known crystallographic plane in a material to create a characteristic scattering pattern. Thermal neutrons are gathered from a source and selected for a single wavelength in the range of 1 Angstrom to 3 Angstroms by a monochromatic crystal such as germanium. This single wavelength beam is then projected through a cadmium alignment slit which selects the size of the neutron beam and ultimately determines the volume of material under study. The beam then interacts with the specimen and is diffracted by planes normal to the incident beam. The diffracted beam is gathered through a second slit onto a multi-detector where the intensity is measured over a range of possible diffraction angles for the particular plane. A Gaussian curve is then fitted to this data allowing the calculation of 2θ, which is the diffracted angle from the highest intensity diffraction plane. With a value of 2θ, the interplanar spacing, d, for a particular plane of Miller indices (*hkl*) can be calculated with the use

of Bragg's law.

$$d_{(hkl)} = \frac{\lambda}{2 \sin \phi_{(hkl)}} \qquad \text{Equation 1}$$

The symbol "λ" is the wavelength of the monochromatic incident beam, $d_{(hkl)}$ is the interplanar spacing for the selected Miller indices and $2\theta_{(hkl)}$ is the angle of diffraction for the equivalent Miller indices..

Once the interplanar spacing, d_{hkl}, is known, elastic strain, ε_{hkl}, can be calculated if a stress free lattice spacing, d^0_{hkl}, is known with the following equation.

$$\varepsilon_{hkl} = \frac{\left(d_{hkl} - d^0{}_{hkl}\right)}{d^0{}_{hkl}} \qquad \text{Equation 2}$$

By orientating the specimen in the transverse, normal and longitudinal directions, and measuring strain on the same volume of material in each of these directions, a value of stress can be calculated using Hooke's Law.

$$\varepsilon^1 = \frac{\sigma^1}{E} - \frac{\nu\sigma^2}{E} - \frac{\nu\,\sigma^3}{E} \qquad \text{Equation 3}$$

In equation 3, E is Young's modulus for this material and ν_{hkl} is the Poisson's ratio for this material.

Equation 3 can be rearranged to calculate stress in a particular direction using the measured values of strain in each of the three directions. For instance, to calculate stress in the x direction (σ_x), which is typically the main stress for crack initiation, the equation will be as follows:

$$\sigma_x = \frac{E}{1+\nu}\sqrt{\left(\frac{1}{1-2\nu}\right)\Delta\varepsilon_x^2 + \left(\frac{\nu}{1-2\nu}\right)\left(\Delta\varepsilon_x^2 + \Delta\varepsilon_y^2 + \Delta\varepsilon_z^2\right)} \qquad \text{Equation 4}$$

2.3.2 X-Ray diffraction

The use of X-ray diffraction to measure stresses is based on the same principle as for neutron diffraction, that is Bragg's Law (Equation 1). The principal differences between X-ray and neutron diffraction is the excitation source and the penetrating power. X-rays can be produced as ionizing particles from the impact of accelerated electrons in a vacuum through a potential field into a positive stationary anode. The majority of the energy in this method is emitted as heat and thereby limits the X-ray production to the rate of heat dissipation, producing X-rays in the order of 1.5 kilowatts to 3 kilowatts. By rotating the anode so that new material is constantly exposed the X-ray intensity can be increased 50 times. [19]

The second principal difference between X-ray and neutron diffraction is in the absorption of X-rays. X-rays are attenuated as they pass through matter. The mechanism of attenuation includes the generation of heat, activation of fluorescent X-rays, excitation of photoelectrons and coherent and incoherent scattering. Depending on the intensity of the beam and the wavelength energy of the X-rays, X-rays may penetrate into the material from a few micrometers to tens of micrometers. [19]

2.3.3 Hole drilling

ASTM method E837-99 provides the methodology for residual stress measurements near the surface of a material by the hole drilling – strain gauge method. [20] The method requires attaching a strain gauge rosette to a surface. A microscope is used to align a drill with the geometric center of the strain gauge and a hole is drilled to a depth of 0.4 times the diameter of the strain gauge circle area. The residual strain surrounding the hole is relieved to near zero. This strain relief is measured with a strain gauge recording instrument. The stress is then calculated from the measured

strains through a set of equations. This method applies only to surface residual stress measurements but others have modified it to allow for stress measurements in the depth direction as well. The equation describing the relation of strain to stress in this technique is as follows:

$$\varepsilon_\tau = (A + B\cos 2\beta)\sigma_{max} + (A - B\cos 2\beta)\sigma_{min} \qquad \text{Equation 5}$$

where

A, B = calibration constants

ε_τ = relieved strain measured by the strain gauge

σ_{max} = maximum principal stress at the hole location before drilling.

σ_{min} = minimum principal stress at the hole location before drilling.

β = angle measured clockwise from the direction of gauge 1 to the direction of σ_{max}.

The calibration constant A can be calculated using Poisson's ratio (ν) and Young's modulus (E) for the particular material with the equations;

$$A = \frac{-a(1+\nu)}{2E} \qquad \text{Equation 6}$$

and

$$B = \frac{-b}{2E} \qquad \text{Equation 7}$$

Where *a* and *b* are dimensionless material independent constants determined experimentally.

This method of measuring residual stress is semi-destructive in that the holes drilled are generally not large enough to destroy a tested component but may be too destructive for further use of test coupons, such as a tensile specimen.

2.4 Test methods for trans-granular SCC

2.4.1 Cyclic loading

Cyclic loading is often used for SCC initiation and crack propagation studies as the severity of the test can be varied from less to more severe and the applied stress can be kept below the yield point for the material. This testing is often used to simulate actual operating conditions that these materials will see. Conversely, the length of the test is often undefined, especially in initiation experiments, as there is no expected ultimate failure of the material if the material is cycled below its fatigue limit in air. Often the very attributes that define SCC, such as minimal fatigue, environmentally assisted and low growth rates, make it very difficult to apply a sufficient degree of realism to a test in order to ensure that the equivalent mechanism is responsible for both test crack initiation and growth and field SCC initiation and growth. [21,22]

Cyclic loads can be applied to a specimen in a number of ways, each with various advantages and disadvantages. On non-machined specimens where the original surface is needed, four-point bending is typically used where a load is applied to two points on the outer surface against two points on an inner surface. This produces a variety of tensile and compressive stresses that may be difficult to interpret. If tensile coupons can be machined from the specimen, they can be placed in a servo-hydraulic loading apparatus where a purely tensile load can be applied, but is limited to modified surfaces. Other researchers [3] have used cantilever cyclic loading where an edge of a curved specimen is clamped and the other end is attached to a loading mechanism. This method can utilize an original surface and geometry but will produce both tensile stresses on the outer surface and compressive stresses on the inner surface, which is different from what an operating pipeline experiences. The most realistic load application to an original surface is achieved through the use of hydraulic loading of an intact and capped piece of pipeline. This method, although very realistic, is limited by the ability to apply high frequencies with accurate loading and is also limited by its higher experimental cost.

Nonetheless, cyclic loading has been successfully used by several researchers (Lambert, Plumtree, Parkins, Fessler, Beavers) to initiate and grow SCC in the lab in what has been thought to be the equivalent mechanism as in the field. [1, 22-24] The key parameters for cyclic loading include the maximum applied stress, the cycling frequency, the strain rate and the R-ratio (minimum load / maximum load). Typically the maximum stress is kept below the specified minimum yield strength (SMYS) which itself is usually 10% below actual yield. This ensures that only elastic deformation occurs in the macroscopic area of the specimen. R-ratio's typically vary from 0.5 to 0.98. Strain rates are a function of both the duration of the test and number of cycles applied and generally remain below 10^{-5} /second. To bring the test duration to reasonable time periods, the loading frequency is typically increased to a point just below where mass transport and electrochemical reaction kinetics in the crack may become rate limiting. By increasing the experimental load frequency by two orders of magnitude greater than the loading pattern typically seen in the field, SCC initiation may be expected in several weeks rather than several years.

It has been shown that crack initiation does not occur using realistic loading condition under cyclic loading conditions in air. [24] In addition to an applied load, a conducive environment must be placed against the surface of the metal. This environment is usually composed of an electrolyte of various compositions, usually with oxygen purged away to prevent rapid corrosion and perhaps a soil with organic content.

2.4.2 Slow strain rate testing (SSRT)

Tensile specimens are one of the most widely used coupons (metal specimens) in the laboratory study of SCC. These coupons are placed under load by a servo-hydraulic loading machine where load can be applied through a constant or variable displacement, load or stress.

The slow strain rate test was derived from this methodology and was originally used

by Parkins in the 1950's for SCC studies. SSRT has been used extensively to screen materials for SCC susceptibility, to perform parametric studies, or to derive information on growth mechanisms. A SSRT applies a constant low strain rate in the order of 10^{-6} $second^{-1}$, or approximately four times slower than a normal tensile test. This slow strain rate typically may lead to test durations of four days to as many as fourteen days. The slow application of a constant strain is designed to allow electrochemical reactions on the steel surface to dominate the cracking mechanism. Often the test is halted before the ultimate strength of the specimen is reached in order to study crack initiation without the interference of a large plastic deformation. In ductile pipeline steels this may mean halting the test at approximately 10% - 15% elongation. Researchers have used this test to estimate the effect of environmental conditions on crack initiation and propagation in the presence of a stress that will ultimately fail the specimen. In particular, the role of hydrogen can be assessed by determining hydrogen concentrations that promote the formation of surface cracks.

One disadvantage of this test may lie in the reproduction of mechanism. Earlier it was stated that a primary criterion for a SCC test is that the mechanism of the test failure should be the same as the in-service failure mechanism. As the SSRT derives the majority of its data from the elastic-plastic region and pure plastic region of the stress – strain curve, the test clearly operates above the loading regime seen on all pipelines. As well the specimen geometry does not allow for natural pipeline surfaces to be used. Due to these constraints each specimen must be examined microscopically to determine the fracture microstructure to ensure that a trans-granular type crack morphology is present. Even this is not a guarantee that the equivalent field mechanism was responsible for the laboratory SCC propagation. To gain useful information from this test a crack propagation mechanism must be assumed. Environmental parameters such as potential and hydrogen concentration can then be tested against the assumed mechanism using SSRT.

Another problem lies in the selection of the variable in the test to be related to the propensity of cracking. Some researchers will use decreasing percent reduction in area (%RA) as an indication of the onset of brittleness and cracking intensity. This

relation was made as a result of the brittle cleavage that trans-granular SCC causes in conjunction with microstructure studies showing a higher chance of causing cracking with decreasing ductility of the metal surface.

Beavers and Parkins have described a standard test procedure for SCC based on a variation of the tensile specimen called the tapered tensile specimen. Parkins speculated that SSRT testing and fatigue pre-cracked specimen testing was too severe, whereas constant load or constant displacement testing was too slow and expensive. Parkins developed what he considered a more realistic test in which a dead weight load was placed on a tapered tensile specimen and a cyclic load was superimposed over the dead weight load. Data analysis compared the number of cracks versus the distance from the high stress end of the coupon. This was converted to a *threshold stress* for each crack using the following equation:

$$\sigma_{th} = \frac{P}{A_1 + \frac{X_n}{L(A_2 - A_1)}}$$ Equation 8

Where:

σ_{th} = Threshold stress.

P = Maximum, minimum or mean load.

L = Gauge length.

A_1 = Specimen cross sectional area at small end of taper.

A_2 = Specimen cross sectional area at large end of taper.

X_n = Specimen cross sectional area at the crack location.

A second computed variable was *cracking velocity*. This value was computed by measuring the depth of the deepest crack and dividing by the total test time. These two variables, threshold stress and cracking velocity, were used in combination with each other by Parkins to define a SCC susceptibility in this test. Environmental chambers were again used to assess the relative contribution of different environmental parameters on SCC as well as the screening of different metals for SCC susceptibility. One interesting conclusion that has come from this test and was

later supported by other researchers was that crack growth rate decreased with increasing test duration. This observation may support a sporadic growth condition or other mechanisms that are inhibited by slow film formation or possibly the onset of crack tip blunting.

Turnbull points out an inherent problem with a taper tension test when used to indicate SCC susceptibility. [31] Under certain conditions the threshold stress, calculated above, is greater than the yield strength due to non-uniform deformation of the specimen. The true strain rate will therefore decrease during deformation, in turn affecting the calculated threshold stresses.

2.5 Proposed mechanisms for tSCC

2.5.1 Hydrogen embrittlement

The process of hydrogen absorption is well documented in the cracking of high strength steels in aqueous environments. Hydrogen is abundant in nature and can be found as a byproduct of cathodic reactions, such as the reduction of water on the surface of the cathode. Line pipe is often an aggressive cathode due to the application of cathodic protection systems, and can easily reach the over-potential of water with the resultant production of diatomic hydrogen gas ($H_{2(g)}$). Diatomic hydrogen cannot in itself diffuse into steel but forms an equilibrium with mono-atomic hydrogen which can readily pass through the interstitial voids in steel with a diffusion coefficient of 10^{-4} to 10^{-8} cm^2 / second. The equilibrium of mono-atomic and diatomic hydrogen greatly favors diatomic hydrogen but the recombination of mono-atomic hydrogen to diatomic hydrogen can be poisoned by sulfur, (as in the case of hydrogen sulfide cracking) as well as arsenic, phosphorus or antimony. [26]

The model of hydrogen embrittlement involves the selective concentration build up of hydrogen at the crack tip. This hydrogen concentration is a result of the increased attraction of hydrogen for the tensile hydrostatic stress caused by stress intensification ahead of the crack tip. [27-31] The build up hydrogen may also be

focused at grain boundaries or dislocations. Although the atomistic mechanistic effect of hydrogen is not yet understood, it is generally believed that hydrogen may weaken bond strength between atoms thereby allowing induced local fracture by cleavage or enhanced micro-plasticity. As the hydrogen in the zone ahead of the crack tip reaches a critical value of concentration and volume, a localized crack can initiate which then can propagate back to the main crack. This is known as discontinuous crack propagation. The average rate of propagation is given as V_t and follows the equation:

$$V_t = \frac{X}{t} \qquad \text{Equation 9}$$

Where *"X"* is the distance between the main crack tip and the hydrogen accumulation zone and *"t"* the time needed for diffusible hydrogen to build to a critical concentration and volume.

As a result of hydrogen embrittlement, the brittle micro-fracture of a ductile alloy can occur in the presence of sustained tensile stresses below the yield strength of the particular metal. The cracks formed are generally sharp, indicating a brittle fracture but may also have some micro-plastic deformation formed during propagation. [32] This combination of brittle and plastic fracture, which has often been observed under high resolution TEM, is often called quasi-cleavage. Some researchers have used the observation of quasi-cleavage as evidence against the cleavage model as a result of hydrogen absorption and bond weakening.

Locally induced micro-plasticity has given rise to a subset mechanism of hydrogen embrittlement. Although this initially appears contradictory to the notion of brittle cleavage, an explanation has arisen. Beachem first suggested that this may be the possible mechanism of hydrogen embrittlement in that the formation of hydrogen in the crack tip is non-uniform. Beachem [9] states "*locally the flow stresses can be reduced resulting in localized deformation that leads to highly localized failure by ductile processes while the total macroscopic deformation remains small.*"

This mechanism proposes that shear localization occurs on a micro-scale yet on a macroscopic scale it appears to be a brittle failure, and is often mistaken as such. The largest obstacle to conclusively show that hydrogen embrittlement can cause trans-granular SCC lies not in the correlation with empirical data, which is very good, but in the atomistic model as to how hydrogen weakens atomic bonds (de-cohesion). To date this information lies only in theoretical calculations with little or no direct evidence.

2.5.2 Surface mobility

Galvele [34] proposed that crack propagation *is "due to the environmentally induced crack propagation due to the capture of vacancies by the stressed lattice at the tip of the crack."* His assumption is that the crack growth rate is controlled by the rate at which these vacancies move from the area of the crack tip and migrate down the crack walls. As well, an aqueous environment is necessary to change the surface self-diffusivity of the metal.

This mechanism is of interest to researchers studying inter-granular SCC of pipelines as it allows a process of brittle fracture to occur in a ductile metal. Galvele's tests were conducted at elevated temperatures (less than half the melting point) and used gold/silver alloys, but despite the temperature and material differences when compared to tSCC in pipelines, it does provide some interesting relationships to low temperature cracking in mild steel. This research was able to predict similar crack velocities as those measured in trans-granular SCC. As well a very good correlation between temperature and cracking velocity was found in terms of surface mobility. Galvele was also able to show that the surface mobility model provided evidence of inter-granular to trans-granular transition based on potential dependence. Previous research by Beavers et al. [6] has theorized that trans-granular cracks initiate in inter-granularly and will then propagate trans-granularly if a suitable aqueous environment exists.

2.5.3 Stress sorption

The mechanism of stress sorption was proposed by Uhlig in 1973 and relates more to the propagation of a crack than the initiation of this crack. Little literature is available on this mechanism as it pertains to line pipe steel. This mechanism suggests that the normally plastic crack tip is acted upon by species in solution to produce increased brittleness. On an atomistic level, the adsorbed species acts to weaken the bond strength between atoms with a resultant decrease in the surface energy. The stress at fracture, σ_f, is reduced in relation to the surface energy, γ, according to the equation;

$$\sigma_f = \frac{\sqrt{E\gamma}}{d} \qquad \text{Equation 10}$$

In equation 10, E is Young's modulus of elasticity and d is the interplanar spacing. The result of stress sorption is that the normally calculated value of K_{IC} for a particular crack is reduced to a value less than the crack tip intensity factor calculated from normal tensile stresses generated by pipeline operation. [35]

The stress sorption mechanism supports empirical evidence pertaining to the environmental influence on the mechanism of trans-granular SCC. Different aggressiveness of absorbable species will be generated according to the particular solution chemistry in contact with the pipe. This has a correlation with laboratory observations in that some solutions are more prone to cause cracking than others. As well, the electrochemical potential of the steel surface is directly influenced by the electrolyte whose ionic species are in a specific oxidation state. This may be an important parallel to SCC of line pipe in that a certain metal surface potential range, which lies between the anodic passivation potentials and anodic dissolution potentials, has been found necessary to allow cracking to occur in both inter-granular and trans-granular SCC. It may also be concluded that the oxidation state of the ionic species in solution at the cracking range provides maximum weakening of the atomic bonding at the crack tip.

Evidence for this mechanism was derived from straining electrode experiments, using a thin wire. A large amount of metal loss was detected in these experiments due to the aggressive nature of the electrolyte on constantly exposed fresh metal. A shortfall of this mechanism when applied to line pipe trans-granular SCC is the question of what will happen to the large amounts of metal dissolved from under the adsorbed film, as this is not typically seen in field SCC.

A second shortfall of this model is the prediction of unrealistically high rates of crack growth.

Finally, a third shortcoming of the stress sorption model is that the straining electrode experiment is designed to constantly expose fresh metal onto which adsorption may occur. A vast majority of research into SCC refers to a rapidly reforming film at the crack tip which would inhibit the adsorption process. It is likely that a film rupture model will need to be added to help explain this mechanism

2.5.4 Slip dissolution

The previous models use mechanical fracture as a means of crack propagation. The slip dissolution model is different from the previous models in that the stress regime is important only in focusing the dissolution process and exposing new material yet the applied stress does not itself break atomic bonding. Crack tip propagation is controlled by the oxidation of the fresh metal surface. The oxidation process itself generates film formation and the application of a continual cyclic stress will cause further film rupture. [15-18]

The rate at which the crack tip can advance in this model is a function of:

I. Film rupture rate at the crack surface.
II. Diffusion of oxidizing species to the crack tip and removal of reduced species away from the crack tip

III. Rate of dissolution as determined by the relative strength of the oxidizing species.

Strain concentration in this model is used to force the dislocations in the material to the metal surface thereby increasing the number of active sites at the metal surface and decreasing the total energy needed for the dissolution process. This model may have limited application to line pipe steels for a number of reasons. Firstly, the rate of crack growth has been shown to correlate with the average oxidation current in slow strain rate tests (SSRT). This may mean that under the less severe stress – strain parameters under which a pipeline operates, compared to the SSRT, a basic principle of crack propagation will be violated. This principle suggests that if crack propagation does not outperform the faradic dissolution rate, the crack tip will eventually degrade into a blunt notch, eventually forming a corrosion pit. It is clear that active corrosion of crack walls in trans-granular cracking of pipelines continues at a slow yet steady pace. The crack tip must propagate more quickly than this dissolution rate. [36,37]

2.5.5 Fast film fracture

To explain the observation that very ductile metals are showing microscopic cracking with distinctive brittle cleavage, Newman and Sieradzki [38] propose that these failures *are "a result of intermittent micro-cleavage events nucleated by a thin surface film".* Although the evidence they provide is based on ductile FCC metals and alloys, this theory has been discussed in terms of BCC materials used to construct line pipe. [27,36,38]

This mechanism was originally demonstrated with brass in sodium nitrate solutions and further evidence of this mechanism was found in the industrially important cracking of austenitic stainless steels in chloride solutions. This mechanism relies on a very thin layer of corrosion product, typically less than 100 nanometers, to form with a high adherence to the underlying base metal. The film must be brittle and be able to be cracked at the strain levels present in the system. Straining will then

cause rapid initiation and propagation of a crack through this surface film, usually at the speed of sound. The energy required to arrest the crack acts in a non-instantaneous manner, allowing the crack to "overshoot" the film, crossing the metal to film interface and propagating into the ductile metal layer onto which the film is adhered. The propagation of the crack into the underlying metal is in itself brittle in nature, and is a function of location, allowing the cracking to proceed either trans-granularly or inter-granularly. The film will then rapidly reform, allowing the process to repeat itself. This film can be composed of either a passivating film formed electrochemically from ionic species in solution or a component of the material itself, such as a de-alloyed layer. On line pipe steels film formation was thought to be a result of a corrosion process forming thin layers of iron chloride ($FeCl_2$), iron oxide (Fe_3O_4) or brittle hydrides.

Hydrogen is also involved in the formation of brittle surface films. Birnbaum [39] describes a mechanism that can be applied to ductile alloys in the presence of hydrogen forming environments. He states that under an applied stress the chemical potential to form a hydride is reduced in areas of tensile concentrations such as a crack tip. Hydrides are characteristically brittle and will lower the value of K_{IC} at which a crack can propagate. The crack then proceeds by brittle cleavage through the hydride and into the interface and is arrested at a point in the underlying ductile material that has a high K_{IC}. The crack is then stopped until a new layer of hydride is formed.

Birnbaum states that this mechanism has a good correlation with empirical data in cases where hydrogen is known to be present in a cracking system. His observations include;

I. *Restricted temperature range.* A high temperature enhances ductile failure before brittle failure. At too low of a temperature, the formation of hydrides and hydrogen diffusion is too slow to effectively propagate a crack.

II. *Increased strain rates.* Ductile fracture processes increase in relation to

increasing strain rate. At a critically high strain rate, the hydride cleavage mechanism is overwhelmed by ductile failure.

III. *The condition of stress.* Hydrides may form without the presence of an applied stress, but it is a stress-stabilized (focused) hydride that can achieve brittle fracture.

IV. *Slowing of crack growth.* As the crack propagates the diffusion of hydrogen becomes rate limiting in the formation of a hydride layer, resulting in reduced cracking velocity.

2.6 Literature survey summary

Research into trans-granular SCC is in many ways in its infancy. Mechanisms have been proposed and supporting evidence has accumulated, but no definitive conclusions exist. Much of the evidence points towards a role of hydrogen in reducing the yield strength of the material.

The need for both stress and a conducive environment to grow cracks has been supported by many researchers. The source of stress may be residual stresses, applied stresses, or a combination of the two. One or the other stresses may be more influential during different periods of the growth cycle of SCC. Applied stresses arise due to the pressure in the pipeline, whereas residual stresses are a result of the manufacturing and fabrication process. Residual stresses can be thought of as being microstresses or macrostresses.

Neutron diffraction will provide a precise method of measuring residual stresses at depth and along the length of a surface. Other methods such as X-ray or hole drilling can also be used to gain confidence in the data generated by neutron diffraction. Neutron diffraction relies on inelastic scattering of a neutron beam by planes of atoms. Bragg's Law can be used to correlate this scattering to the interplanar spacing. Differences between the measured interplanar spacing and the

stress free interplanar spacing results from residual stresses. By measuring this strain in the three coordinate directions, and by applying Hooke's law, an absolute measurement of stress can be found for a volume of material. This stress is an average of the microstresses and is termed pseudo-macrostresses (PM). PM stresses balance to zero over an unconstrained volume. This balance is useful in validating measured data.

To initiate cracks on coupons a loading technique such as cyclic loading or slow strain rate loading can be used. Cyclic loading is more realistic but does not necessarily produce cracking. SSRT is more aggressive and will eventually fail the material but may overwhelm or mask the residual stresses and/or fail the material by a different mechanism than by tSCC.

The literature review supports the need for an investigation between residual stresses and tSCC initiation and early stage growth beyond the empirical observations made by Beavers and Johnson [18]. Neutron diffraction was found to be a useful measurement technique for this investigation. Competing qualities of the SSRT and cyclic loading testing suggest that both of these methods of crack initiation and growth provide useful mechanistic and growth information, and therefore will be suitable for use in the following study. The literature review also suggests that a tSCC growth mechanism involving hydrogen has the greatest support in literature and will therefore form the premise behind the interpretation of results derived from the following study.

3.0 METHODS AND MATERIALS

3.1 Experimental Design Overview

The experimental objective of this project is to;

- Identify the effect of compressive and tensile residual stresses on crack initiation and growth.
- Provide a mechanistic explanation of the relationship between residual stress and tSCC, if observed.

A such, the experimental methodology was designed to quantify the frequency of initiation and growth rate of stress corrosion cracking on tensile specimens containing measured amounts of artificially induced residual stress on the specimen surface and through the specimen depth. Two types of crack initiation and growth experiments were performed. A four month controlled cyclic loading test was performed to allow more time for growth under a loading regime similar to that found on operating pipelines. The risk in cyclic load tests is a decreased probability of the timely initiation of cracks due to the milder loading. Modified slow strain rate experiments were performed to increase the probability of success of crack initiation resulting from the aggressive energy input into the tensile specimens. The disadvantage of SSRT is a likelihood of ductile failure rather than brittle cracking, as well as a short time period for testing (12 days), thereby limiting the environmental crack growth aspect of tSCC. The use of both tests was deemed necessary to increase the probability of delivering usable results. Table 1 provides an overview of the testing method.

3.2 Material selection

Test material for the experimental program originated from a single, undamaged, section of 1066.8 mm (42 inch) diameter, high pressure, natural gas pipeline removed from service after a nearby tSCC rupture. The pipeline had been in –

service for approximately 19 years before the failure occurred. The wall thickness of this section of pipeline is 9.88 mm while the pipe grade is 448 MPa (65 ksi). The pipeline operates at an average pressure of 6600 kPa (957 psi). A stress - strain curve for the as received material was obtained and the actual yield strength was found to be 480 MPa while the ultimate strength was 607 MPa (Figure 1). The microstructure of this material is ferrite and pearlite with an average grain size being 6 μm – 10 μm. The material was found to have a low carbon composition (Table 2). The pipeline steel was deemed to be susceptible to trans-granular stress corrosion cracking due to the particular environment in which the pipeline operated, the loosely adhered polyethylene tape coating on the pipe surface and the above mentioned in-service tSCC failure.

3.3 Fabrication of test specimen and test apparatus

3.3.1 Residual stress plates and tensile specimens

The experimental design necessitated a test specimen with a large and uniform residual stress gradient in both the longitudinal and through thickness directions of the test specimen. The large residual stress gradient was necessary in order to differentiate cracking on the basis of residual stress levels alone. To provide these stress gradients, one-piece plates of steel were machined from the pipeline in a "roof" like shape that maximized plate thickness (Figure 2a). Four steel plates were removed from the pipeline diameter, two of which had an angle of 165.6 degrees and two of which were 171.0 degrees (Table 4). The plates had a thickness of 6 mm and total length of 128 mm (Figure 2b). The test plates were then subjected to three point bending until a center axis of the plate was straight when no force was applied (Figure 3). The load necessary to accomplish the three point bending was measured versus the displacement (Figure 4). The plate was then machine ground to remove the peak and valleys formed from the deformation process, resulting in a flat plate. One surface would be expected to have tensile residual stresses, while the opposing surface would have compressive residual stresses (Figure 5).

The position of the final 3.4 mm steel plate from within the original steel plate can be approximated by subtracting the measured amounts of material removed from the bottom and top surfaces (Figure 6). Finally, tensile specimens with dimensions of 32 mm in gauge length, 3.4 mm in thickness and 7 mm in width were cut from the steel plates using electrical discharge machining (EDM) (Appendix A). EDM has an advantage over regular machining in dimensional accuracy as well as the ability to machine without introducing significant heat into the coupon. As such, the three tensile specimens removed from each plate were dimensionally exact copies of each other. The tensile specimens were removed from the residual stress plates in such a manner that the maximum residual stress on the specimen would be expected at the centerline of the gauge length while decreasing to the gauge length shoulders (Figure 7).

Each tensile specimen was stamped to identify its origin as well as the orientation of the specimen from within the original plate. The first number in the two digit label indicated the plate from which the tensile specimen originated. The second number differentiated tensile specimen originating from the equivalent plate (Table 4).

The tensile specimens were polished to a 400 grit finish before residual stress measurements were made. After completion of the measurements and prior to testing, a mirror finish polish was applied to both specimen surfaces.

3.3.2 Environmental chamber design

Both the cyclic loading experiment and modified slow strain rate experiment were performed in an environmental chamber. The function of the environmental chamber was to immerse the tensile specimen in an electrolyte during testing while excluding oxygen (Figure 8). The chamber was constructed of plexiglass with a solution volume of 700 milliliters. A port was constructed to accommodate a counter-electrode in the case where applied cathodic protection was necessary (Appendix B). Two additional ports were constructed to allow for the purging of the solution with a gas, in this case a 5% carbon dioxide and 95% nitrogen gas mixture. The

chamber was completely sealed by the use of rubber O-rings onto specially designed cylindrical grips that attached to the load frame (Appendix C).

The solution used in all cracking experiments was composed of a synthetic electrolyte similar in composition to field electrolyte extracted from beneath areas of loosely adhered coating where tSCC was found to be present (Table 3).

3.4 Pre-conditioned tensile specimen

A single residual tensile specimen (32) was selected for cyclic pre-conditioning. Pre-conditioning consisted of applying a cyclic load to the tensile specimen in air on a load frame. The cyclic loading pattern consisted of a series of cycles with different R-ratio's (Figure 9) that was repeated approximately 267 times. This subjected the tensile specimen to 6667 cycles at a R-ratio of 0.9, 800 cycles at a R-ratio of 0.8 and 533 cycles at a R-ratio of 0.5.

The maximum stress for all applied cycles was 90% of the SMYS. A constant strain rate of 5×10^{-5} / second was used. The load pattern was derived as a simplification of actual pipeline operation and was meant to represent approximately 15 years of service.

The pre-conditioning was intended to moderate the residual stress on the tensile specimen in a similar manner that would be experienced by an operating pipeline. By measuring the stresses in identical pre-conditioned and unconditioned tensile specimens, the effect on residual stress of the moderate pressure cycles occurring on pipelines could be quantified.

3.5 Neutron diffraction analysis of tensile specimens at Chalk River Laboratories

The tensile specimens were brought to the Chalk River Laboratory at Chalk River, Ontario for residual stress measurements by neutron diffraction. The Neutron

Program for Materials Research at Chalk River is operated by the Steacie Institute of Molecular Science of Ottawa, Ontario, Canada and is supported by the National Research Council (NRC) of Canada. Non-proprietary University research can be performed collaboratively at this facility with financial support being derived from the NRC.

Time constraints limited the use of this expensive facility to residual stress measurements on a single tensile specimen from each of the four residual stress plates. As a result of the precise electrical discharge machining method used to create the tensile specimens, as well as the uniformity of the residual stress plates from which the tensile specimens were cut, the measured tensile specimen obtained from each residual stress plate was thought to be an adequate representation of the remaining two tensile specimens cut from the same plate. Additionally, the pre-conditioned specimen was also measured. A total of five tensile specimens were measured.

Residual stress measurements were performed on the E-4 neutron spectrometer, also known as the Brockhouse spectrometer. This spectrometer was the original device developed by B.N. Brockhouse, the Nobel Prize Laureate who pioneered this technique (Figure 10).

A jig was designed and built to support the tensile specimen and provide the correct mounts for the 2-coordinate table upon which the tensile specimen is mounted (Figure 11, Appendix D). A small load of approximately 0.2 kiloNewtons was applied by the jig which equated to a maximum of 8 MPa of applied stress on the tensile specimen during measurement. This was deemed necessary in order to keep the specimen flat for ease of measurement alignment in the spectrometer.

The E4 neutron spectrometer is composed of four components; the nuclear reactor source, the monochromator, the robotic specimen table and the neutron detector. The nuclear reactor provides a high flux source of neutrons of many different wavelengths, which pass through a port in the reactor wall and arrive at the

monochromator. The monochromator is a single crystal of germanium, which can be orientated to select a 1 to 3 Angstrom wavelength of neutrons and direct this neutron flow as an incident beam onto the specimen. As most metals, including steel, do not block the neutron path, the beam can be focused to measure at any point in the body or surface of the specimen. Finally, the detector, composed of a thin filament grid of wires, measures the angle of the deflected neutron beam.

The tensile specimen was oriented in relation to the incident beam to diffract this beam according to the selected plane, in this case the (110) plane (Figure 12). The detector measures the diffracted beam including the small deviations from the theoretical diffraction angle. A Gaussian curve of measured neutron "counts" is collected, where the magnitude of the counts is measured against the diffraction angle (Figure 13). The diffraction angle at the maximum magnitude was then used with Braggs Law (Equation 1) to calculate the interplanar spacing between adjacent layers of iron atoms (Figure 12). This spacing is a direct indication of strain between the adjacent layers when compared to the theoretical spacing for the body cubic centered iron lattice composing this material (Figure 12). When the specimen is oriented and measured in all three spatial directions, the strain in each direction was quantified. With these three values of strain, the axial residual stress was calculated by use of Hooke's law (Equation 4).

The measured Gaussian curve of neutron counts reflects the statistical nature of the detected diffracted neutrons. A unit volume containing thousands of grains are measured rather than a single grain (Figure 14). Only a fraction of the grains in the measured unit volume will align with the beam to produce a (110) diffraction pattern. As well the diffracted crystals will have a distribution of interplanar spacing, resulting in a range of measured angles. The unit volume measured for these tensile specimens was 1 mm^3. The symmetry of the unit volume can be altered by changing the slit dimensions of the incident beam. In this case, the depth direction was minimized to be 0.7 mm, while the surface width was the maximum length direction for the measured unit volume. As a result, for these tensile specimens measuring approximately 3.4 mm in thickness, five depth measurements were

adequate to quantify the residual stress in the depth direction from the front surface to the back surface of the tensile specimen. The five depth measurements were performed at seven equally spaced points along the gauge length, in increments of 5 mm, for a total gauge length measurement of 30 mm.

Each strain measurement of a unit volume of material was made in three spatial directions in order to derive the gauge length stress. This multi-spatial measuring resulted in a total of one hundred and five strain measurements per tensile specimen, with each measurement needing approximately twenty minutes to accumulate the necessary number of neutron counts to produce a statistically valid Gaussian curve. As a result of the high degree of automation of the spectrometer in moving and aligning the specimen, the measurements can be made almost continuously. Thirty to forty hours was required to measure stress at thirty-five locations on each tensile specimen.

The final output from the residual stress measurements is a residual stress versus location plot for each group of identical tensile specimens. The location parameter indicates the midpoint of the unit volume measured. The stress value indicates the increase or decrease in longitudinal stress (the gauge length direction), when compared to a stress free specimen.

3.6 Cyclic loading test for tSCC

Four environmental cells were placed in series in an Enduratec pneumatic load frame, with each cell containing a single tensile specimen (Figure 15). The chambers were purged with gas containing five percent carbon dioxide with the balance being nitrogen. A de-aerated electrolyte was then introduced into the cell. The cells were purged with the above gas for the duration of the test. No cathodic current was applied to the tensile specimens. A cyclic load pattern was applied during testing (Figure 16). The maximum applied stress was 448 MPa or 100% of SMYS while the minimum applied stress was 354 MPa or 80% of SMYS. This stress cycle produced a R-ratio of 0.8. The test duration was 2631 hours, or approximately

four months in which 517 cycles were applied. The loading rate was 3.4×10^{-8} / second while the unloading rate was a magnitude faster than the loading rate at -4.7×10^{-7} / second. At the maximum applied load, a static hold time of two hours was applied. At the end of the test the specimens were dried and inspected optically on the surface for signs of cracking or pitting. Further cross-sectional examination was performed to detect cracks hidden by corrosion.

3.7 Modified slow strain rate testing for tSCC

Modified slow strain rate tests were performed on six tensile specimens. Tensile specimens were placed in the identical environmental cells and load frame as in the cyclic loading tests. A modification in the traditional slow strain rate tests was made by not surpassing the ultimate tensile strength of the material during the length of the test, thereby preventing failure. Instead of progressing to failure, the coupon was cycled between the ultimate material strength and the specified minimum yield strength of the material (Figure 17). The strain was applied at 2.1×10^{-8} /second, with the total test duration equal to twelve days. The purpose of modifying the traditional slow strain rate test was to extend the test length so that the environment had sufficient time to act on the propagating crack. By not exceeding the ultimate tensile strength of the specimen, uniform plastic deformation was maintained across the gauge length and localized plastic deformation (necking) was avoided. Due to the short duration of the test minimal corrosion was expected to occur. Post-test inspection was performed by cross-sectioning and metallurgical examination.

3.8 Metallurgical examination for SCC

Examination for cracking was performed by cross-sectioning the tensile specimen down the gauge length and consecutively grinding, polishing and inspecting each half of the tensile specimen from the inner depth face to outer depth face in increments of 0.5 mm. Each increment was polished to a 6 μm finish and etched with Nital (5% nitric acid, balance ethanol) for 45 seconds to resolve grain boundaries. The surfaces were inspected by digital optical microscopy or scanning

electron microscopy in the case where the cracks were very small. The deepest point of the crack was recorded and the location on the tensile specimen was measured relative to the gauge centerline. A tabulation of tensile specimens and the procedure or testing performed on the tensile specimen is provided (Table 4).

4.0 RESULTS

4.1 Residual Stress Analysis of Test Specimens

Strain in three dimensions was measured by neutron diffraction on tensile specimens 13, 21, 32, 33 and 41 (Table 4). The residual stress in the axial direction was calculated and plotted versus both distance along the gauge length and the depth direction (Figures 18 to 22). The axial direction is equivalent to the gauge length direction of the tensile specimen and is also equivalent to the hoop direction of the original pipeline material from which the residual plates and ultimately the tensile specimens were derived.

The data points plotted in figures 18 to 22 provide the residual stress measurement center point in the gauge length direction and in the depth direction of the 1 mm^3 volume of measured material, or "strain pixel." In the depth direction, the measured volume extends 0.35 mm on each side of the center point. For example, at a measured depth of 0.4 mm the measured volume extends in depth from 0.05 mm (surface) to 0.75 mm. Similarly, the center point along the gauge length represents a length extending 0.5 mm on each side of the indicated distance. Finally, the measured width of the strain pixel was 1.43 mm, which was centered in the middle of the 7 mm gauge width. The width direction was assumed to have a relatively uniform residual stress profile. Each line in these figures (Figure 18-22) represents a particular depth from the original surface while each data point on a single line represents a measurement along the gauge length. The line itself is interpolated between points. As the residual stress measurements were made using a specimen holding jig that applied only a small stress, the measured stresses are mainly a result of residual stresses.

Both tensile specimen 32 (Figure 20) and 33 (Figure 21) were measured for residual stress levels by neutron diffraction despite being cut from the same plate. This duplicate measurement allowed for the effect of the pre-conditioning in air, which was performed on tensile specimen 32, to be evaluated. The effect of pre-conditioning on tensile specimen 32 (Figure 20) was an overall reduction in peak

residual stress when compared to the unconditioned tensile specimen 33 (Figure 21). The maximum reduction was approximately 50% for the large residual stresses in the 300 MPa range. Residual stresses less than 50 MPa were not greatly affected by pre-conditioning.

Utilizing data from tensile specimen 21 allowed a three-dimensional plot of the absolute axial strain to be plotted (Figure 23). This figure provides a visual illustration of the deformation in the tensile specimen as a result of the bending, flattening and machining process of the original plate. Noticeable in this figure is the presence of a zero strain area in the tensile specimen at a depth of 2.4 mm – 2.7 mm. This measured zero strain axis corresponds well to the original proposed zero strain axis of 3.0 mm found at the center of the plastically deformed 6 mm plate. This axis equates to 2.4 mm when measured from the tensile specimen surface (Figure 6).

4.2 Cyclic loading experiments

The four-month cyclic loading experiments exhibited some corrosion on the four tensile specimens in this test despite best efforts to exclude oxygen with a continuously applied purge gas. The corrosion damage was in the form of micro-pitting, with little evidence of general corrosion. As the compressive residual stress surface and edges of the tensile specimens were sealed with a coating, only the tension side was pitted. To evaluate where anodic dissolution occurs with respect to residual stress levels, the location of the pitting was measured and related to the previously measured level of surface residual stress (Table 7, Figure 24). In this figure, maximum pitting occurred at approximately 250 MPa while relatively little pitting occurred below 150 MPa. Only a few pits were located in areas where compressive residual stresses were measured.

Initially no cracking was detected on the surface of the tensile specimen when inspected by both optical microscopy and dye penetrant. This lack of crack detection was likely due to the pitting that occurred on the surface, which created a large amount of background fluorescence, obscuring the cracks. Further inspection by

initial random cross-sectioning and later more systematic cross-sectioning revealed a total of 19 relatively deep cracks ranging from 0.14 mm to 0.82 mm in depth (Figures 25 – 41). All these cracks originated at the bottom of corrosion pits, contributing to the difficulty in surface detection. The common feature of these cracks is the corrosion damage occurring along the walls of the crack as well as at the tip, effectively blunting the cracks. As a result of this corrosion damage it was not possible to visualize the trans-granular nature of crack growth. As well, any surface microstructure differences at the crack initiation point were obliterated by the corrosion damage. The location of these cracks relative to the measured residual stress was tabulated and graphically illustrated (Table 7, Figure 42).

4.3 Modified slow strain rate experiments

A total of six tensile specimens were subject to individual twelve day modified slow strain rate tests. Some pitting occurred on the surface, although these pits were approximately an order of magnitude shallower than those cracks detected on tensile specimens from the cyclic loading experiments. A total of 10 cracks were detected on the six tensile specimens. These cracks were also an order of magnitude shallower than those detected in the cyclic loading experiment. These cracks ranged from 8.0 μm to 293 μm in depth, with the average crack depth being approximately 35 μm. Aside from the shorter length, the SSRT induced cracks distinguished themselves from the cyclic load induced cracks by their sharper crack tips and minimal wall damage by corrosion (Figures 43-46). The deepest crack, 293 μm, was found as a single crack on the pre-conditioned tensile specimen and was approximately five times longer than the second deepest crack.

Only the edges of these tensile specimens were coated and sealed. Despite both surfaces being exposed to electrolyte, all cracks originated on the surface of the coupon containing tensile residual stresses.

Visual differences existed between surface areas with compressive residual stresses and tensile residual stresses. Surface areas with tensile residual stresses

were darker and exhibited a striated appearance. Conversely, surface areas with compressive residual stresses were covered with a lighter, more uniform deposit (Figure 47).

The crack location relative to the gauge length and the crack depth was tabulated along with the corresponding surface residual stress measurement (Table 7). Residual stress levels are compared to the frequency of cracking in a histogram (Figure 48).

A third histogram is presented which plots the frequency of crack initiation with the level of residual stress from both the SSRT and cyclic load experiment (Figure 49). In this figure, the number of initiation points is normalized for the area of the tensile specimen at a particular residual stress level. Normalization removed the influence of the variable area of different residual stress levels on the tensile specimen surface.

To determine the relationship between the incidence of cracking and the change in residual stress, the change in residual stress at each cracking location was calculated based on the slope of the line depicting the measured surface residual stress. As well, the maximum rate of surface residual stress change between data points was also determined for each tensile specimen (Table 8). The rate of change of residual stress for each crack was then expressed as a percentage of the maximum rate of residual stress change observed for the corresponding tensile specimen and plotted as a histogram (Figure 50). This histogram provides the frequency at which the combined 29 cracks initiate in relation to the maximum residual stress changes occurring along the gauge length surface.

The combined residual stress and applied stress was calculated on data from tensile specimen 13 at each depth through the center point (0 mm) of the gauge length direction (Figure 51). The maximum and minimum levels of stress depicted in this figure were derived by adding the appropriate level of residual stress for a particular depth to the maximum and minimum applied stress created by the cyclic

load pattern used for testing. This calculation allowed the determination of the crack stress intensity for a theoretical crack propagating through the tensile specimen at this location. The crack stress intensity on the second y-axis versus depth is also shown (Figure 51). This figure illustrates that a crack would initially encounter a stress intensity of approximately 10 $MPa\sqrt{m}$ at a point just below the surface and this would increase to a maximum of 30 $MPa\sqrt{m}$ at a depth of 0.5 mm for the crack depths measured in this test. After this depth, compressive residual stresses prevent the stress intensity from increasing further until a depth of 1.5 mm is reached.

The difference between the maximum crack stress intensity and the minimum crack stress intensity can be expressed as a change in stress intensity or ΔK. The value of ΔK is often associated with the fatigue growth of a crack. Fatigue growth of a crack usually occurs with the higher levels of ΔK found with cracks considerably deeper than those created in these tests. An illustration showing the magnitude of ΔK that the cracks in this test could experience is presented (Figure 52). In this figure the depth versus ΔK is shown where the value of ΔK was calculated from the data provided in the previous figure (Figure 51).

5.0 DISCUSSION

5.1 Stress analysis of tensile specimens.

Residual stresses on the tensile specimens were relatively large, ranging from a minimum of -280 MPa to a maximum of 300 MPa (Figures 18-22). The maximum residual stress was found to be 67% of SMYS, inferring only elastic stress was present. In all but one series of tensile specimens a compressive and tensile surface were present as originally predicted (Figure 5).

The variation of residual stress profiles between different tensile specimens is large. This variation is not surprising considering that substantial amounts of material was removed from the original plates after bending in order to make them flat. The machined flat plate had more material removed from the bottom surface than from the top surface, and this varied slightly between plates (Figure 6). As a result, it would be difficult to accurately predict the final stress condition of the new surfaces without measuring this stress.

The effect of the pre-conditioning on the tensile specimen was a reduction in the maximum residual stress from an original range of 580 MPa (Figure 21) to a lesser range of 340 MPa (Figure 20). As well the original stresses were re-distributed to a small degree along the gauge length. There was a decreasing effect of pre-conditioning on areas with less residual stress. Generally, below 50 MPa, little reduction in residual stress resulted from the pre-conditioning.

The plastic deformation and machining used to create the tensile specimen yielded sufficient residual stress gradients in both the gauge length and depth direction. The extent of plastic deformation is visible when the absolute percent strain in the gauge length is plotted in three dimensions (Figure 23). In this figure, the neutral axis is visible at approximately 2.5 mm to 2.7 mm from the tensile specimen surface. This measured neutral axis closely aligns with the original predicted neutral axis located at 3.0 mm from the surface of the deformed plate from which the tensile specimens

were machined (Figure 6). The alignment between the original predicted neutral axis and the measured neutral axis provides a degree of confidence in the neutron diffraction measurement technique. The increase strain towards the center of the gauge length and towards the outer surfaces was also predicted and is distinguishable in this figure.

The minimum observed change in stress across the entire gauge length surface was 70 MPa while the maximum observed surface change in stress was 300 MPa. The residual stress gradients present dominate other possible small differences in material properties or mechanical properties present on these uniformly machined and mirror polished tensile specimens. As such, it is likely that initiation locations of cracks are predominately influenced by the level of residual stress.

5.2 Occurrence of corrosion

A lack of cathodic protection or active oxygen scavenging during the four month cyclic loading tests allowed for extensive pitting to occur on the face of the residual stress tensile specimens. The pitting occurred despite attempts to limit oxygen at the specimen surface by constant purging of the sealed environmental chamber with an oxygen free gas.

The observed pitting was not random and occurred in clusters on the surface whereas other surface areas remained completely non-corroded. It was evident that galvanic action had occurred over substantial distances of the coupon face (Figure 47). The opposing compressive surface and sides of the tensile specimen had been sealed with an insulating coating and therefore did not participate in the galvanic couple.

To determine if the frequency of corrosion pitting was influenced by surface residual stress differences, approximately 70 corrosion pits were located and compared to the measured residual stress level for that location (Table 7, Figure 24, 47). Although the occurrence of pitting was not normalized for the exposed surface area

at a particular stress range, the majority of the tensile specimen residual stress surface area fell between 100 MPa to 200 MPa, especially since the compressive surface was masked. A peak in corrosion pitting at 250 MPa suggests that areas of high tensile residual stress are anodic with respect to areas with lower residual stress levels. The steep fall of the curve from 250MPa to 100 MPa suggests strong galvanic coupling arises with surface stress differences greater than 100 MPa to 150 MPa. A difference of 100 MPa to 150 MPa is typical of what has been observed on operating pipelines where the average residual stress at a tSCC colony was measured to be 216 MPa compared to 108 MPa in non-SCC areas. [18].

5.3 Residual stress versus crack initiation

5.3.1 Crack initiation under cyclic loading conditions

In the cyclic loading experiment, performed on four tensile specimens, nineteen cracks were found and examined (Table 7, Figures 25–41). As the compressive residual stress surface and the edges of these four tensile specimens were coated, the cracks were all found on the surface containing tensile residual stresses. The cracks were initially not detected on the surface of the specimen due to the pitting and general corrosion that had occurred. After revisiting and cross-sectioning these tensile specimens a few months after the completion of the test, the cracks were detected. Despite limiting oxygen ingress, the cracks all exhibited extensive corrosion of the crack walls and crack tip. It is unknown whether the corroding of the crack occurred during the four month long exposure in the test solution, from residual solution trapped in the crack during storage in a dessicator after the test, or during both periods. As some pitting occurred during the much shorter SSRT, and the tensile specimens were stored in a dessicator, it is likely that the corrosion of the cracks in the four month long cyclic loading test also occurred during the test.

As a result of the dissolution of the crack wall, crack tip and the crack mouth, it was not possible to determine if the crack propagated trans-granularly. As well, any surface inclusions or variant microstructure were obliterated by the corrosion pit and

therefore difficult to detect.

The calculated cracking velocity based on an average crack size of 530 μm is 5.6×10^{-8} mm/second. The blunting of the crack tip by corrosion likely affected the cracking velocity. To prevent this corrosion, active oxygen scavenging by a small cathodic current, or perhaps sacrificial steel in solution would be necessary. The cathodic current would need to be of sufficient magnitude to prevent rapid anodic dissolution and corrosion of the crack while still allowing for micro-pitting of the surface.

When crack initiation location is compared to the level of residual stress at this location, the maximum frequency of crack occurrences was found at 151 MPa to 200 MPa with smaller peaks at the next highest residual stress range (200 MPa to 250 MPa) and next lowest range (100 MPa to 150 MPa) (Figure 42). A minor amount of cracking was found in the range of 1 MPa to 50 MPa and no cracking occurred on surface areas with compressive residual stresses. This observation supports a preference for cracking to occur at higher levels of residual stress when these stresses are available.

5.3.2 Crack initiation under SSRT conditions

The SSRT micro-cracks initiated and grew to depths between 8.0 μm and 72 μm while remaining relatively corrosion free, except near the crack mouth. In this case, the trans-granular nature was evident due to the sharper nature of the cracks. The cracking velocity, based on an average 35.1 μm crack depth, was 3.4×10^{-8} mm / second. The pre-conditioned tensile specimen was an exception in that a single crack formed and grew to a depth of 293 μm, approximately 5 times greater than that of the next largest crack detected in the SSRT experiments (Figure 43). The growth rate for this single, deeper crack was 2.8×10^{-7} mm/second. This single crack initiated in a small tensile residual stress region near the shoulder of the gauge length. The remaining crack free surface and the opposing crack free specimen face were measured to have compressive residual stresses (Figure 20).

One possible explanation for the substantially longer crack in a pre-conditioned specimen may be that the crack initiated during pre-conditioning in air as a fatigue crack. Although the pre-conditioning was well below the normal fatigue limit for this material, no initial accounting was taken for the additional residual stresses in the fatigue calculation. As a result of the combined tensile and residual stress, small areas of plastic deformation or persistent slipbands may have occurred, thereby lowering the fatigue threshold at specific locations.

Although the large crack in the pre-conditioned tensile specimen was surprising, it was not surprising that the identical tensile specimen 33, which was not pre-conditioned, was the only tensile specimen in which no cracks initiated. In reviewing the residual stress measured on the surface of both specimen 32 and 33 (Figures 21,22) it was found that all the surface area of both tensile specimens were composed of almost completely compressive residual stresses. Similar to the pre-conditioned tensile specimen 32, one small area near the gauge length shoulder of tensile specimen 33 had tensile residual stresses. The lack of any crack initiation in a specimen that has surfaces predominately in compression suggests that a compressive surface area inhibits cracking.

Nine cracks initiated in the remaining four tensile specimens tested under SSRT conditions (Table 7, Figures 44-46). The tensile specimens in these tests had both a surface with predominately tensile residual stresses and a surface with predominately compressive residual surfaces. In all cases the cracks initiated on the surface with larger tensile residual stress. All cracks initiated in the bottom of a micro-pit that was only visible under a microscope. Many micro-pits had no cracks, suggesting the pits formed prior to the cracks. In the SSRT only the tensile specimen edges were coated, the opposing gauge surfaces were left with a mirror finish. The tensile specimen surface under compressive residual stress had far fewer pits than the surface experiencing tensile residual stresses (Figure 47). As well, surface areas with compressive residual stresses generally had a uniform, light carbonate appearance while surface areas with tensile residual stresses were darker and striated in appearance. EDX analysis suggests that the lighter deposits

had a higher concentration of calcium, likely calcium carbonate. Calcium carbonate forms in the presence of cathodic potentials. This observation suggests that surface areas with compressive residual stress levels were cathodic with respect to those surface areas containing tensile residual stress levels. The possible anodic and cathodic interactions between opposing surfaces pre-disposes the tensile surface to pitting with the resultant stress intensification and an increased probability of cracking.

The cracks were located with respect to the mapped residual surface stress and compared as a frequency of cracking versus residual stress (Figure 48). Although only 10 cracks were found, eight of these initiated in stress ranges of 150 MPa to 200 MPa, while the remaining two initiated at stress levels between 100 MPa to 150 MPa. As in the testing under cyclic loading conditions, the observed residual stress cracking range found in the SSRT supports the preference for cracking at elevated residual levels.

The relationship between the change in residual stress versus distance along the gauge length $\left(d\sigma/dx\right)$ and cracking frequency was determined. This value was determined from the absolute value of the slope of the interpolated line between two consecutive surface residual stress data points at the location of each crack. This value was compared to the maximum slope $\left(d\sigma_{max}/dx\right)$ of the surface stress change for each corresponding tensile specimen (Table 8). The resulting frequency histogram indicates that cracking did not initiate at the point of greatest change in residual stress levels when determined using this method (Figure 50). Rather, the majority of cracks initiated at $d\sigma/dx$ values less than 50% of $d\sigma_{max}/dx$. It was stated previously that cracks were typically associated with corrosion micro-pits and that these micro-pits occurred at areas of high residual stress thought to be anodic with respect to areas of lower or compressive residual stress. This earlier statement is not supported by the relationship of $d\sigma/dx$ for a crack versus $d\sigma_{max}/dx$ for each tensile specimen as illustrated in the above histogram. This may indicate that the

anodic and cathodic interactions that may occur between areas of high and low residual stress levels is below the 5 mm resolution of the measured residual stress data points. Alternately, interactions between high and low residual stress areas may occur over a much greater area than resolved in the calculation of $d\sigma/dx$. The long range interactions are likely, as definitive differences in surface deposits were found between the two well separated surfaces of the tensile specimens in the SSRT. These differences are likely a result of the surface with tensile residual stresses being anodic with respect to the surface having a majority of compressive residual stresses. The micro interactions are also likely, as local areas of plastic deformation can occur on the grain or phase size. A combination of these galvanic actions makes the relationship of cracking frequency with change in residual stress difficult to quantify.

5.4 Crack growth

No cracks grew in depth past 0.7 mm in the SSRT. Only a few cracks grew marginally past 0.7 mm in depth in the cyclic loading experiment. The depth of 0.7 mm is significant in that the volume from 0 mm (surface) to 0.7 mm is encompassed in the first gauge volume of material measured by neutron diffraction for residual stress levels. As such, little can be said about the effect of changing residual stresses on cracking velocity until the crack propagates past 0.7 mm and into a new gauge volume.

A calculation for the total stress that a hypothetical crack would encounter as it progresses through the specimen was attempted (Figure 51). This calculation was based on the summation of the applied stress and the changing axial residual stress found at the various depths though the tensile specimen in the direction of crack propagation. The calculation for total stress was made based on the superposition principle, which states that separate components of stress, strain, displacement and stress intensity can be summed, as long as they act in the same direction and are in the linear elastic region. The axial residual stress depth profile used in this calculation was derived from the residual stresses measured for tensile specimen

13 at the center of the gauge section. This tensile specimen contained the highest levels of measured residual stress. The remaining three tensile specimens used in the cyclic loading experiment typically did not have total stress levels that exceeded the material yield strength and never did the total stress exceed the ultimate strength. For a total stress determined to be greater than the yield strength of the material, a more complex finite element method of determining the total stress would be necessary, but this calculation is beyond the scope of this project. Similarly, the stress intensity can be calculated, in the linear elastic region, using the combined stresses and the crack depth for a theoretical crack by use of the stress intensity equation below (Figure 51).

$$K_I = \sigma_t \bullet \sqrt{\frac{\pi a}{Q}} \bullet F(a/w) \qquad \text{Equation 11}$$

Where

σ_t = hoop stress of the pipe
a = crack depth
2c = crack surface length
w = pipe wall thickness
Q = elliptical crack shape correction factor
F (a/w) = geometry correction factor for a particular crack depth. (back surface correction factor)

The solution for the geometry correction factor (F(a/w)) originated from the Wang & Lambert weight function method for long shallow cracks, specifically tSCC cracks similar to those found in this testing. [3]. In the calculation for stress intensity, an aspect ratio of eight times the surface length over depth was used to represent the long shallow nature of the cracks observed in the cyclic loading experiment. The stress history for the cyclic loading pattern was used to calculate the maximum and minimum applied stress for this calculation.

The stress profile (Figure 51) indicates that an initiated crack would experience high levels of total stress for the first 0.5 mm in depth. The actual values for stress in the first 0.5 mm of depth are shown to be above the yield strength of the material and

are therefore not plausible due to the onset of plasticity. Without a more complex analysis, it would be expected that in this high tensile residual stress area local yielding between grains or weaker phases may occur and some residual stress relaxation would occur in the first few cycles due to local plastic deformation. Generally a high stress would likely remain. Areas of local yielding at the surface will have a strained structure that could possibly expose fresh metal to the aqueous environment. It is these areas of local surface yielding that are theorized to be susceptible to anodic dissolution that then can form corrosion pits leading to stress intensification and crack initiation.

Total stress was predicted to drop rapidly at a depth of 0.5 mm to 1.5 mm. This drop in stress equates to a period in which the crack stress intensity remains static at approximately 30 MPa$\sqrt{m}$ or decreases slightly. The static crack stress intensity is a result of a decreasing applied stress balancing the increasing crack depth as described in equation 11. It was interesting to observe that all the cracks formed in the cyclic loading experiment had experienced blunting and a cessation of brittle crack growth in this depth range where crack stress intensity decreased or remained static.

Crack tip blunting by corrosion, as experienced by the cracks in the cyclic load experiment, occurs when cracking velocity falls below the anodic dissolution rate of the crack tip. Therefore blunting by corrosion may indicate an initial high cracking velocity necessary to form the crack, followed by a slowing cracking velocity and final dormancy, assuming the anodic dissolution rate remains constant or decreases. As all the cracks experienced initial residual stress levels of 100 MPa to 200 MPa and the equivalent applied stress, the high cracking velocity of these cracks occurred where there was a rapid rise in stress intensity as observed in the first 0.5 mm of depth, equating to a rate of change of approximately 40 MPa$\sqrt{m}$ per millimeter of depth (Figure 51). As well a crack stress intensity value of 10 MPa$\sqrt{m}$ was obtained just below the surface of the tensile specimen, which is relatively large for a recently initiated crack and is likely sufficient to keep the crack open.

Increasing crack stress intensity creates a number of conditions for a propagating crack. Firstly, the crack tip opening displacement (CTOD) is directly proportional to crack tip stress intensity. It would be expected that a crack would be continuously widening in an increasing crack stress intensity condition. A continuously widening crack would prevent the wedging of the crack by anodic corrosion products, which are known to form during tSCC growth. Wedging of the crack reduces crack closure thus reducing the effective stress range. As cracks typically propagate only under cyclic stress conditions, a reduction in the stress amplitude could reduce cracking velocity. Secondly, a widening crack would allow for increased volume for the diffusion of ions necessary for the environmental growth of the crack. Finally, the plastic zone ahead of the crack tip would be increasing, increasing the probability of successfully competing with other voids as well as the trailing deformed material along the crack wall for hydrogen in the steel. As such, it can be theorized that increasing crack stress intensity, above a threshold level necessary to keep a crack in an open state, is a necessary condition to keep the cracking velocity greater the anodic dissolution rate.

Conversely, a crack which is not continually widening due to a static or decreasing crack stress intensity may have a slowing cracking velocity due to a combination of diffusion limitations, stress relief caused by wedging of the crack with anodic products and a constant plastic zone size containing constant levels of hydrogen.

The effect of a compressive residual stress field is to decrease the crack stress intensity. The compressive field encountered between the depths of 0.5 mm and 1.5 mm on a tensile specimen in the cyclic loading test likely resulted in crack blunting and crack dormancy for these cracks by the above mechanism.

The above observations and theory provide a plausible explanation as to why the vast majority of tSCC located on operating pipelines are dormant cracks that have penetrated less than 10% into the wall thickness, or less than 1 mm in depth. This is especially probable in areas where surface tensile residual stresses are known to exist, such as the base of welds where tSCC commonly occurs.

At a depth of 1.5 mm, total stress again rises rapidly until a depth of 2 mm due to increasing tensile residual stresses equating to a rapid rise in crack stress intensity, peaking at 70 MPa$\sqrt{m}$. None of the measured cracks penetrated into this region, therefore it was not possible to determine if the rapidly rising crack stress intensity increased cracking velocity.

Another possible influence in crack growth is the change in crack stress intensity (ΔK). ΔK is calculated by substituting $\Delta\sigma$ for σ in equation 11 where $\Delta\sigma$ is the difference between the maximum and minimum total stress for each cycle. Fatigue growth of cracks is related to ΔK by use of the Paris equation with the general form of;

$$\frac{da}{dn} = C\Delta K^m \qquad \text{Equation 12}$$

where $\frac{da}{dn}$ is the growth of the crack per applied cycle, C and m are dimensionless, empirically derived constants for a particular material and stress conditions. Although the Paris equation does not account for mean stress, it is generally applicable for a constant mean stress in the linear elastic region.

Fatigue growth can be expected to begin influencing crack growth when the value of ΔK increases into the range of 10 MPa$\sqrt{m}$ to 20 MPa$\sqrt{m}$. The value of ΔK was found to increase with depth for an average tensile specimen (Figure 52). This occurs as a result of the increase in crack length. Crack length affects the value of K in a non-linear fashion due to the square root function applied to crack length (a) in equation 11. The applied cyclic load is constant and the additional amount of residual stress is added equally to the minimum and maximum applied stress, thereby negating this addition when the difference is calculated. Therefore, for the equivalent stress amplitude ($\Delta\sigma$), the value of ΔK increases in proportion to increasing crack length.

The value of ΔK is small for even the deepest cracks measured in this experiment, typically below a maximum of 5 $MPa\sqrt{m}$, which is far below both a mathematical and realistic threshold for significant fatigue growth. It is unlikely that the cracks measured in this experiment were influenced by fatigue growth to any significant degree.

5.5 Proposed mechanism

A hypothesis was proposed early in this paper that stated:

Surface residual stresses provide anodic or "high energy" sites that focus initial grain dissolution and lead to stress intensification, a pre-cursor to cracking. Below surface residual stresses provide a tensile stress necessary to keep small cracks open and allow growth. Therefore propagation of a crack into compressive residual stresses will create dormancy, while a tensile residual stress will allow growth to continue.

In support of this hypothesis it was demonstrated that high levels of residual stress provide anodic sites for pitting to occur. The pitting likely forms prior to advent of cracking. The micro-pits observed, ranging down to a few grains in depth, allowed for a focal point for crack initiation if the surface is in tension. Micro-pits, such as the one observed in the SSRT, would likely not be assessed as being a pit when observed in the field on an in-service pipeline as they would be too difficult to detect on a mill scale surface and largely obliterated after grinding and polishing. The deeper pits observed in the cyclic loading tests were typically less than 50 microns in depth and again would be difficult to observe on pipelines in service. It is likely that the initial pitting occurs rapidly thereby relieving some of the energy associated with the surface stress and resulting in a decreasing pitting rate.

The resultant micro-pits formed locations for cracks to initiate. All the cracks observed in both tests were associated with micro-pitting. In the case of the cyclic

load tests the micro-pits progressed from a few grains to a dozen or more grains during the course of the test and would likely obliterate the newly formed crack if the corrosion rate was increased by the ingress of oxygen. The micro-pits created a stress intensifier, which in the presence of a residual tensile stress found to be 150 MPa or greater, allowed for sufficient stress intensity to propagate the crack. No cracks propagated in the compressive face or at a compressive surface stress location. This observation supports a threshold crack stress intensity for crack growth.

When the frequency of all of the initiated cracks are plotted against the residual stress level and normalized for exposed area at a particular residual stress level a relationship is observed (Figure 49). The relationship indicates that between -280 MPa to +300 MPa of surface residual stress levels, 71% of the cracking occurs in the range of 150 MPa to 200 MPa. A total 98% of the cracks initiated in the stress range of 100 MPa to 250 MPa. These results indicate that tSCC occurs preferentially in areas of high residual stress. The absolute value of residual stress influences the site of cracking initiation more than the change in the value of residual stress at the cracking location. This may indicate that the anodic - cathodic interactions between areas of high and low residual stress levels occur over a large area.

The decreasing cracking velocity for those cracks formed in the cyclic loading experiment occurred when many of these cracks encountered compressive residual stresses. Compressive stresses likely reduce cracking velocity below that of the anodic dissolution rate resulting in crack blunting and dormancy. All the cracks created in the cyclic loading experiment were blunted by corrosion. Some cracks would likely be obliterated completely by corrosion and turn into large pits (Figure 37, 40). The effect of fatigue was determined by calculating ΔK for these cracks and was found to be below the threshold for significant fatigue growth. Therefore, the majority of growth would be due to an environmental mechanism, where the role of stress would be synergistic to an environmental mechanism. The role of stress is predominately to keep the crack open, to create anodic and cathodic interactions

around and inside the crack and in focusing the accumulation of hydrogen at the crack tip.

6.0 CONCLUSIONS

The experimental portion of this thesis was designed to provide data to support a role of residual stress in the initiation and propagation of trans-granular stress corrosion cracking in pipeline steels. Essentially cracks were initiated on tensile specimens that were designed to be uniform in their material and mechanical properties, except for the large gradients in residual stress. To have residual stress gradients sufficiently large as to dominate, by several orders of magnitude, any other non-uniformity in properties, the residual stress was artificially induced by bending. The stresses were then extensively mapped across the length and through the depth of the specimen by non-destructive neutron diffraction. The correlations found were then inferred to be mainly a function of the level of residual stress present in the steel. Several high confidence correlations were made in these experiments as follows.

I. The formation of micro-pitting (less than 50 μm deep) occurred preferentially in areas where the tensile residual stresses were 200 MPa to 250 MPa, some of the highest residual stresses encountered.

II. Little pitting or general corrosion occurred on surfaces with compressive residual stresses. These surfaces contained cathodic surface deposits.

III. All twenty-nine cracks detected on the ten tensile specimens from both experimental testing methods formed at the base of micro-pits.

IV. Crack initiation occurred with a 71% normalized frequency in areas where the surface residual stress was in the range of 150 MPa to 200 MPa.

V. No cracking initiated at surface areas measured to have compressive residual stresses.

VI. The SSRT cracks formed were trans-granular in nature.

VII. The value of ΔK was calculated and determined to be too small to influence the growth of these cracks by fatigue.

The analysis and interpretation of these findings is somewhat more subjective and recognizes that in crack initiation and in the early stages of crack growth, residual stresses and total stress act in support of an environmental mechanism. The mechanical effect of stress such as in fatigue will be relatively unimportant at this stage of crack growth. As such, differences in stress will likely support an environmental mechanism of crack growth by:

I. Creating electrochemical potential gradients across the steel surface that can cause localized pitting and stress intensification.

II. Focusing the accumulation of hydrogen at the crack tip, thereby embrittling the crack tip according to the hydrogen mechanism of crack growth reviewed in section 2.5.1.

III. Increasing the crack tip opening displacement, thereby preventing diffusion limitations to the crack tip.

A mechanism describing the effect of residual stress on crack initiation and propagation was proposed and supported by the experimental data. The proposed mechanism suggests:

I. Tensile surface residual stresses are areas of high energy and as such become anodic with respect to neutral or compressive areas of residual stress. This galvanic action can occur over several millimeters, across adjacent phases or even adjacent grains.

II. Trans-granular stress corrosion cracking is initiating in the micro-pits due to the stress intensification resulting from both the pit and the superimposed

tensile residual stress. This stress intensification results in a relatively high stress intensity for a short crack (>10 MPa$\sqrt{m}$). Overcoming a stress intensity threshold is likely required for crack growth.

III. Increasing crack stress intensity is required to propagate the crack. Increasing crack stress intensity continuously widens the crack. A widening crack reduces diffusion limitations to the tip of the crack, a widening crack prevents wedging of the crack and increases the plastic zone size thereby focusing hydrogen accumulation at the crack tip.

IV. Surfaces with compressive residual stresses act to inhibit crack initiation by remaining cathodic thereby inhibiting pitting. As well, initial crack stress intensity would be below a threshold needed to keep the crack in an open state.

V. Compressive residual stresses reduce crack stress intensity, thereby decreasing cracking velocity. When the cracking velocity drops below the anodic dissolution rate of the crack tip, blunting of the crack tip occurs. Very little material needs to be removed from the crack tip to cause blunting. A large drop in crack stress intensity results from blunting and causes eventual crack dormancy.

It is sufficient to state that all the environmental growth models proposed for tSCC involve a tensile stress. The tensile stress undoubtedly has a mechanical aspect in crack growth but may also act as a driver for cathodic reactions, for the focus of hydrogen at a crack tip or in other synergistic methods. Therefore the above role of residual stress proposed does not preclude other mechanisms and can typically be incorporated as one component in what will clearly be a much more complex mechanism to describe trans-granular SCC.

7.0 REFERENCES

[1] Zhang, X.Y., Lambert, S.B., Sutherby, R., Plumtree, A. *"Trans-granular Stress Corrosion Cracking of X-60 Pipeline Steel in Simulated Ground Water."* Corrosion – Vol. 55, No. 3. NACE International. Houston, TX. 1999.

[2] Parkins, R.N. *"A Review of Stress Corrosion Cracking of High Pressure Gas Pipelines"* Proceedings of Corrosion 2000. Paper 00363. NACE International. Houston, Texas. 2000.

[3] Lambert, S.B., Plumtree, A., *"Modeling of Environmental Crack Growth in Pipeline Steel."* Corrosion 2000 Proceedings. Paper No. 00364. NACE International, Houston TX. 2000.

[4] Parkins, R.N. *"Overview of Inter-granular Stress Corrosion Cracking Research Activities."* Report PR-232-9401 to PRCI at the American Gas Association, November, 1994.

[5] Meletis, E.I. *"A Review of Present Mechanisms of Trans-granular Stress Corrosion Cracking."* Department of Materials Science and Engineering. Louisiana State University. Baton Rouge, Louisiana, U.S.A.

[6] Beavers, J.A., Durr, C.L., Shadememan. *"Mechanistic Studies of Near-Neutral pH SCC on Underground Pipelines".* Materials for Resource Recovery and Transport. Canadian Institute of Mining, Metallurgy and Petroleum, Quebec, P51, 1998.

[7] Parkins, R.N., Blanchard, W.K., Delanty, B.S. "Stress corrosion cracking: A Summary" Corrosion 50, 394, 1994

[8] Birnbaum, H.K., *"Mechanisms of Hydrogen Related Fracture of Metals."* in Environment Induced Cracking of Metals, Eds. R.P. Gangloff and M.B. Ives. NACE International. Houston, TX. 1990.

[9] Beachem, C.D., Metallurgical Transactions, 3, 437, 1972.

[10] Cracknell, A., Petch, N.J., Acta Metallurgica, 3, 200, 1955.

[11] Oriani, R.A., Josephic, P.H., Acta Metallurgica, 29, 669, 1981.

[12] Jack, T.R., Van Boven, G., Wilmott, M.J., Sutherby, R.L. *"Parameters Affecting the Growth of Low pH Stress Corrosion Cracking of Pipeline Steels."*, Canadian Western Regional Conference, Calgary, p504, NACE International. Houston, TX. 1994.

[13] Holden, T.M.; Root, J.H.; Rogge, R.B.; Clarke, A.P.; *"The Application of Neutron Diffraction to Materials Science Problems in the Canadian Nuclear Industry."* CAN Conference, Saskatoon. June 1995.

[14] Holden, T.M. et al. *"Application of Neutron Diffraction to Engineering Problems".* Atomic Energy of Canada, Chalk River Ontario. Proceedings of the Fifth Canadian Conference on Nondestructive Testing. October 28, 1984

[15] Holden, T.M., Roy, G. *"The Application of Neutron diffraction to the Measurement of Residual Stress and Strain."* Handbook of Measurement of Residual Stresses, Society for Experimental Mechanics Inc. Fairmont Press, N.J. 1996.

[16] Schajer, G.S. *"Application of Finite Element Calculations to Residual Stress Measurements."* Journal of Engineering Materials and Technology. Vol. 103. April 1981.

[17] Mura, T. *"Micro-mechanics of Defects in Solids."* Marting Nijhoff Publishers, the Hague, Netherlands, 1982.

[18] Beavers, John A., Johnson, Joshua T., Sutherby, R.L. *"Material Factors Influencing the Initiation of Near-Neutral pH SCC on Underground Pipelines."* Proceedings of International Pipeline Conference. IPC00-0047. June, 2000.

[19] Noyan, I.C., Cohen, J.B. *"Residual Stress – Measurement by Diffraction and Interpretation."* Springer – Verlag New York Inc. 1987.

[20] *Standard Test Method for Determining Residual Stresses by the Hole-Drilling Strain-Gage Method.* ASTM Method E 837-99. ASTM . West Conshohocken, PA. 1999.

[21] Beavers, J.A., Parkins, R.N. *"Recent Advances in Understanding the Factors Affecting SCC of Pipe Steels."* Symposium on Line Pipe Research, Houston, Texas. 1986.

[22] Harle, B.A., Beavers, J.A., Jaske, C.E. *"Low pH Stress Corrosion Cracking of Natural Gas Pipelines". Unpublished internal memo.*

[23] Wang, Y.Z., Revie. R.W., Shehata, M.T. *"Initiation of Stress Corrosion Cracking in Pipeline Steel."* Summary Report to GRI. Chicago, Illinois. May 1997.

[24] Beavers, J.A., Parkins, R.N. *"Standard Test Procedure for Stress Corrosion Cracking Threshold Determination."* Corrosion 86. Paper 321. NACE International. Houston, Texas. 1986.

[25] Jack, T.R., Erno, B., Krist, K., Fessler, R.R. *"Generation of Near Neutral and High pH SCC Environments on Buried Pipelines."* GRI 1999.

[26] Vrable, J.B. *"Stress Corrosion and Hydrogen Embrittlement of Line – Pipe Steel in Underground Environments."* Materials Performance. Vol. 11 No. 2. NACE International, Houston, Texas. Feb, 1972.

[27] Sieradzki, K., Newman, R.C. *"Brittle Behavior of Ductile Metals During Stress – Corrosion Cracking."* Philosophical Magazine. Vol. 51. No.1. pp.95-132. 1985.

[28] Qiao, L.J., Luo, J.L., Mao, X. *"Hydrogen Evolution and Enrichment Around Stress Corrosion Crack Tips of Pipeline Steels in Dilute Bicarbonate Solution."* Corrosion. Vol. 54, No. 2, pp.115-120. NACE International. Houston, Texas. Feb. 1998.

[29] Qiao, L., Mao, X. *"Thermodynamic Analysis on the Role of Hydrogen in Anodic Stress Corrosion Cracking."* Acta Metallurgica Materials. Vol. 43, No. 11, pp. 4001-4006. Elseevier Science Ltd. Great Britain. 1995

[30] Pound, B.G. *"Hydrogen Entry and Trapping in High Strength Alloys."* Proceedings of the First International Conference on Environment-Induced Cracking of Metals. pp.203-217. NACE. Houston, Texas. Oct. 1988.

[31] Turnbull, A., Saenz, M. *"Relative Importance of Crack Tip Charging and Bulk Charging in Hydrogen Assisted Cracking in Aqueous Solutions."* Proceedings of the First International Conference on Environment-Induced Cracking of Metals. pp.193-196. NACE. Houston, Texas. Oct. 1988.

[32] Kasul, D.B., White, C.L., Heldt, L.A. *"Relationships Between Plasticity and Stress Corrosion Cracking."* Proceedings of the First International Conference on Environment-Induced Cracking of Metals. pp.219-227. NACE. Houston, Texas. Oct. 1988.

[33] Jones, D.A. *"The Contribution of Localized Surface Plasticity to the Mechanism of Environment-Induced Cracking."* Proceedings of the First International Conference on Environment-Induced Cracking of Metals. pp.265-270. NACE. Houston, Texas. Oct. 1988.

[34] Galvele, Jose, R. *"Surface Mobility Mechanism of SCC."* Proceedings of the Parkins Symposium on Fundamental Aspects of Stress Corrosion Cracking. The Minerals, Metals & Materials Society, 1992.

[35] Uhlig, H.H. *"Proceedings of the International Conference on Stress Corrosion Cracking and Hydrogen Embrittlement of Iron Base Alloys."* Ed. Etienne, St., NACE. Houston, Texas. 1973.

[36] Newman, R.C. *"Stress Corrosion Cracking Mechanisms."* UMIST, Manchester England, pp. 311-372. 1995.

[37] Atrens, A., Wang, Z.F. *"Stress Corrosion Cracking."* Materials Forum. No 19. Pp.9-34. NACE International. Houston, Texas. 1995.

[38] Sieradzki, K. *"Atomistic and Micromechanical Modeling Aspects of Environment-Induced Cracking of Metals."* Proceedings of the First International Conference on Environment-Induced Cracking of Metals. pp.125-137. NACE. Houston, Texas. Oct. 1988.

[39] Birnbaum, H.K. *"Mechanisms of Hydrogen Related Fracture of Metals."* Proceedings of the First International Conference on Environment-Induced Cracking of Metals. pp.21-29. NACE. Houston, Texas. Oct. 1988.

8.0 TABLES

TABLE 1: Experimental methodology flowchart.

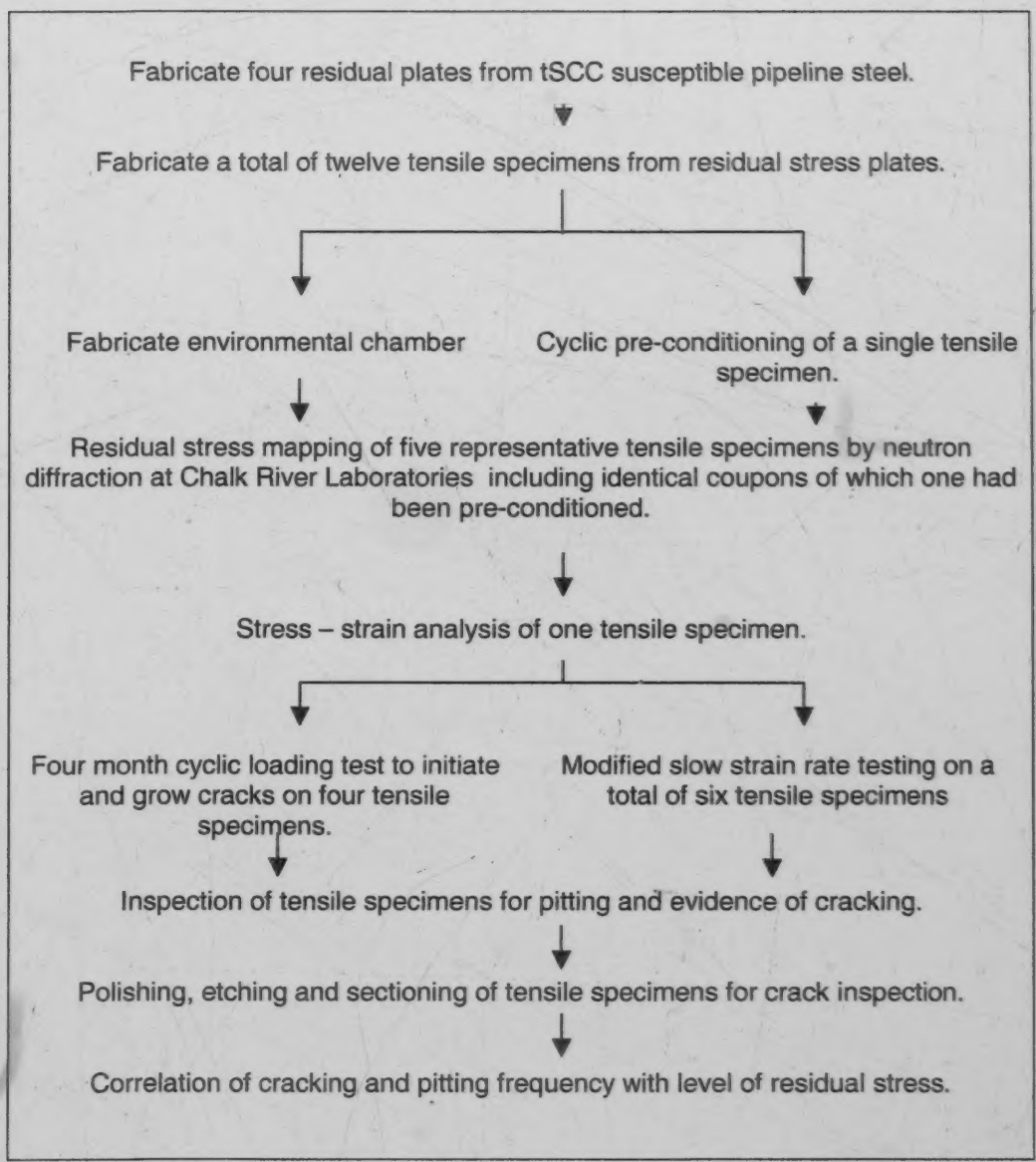
Fabricate four residual plates from tSCC susceptible pipeline steel.
Fabricate a total of twelve tensile specimens from residual stress plates.
Fabricate environmental chamber
Cyclic pre-conditioning of a single tensile specimen.
Residual stress mapping of five representative tensile specimens by neutron diffraction at Chalk River Laboratories including identical coupons of which one had been pre-conditioned.
Stress – strain analysis of one tensile specimen.
Four month cyclic loading test to initiate and grow cracks on four tensile specimens.
Modified slow strain rate testing on a total of six tensile specimens
Inspection of tensile specimens for pitting and evidence of cracking.
Polishing, etching and sectioning of tensile specimens for crack inspection.
Correlation of cracking and pitting frequency with level of residual stress.

TABLE 2: Chemical composition of X65 pipeline steel.

Element	Weight percent composition
Carbon (C)	0.20
Chromium (Cr)	0.09
Copper (Cu)	0.06
Manganese (Mn)	1.52
Molybdenum (Mo)	0.03
Nickel (Ni)	0.031
Niobium (Nb)	0.029
Phosphorus (P)	0.004
Silicon (Si)	0.28
Sulfur (S)	0.01

TABLE 3: Experimental electrolyte composition.

Ion	Concentration (mg/l)
$MgSO_4 \cdot 7H_2O$	27.4
$CaCl_2$	25.5
KCl	3.5
$NaHCO_3$	19.5
$CaCO_3$	60.6

TABLE 4: List of tensile specimens and testing performed.

Residual Plate #	Initial bending angle (°)	Tensile specimen #	Experimental Procedure
1	165.6	11	Destructively tested for stress – strain curve.
		12	Not used – machined outside of specification
		13	Neutron Diffraction Analysis Cyclic loading experiment
2	165.6	21	Neutron Diffraction Analysis Cyclic loading experiment
		22	Cyclic loading experiment
		23	Modified SSRT
3	171.0	31	Cyclic loading experiment
		32	Neutron Diffraction Analysis Modified SSRT
		33	Neutron Diffraction Analysis Modified SSRT
4	171.0	41	Neutron Diffraction Analysis Modified SSRT
		42	Modified SSRT
		43	Modified SSRT

TABLE 5: Frequency of corrosion pitting versus measured surface residual stress in a four month cyclic loading tests on tensile specimens 13, 21, 22,31.

Measured surface residual stress. [MPa]	# corrosion pits observed
-300	3
-250	0
-200	2
-150	2
-100	1
-50	1
0	3
50	5
100	4
150	6
200	11
250	18
300	12

TABLE 6: Location, depth and measured residual stress of blunt cracks formed on tensile specimens subject to cyclic loading in an electrolyte.

Tensile Specimen #	Distance from center of gauge section (mm)	Crack depth (um)	Measured residual stress (MPa)
13	2.1	640	231
13	2.0	820	229
13	-1.5	610	193
13	-3.7	480	215
13	-4.2	750	232
13	-2.2	780	200
21	-3.4	740	161
21	-3.9	550	161
21	-4.2	480	161
21	-4.0	230	161
22	4.3	620	148
22	4.8	750	150
22	6.7	280	157
22	-3.1	420	161
22	5.0	550	150
22	0.9	440	166
22	6.8	610	159
31	14.1	140	11
31	14.2	180	14

TABLE 7: Location, depth and measured residual stress of sharp cracks formed on tensile specimens subject to SSRT in an electrolyte.

Tensile specimen #	Distance from center of gauge length (mm)	Measured surface residual stress (MPa)	Crack depth [μm]
23	7.1	152	39.4
32	13.2	120	293.0
33	NO CRACKS FOUND		
41	-5.1	152	34.7
41	-5.1	152	8.0
41	-5.1	152	21.4
42	-10.1	186	41.8
42	-2.2	141	19.9
42	-2.2	141	11.0
43	-4.2	189	72.0
43	-4.2	189	68.0

TABLE 8: Rate of change of surface residual stress at cracking locations and rate of change as a percentage of the largest rate of change found on the corresponding tensile specimen.

Tensile Specimen	$d\sigma/dx$ (MPa/mm)	$d\sigma_{max}/dx$ (MPa/mm)	Percentage of maximum (%)
13	28	29	97
13	28	29	97
13	9	29	31
13	13	29	45
13	15	29	52
13	10	29	34
21	2	19	11
21	2	19	11
21	2	19	11
21	2	19	11
22	7	19	37
22	7	19	37
22	4	19	21
22	2	19	11
22	4	19	21
22	7	19	37
22	4	19	21
31	24	24	100
31	24	24	100
23	4	19	21
32	6	31	19
41	8	18	44
41	8	18	44
41	8	18	44
42	1	18	6
42	1	18	6
42	1	18	6
43	1	18	6
43	1	18	6

9.0 FIGURES

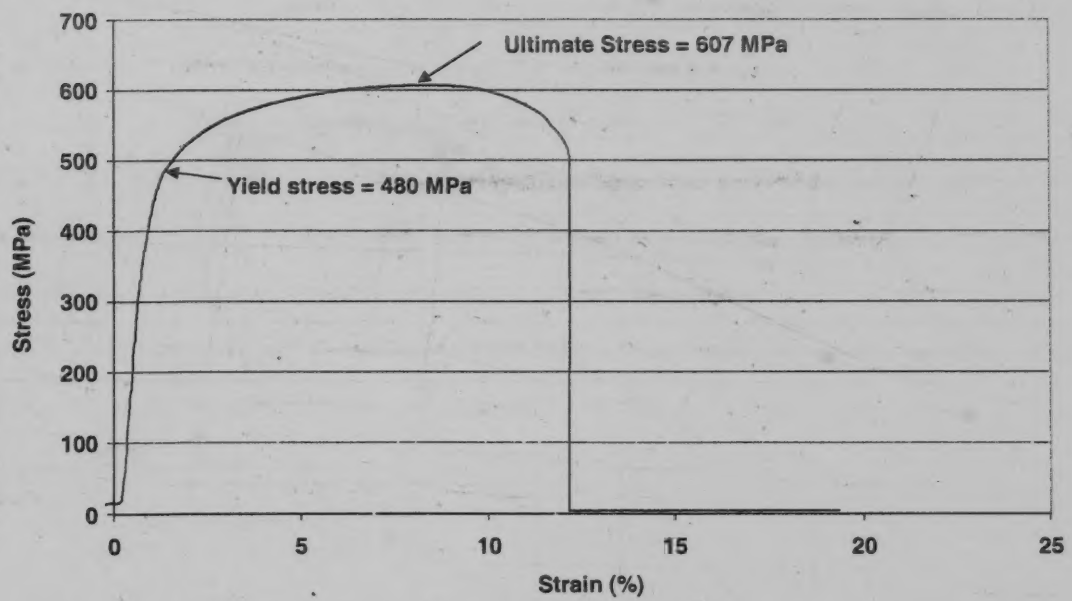

Figure 1: Stress - strain curve performed on a residual stress tensile specimen.

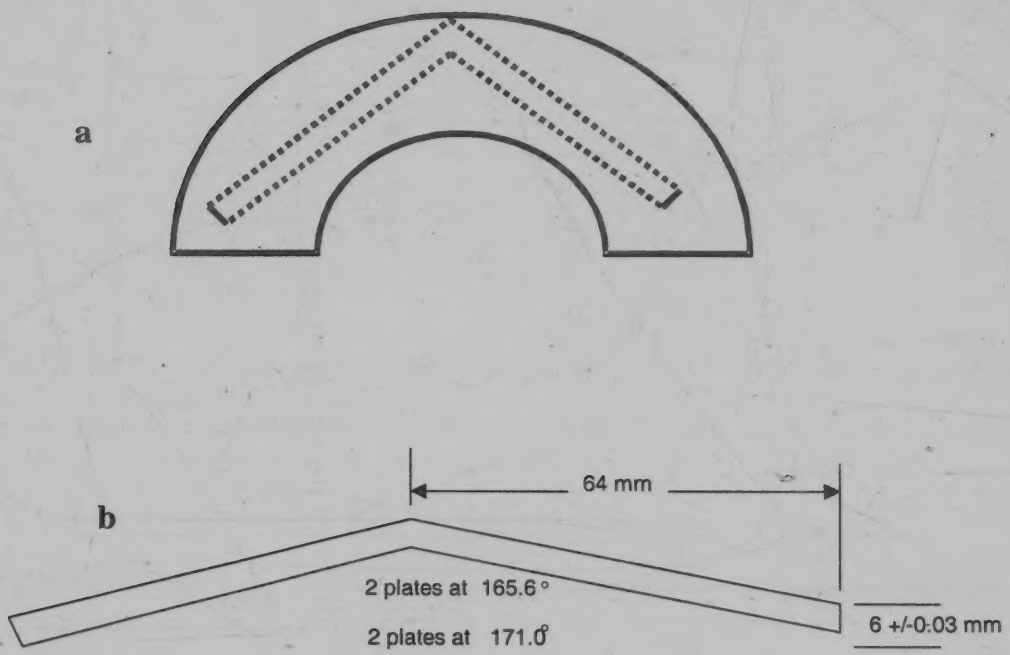

Figure 2: Orientation of the residual stress test plate when removed from the pipeline (**a**) and the residual stress test plate dimensions before three point bending. (**b**)

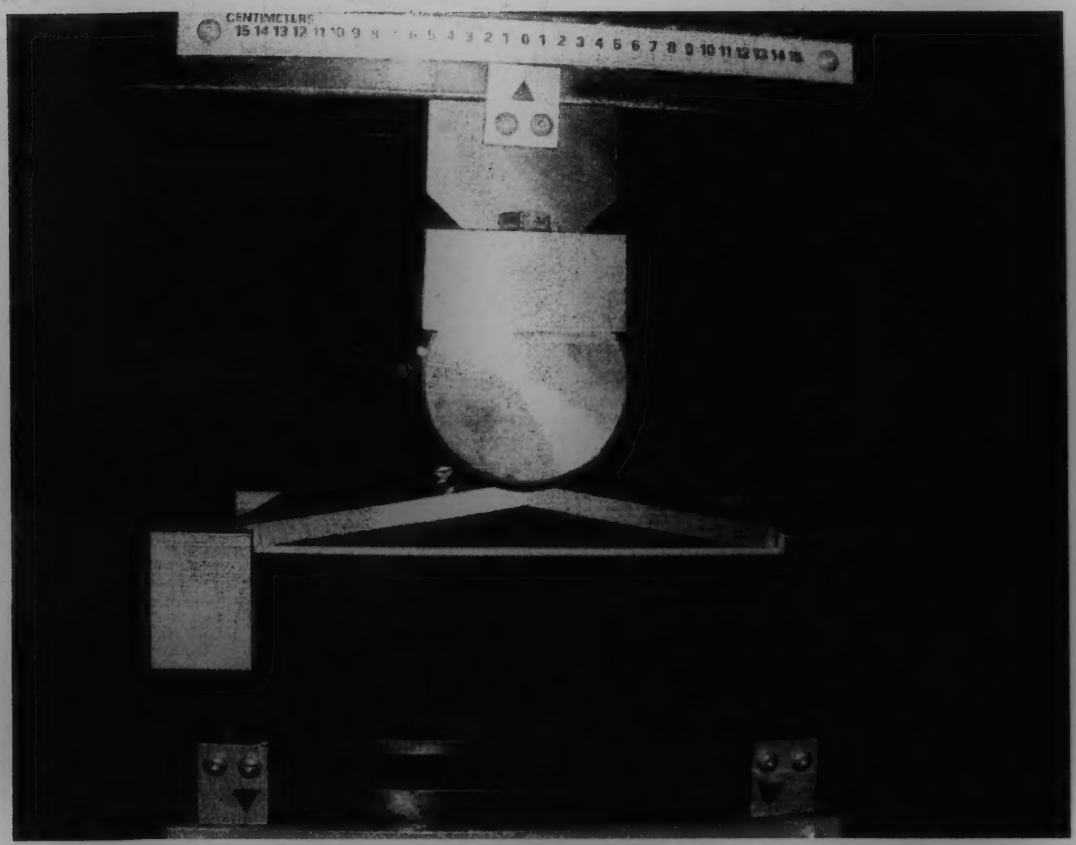

Figure 3: Deforming of test steel into a high residual stress test plate by three point bending.

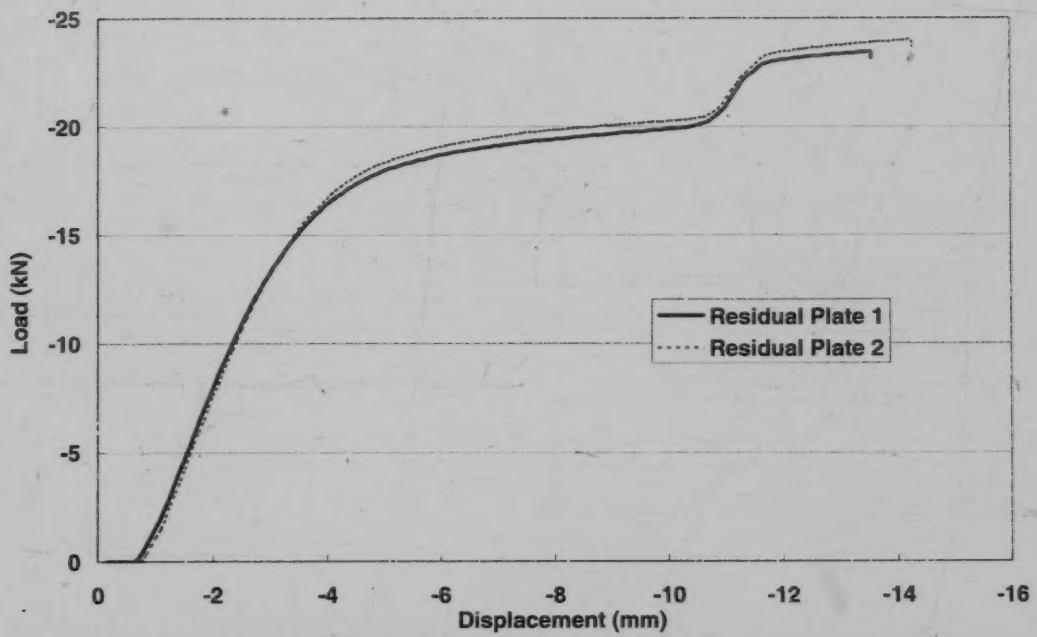

Figure 4: Applied load versus displacement in three point bending of a residual stress plate.

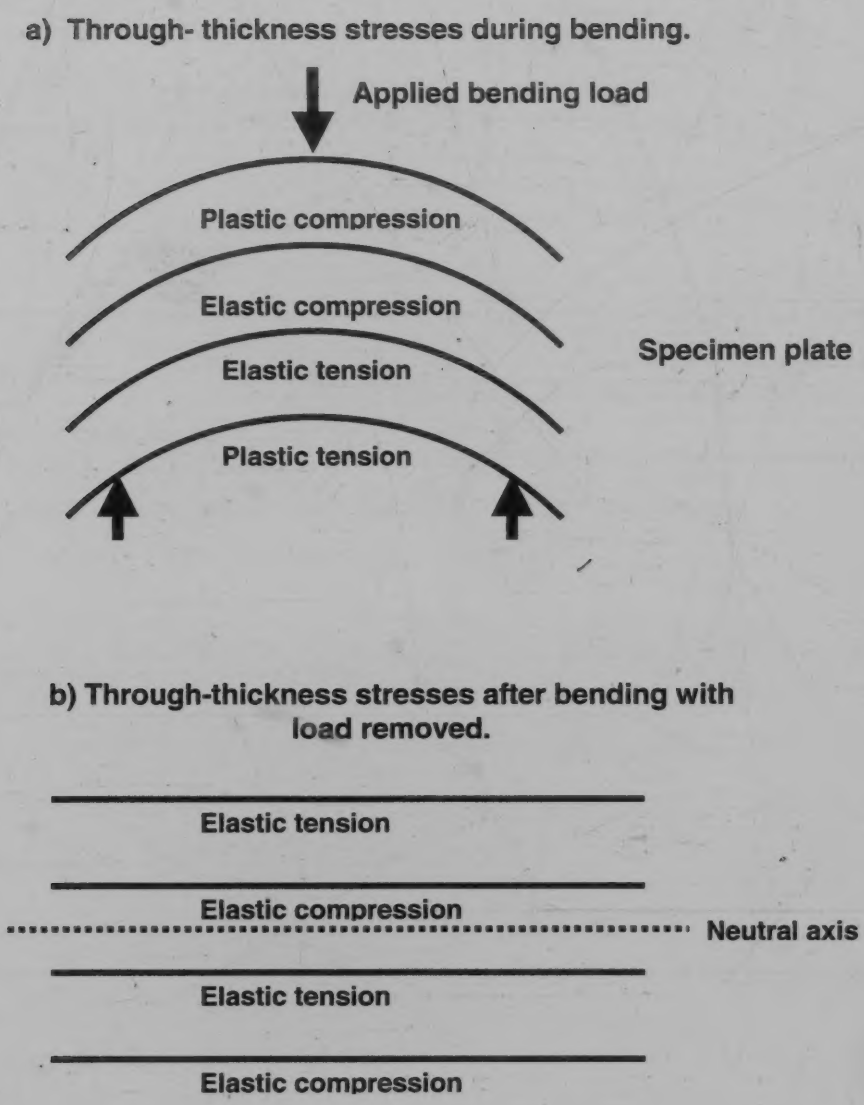

Figure 5: Predicted stress profile during and after bending.

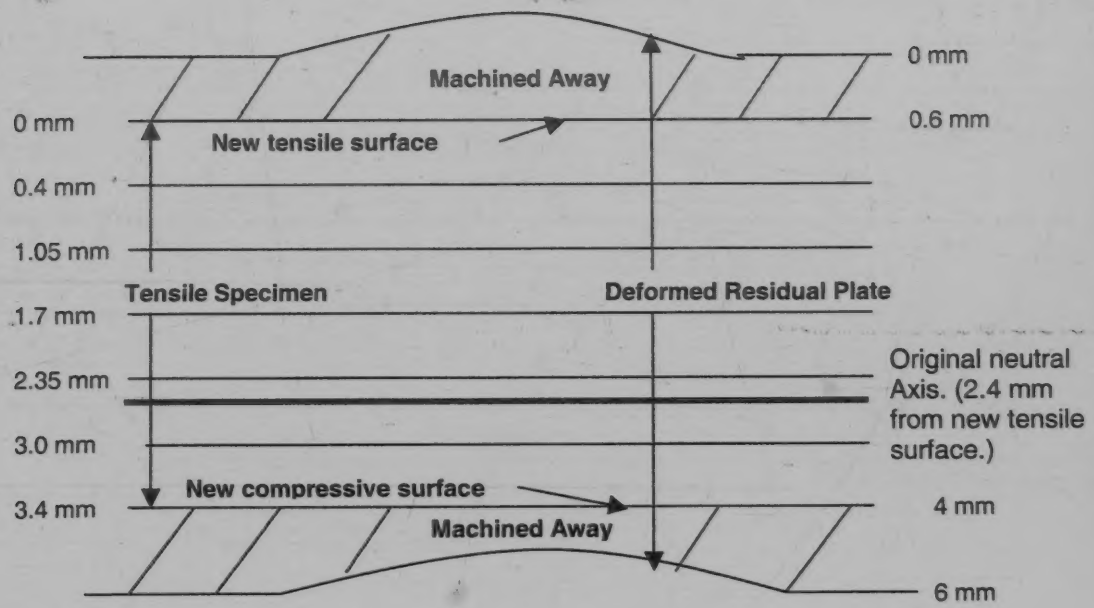

Figure 6: Illustration of tensile specimen orientation after machining from residual stress plate.

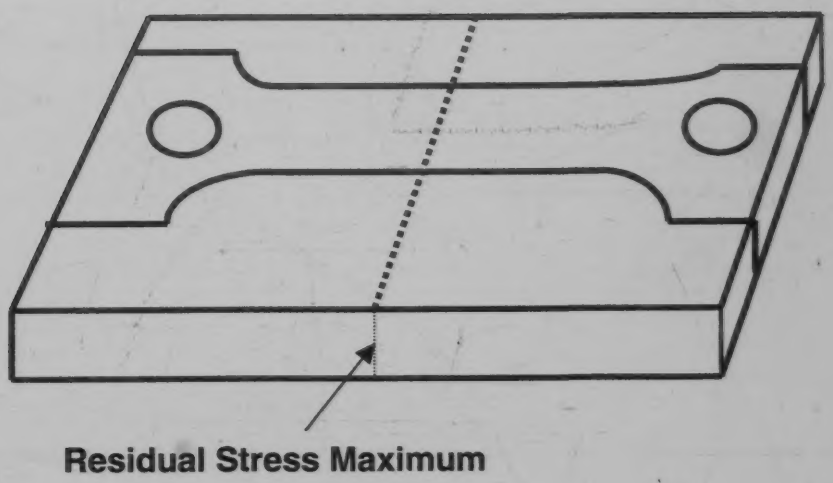

Figure 7: Orientation of the tensile specimen with respect to residual stress plate and maximum expected residual stress field.

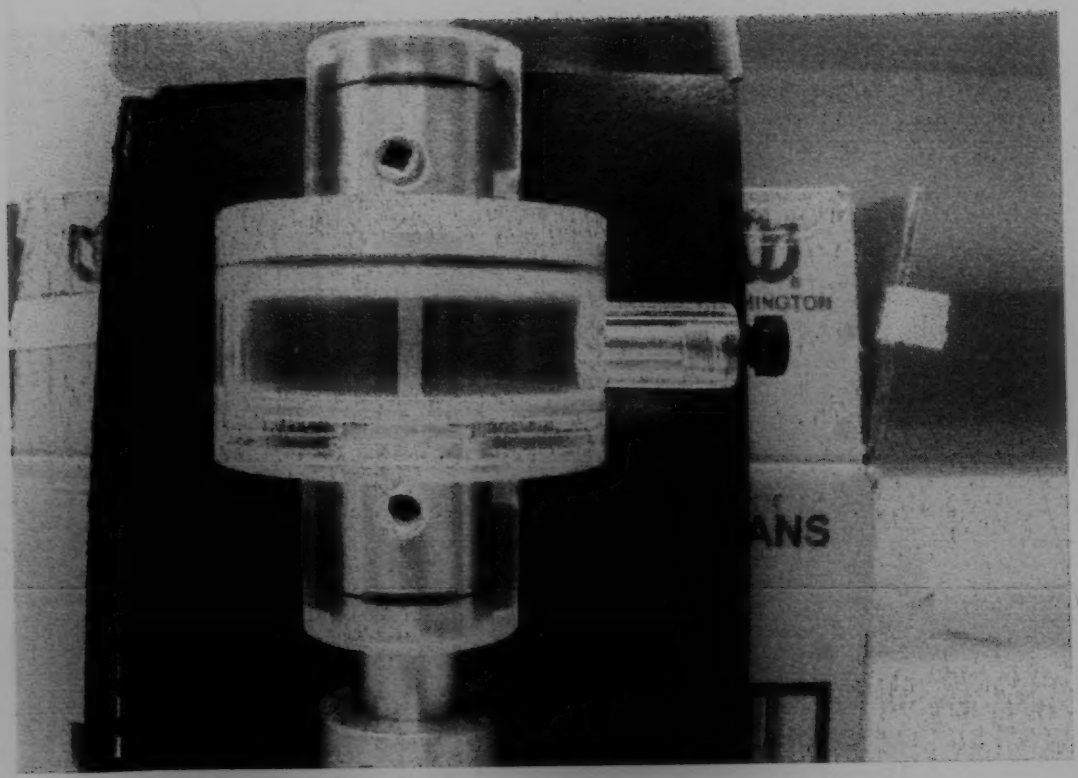

Figure 8: Environmental chamber with tensile specimen mounted in grips.

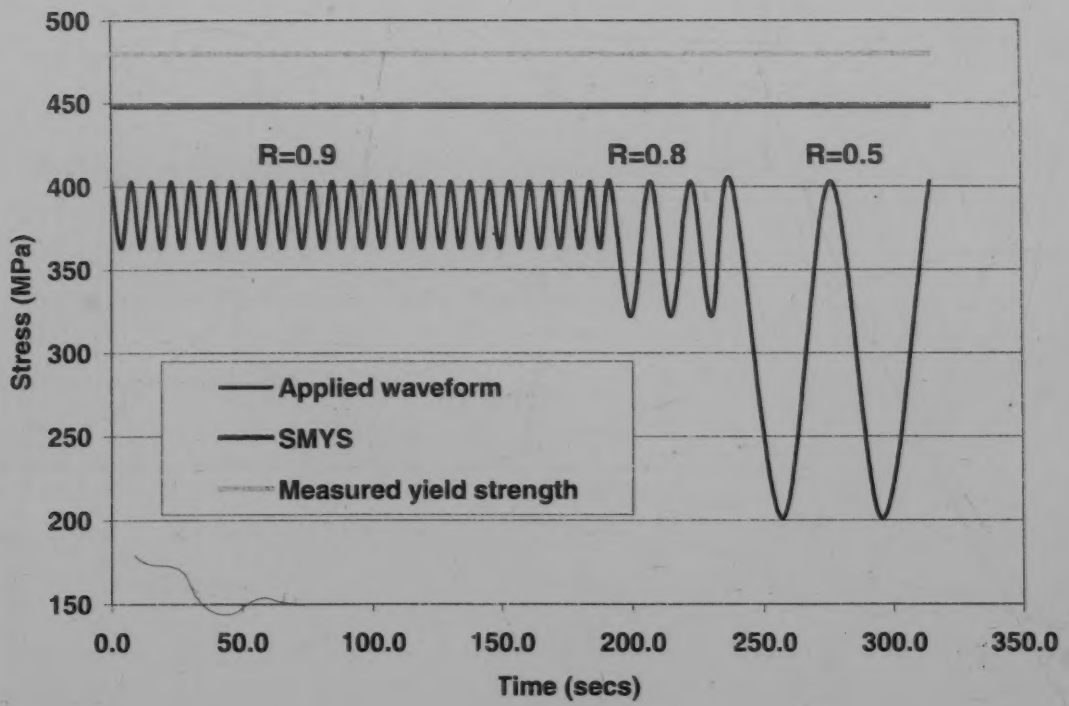

Figure 9: Load pattern used in pre-conditioning of tensile specimen 32. A total of 8000 cycles were applied with a constant strain rate of 5×10^{-5} / second.

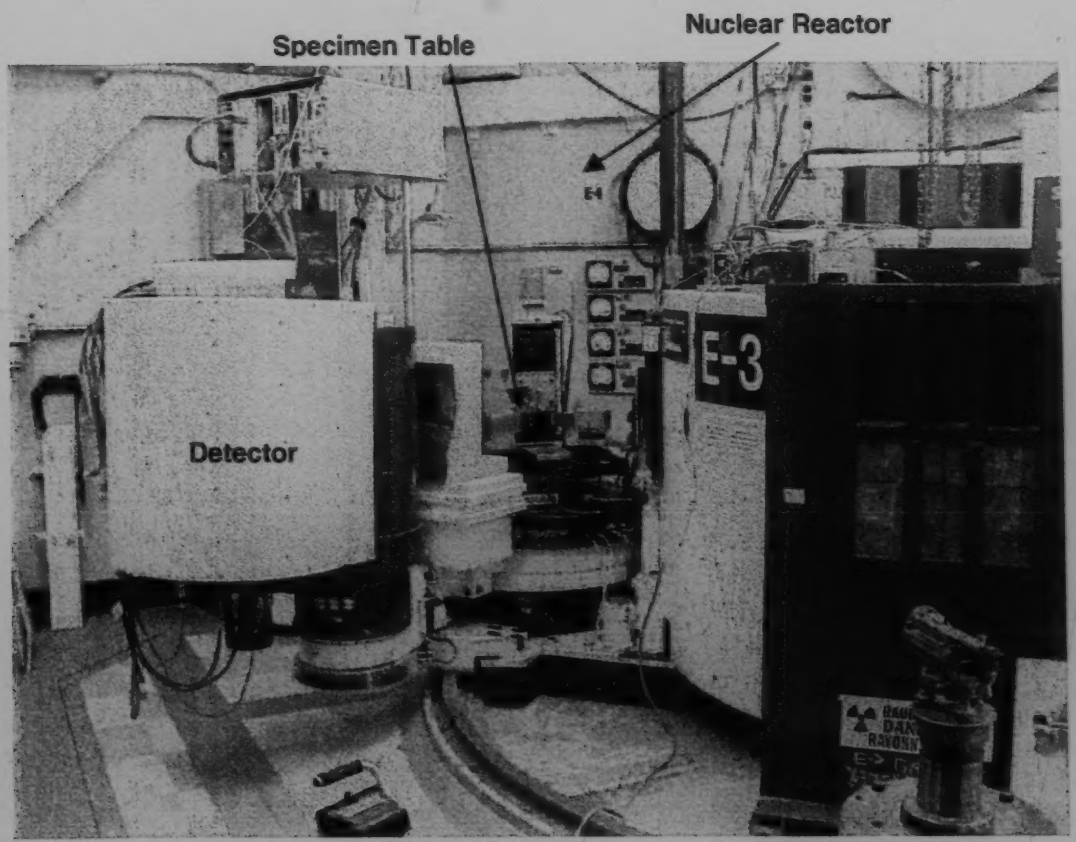

Figure 10: Neutron spectrometer used to measure residual stresses in tensile specimens.

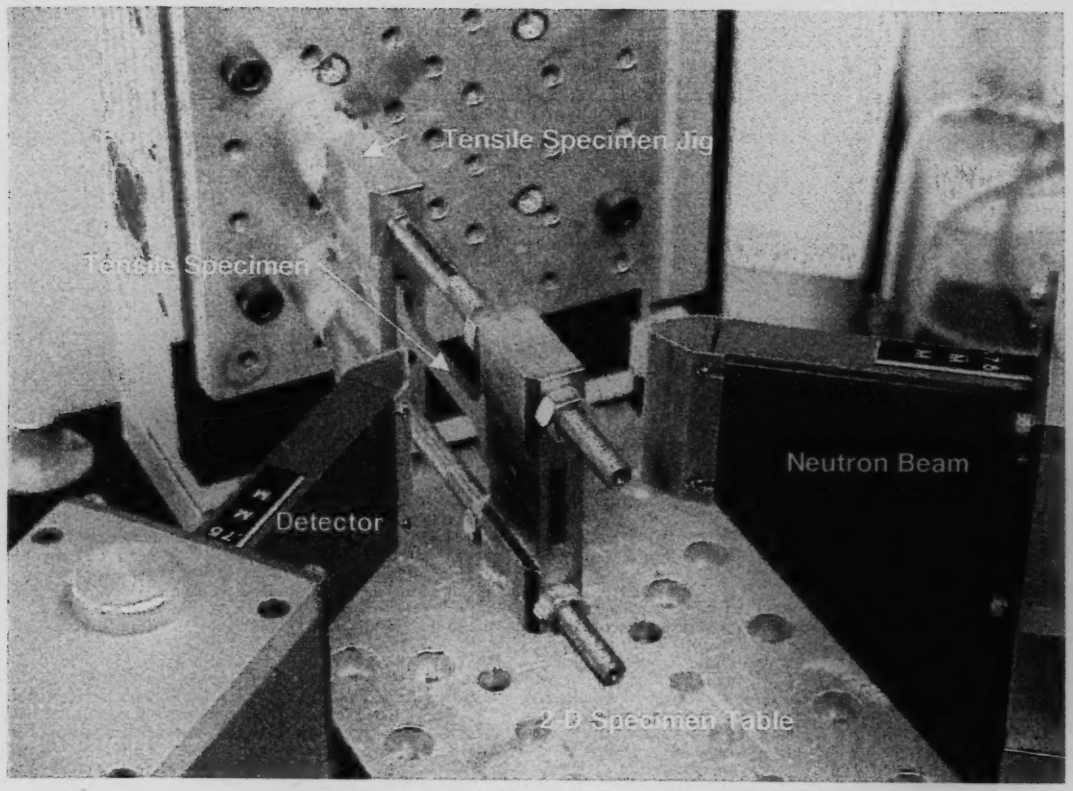

Figure 11: Positioning of tensile specimen on the specimen table in the neutron spectrometer.

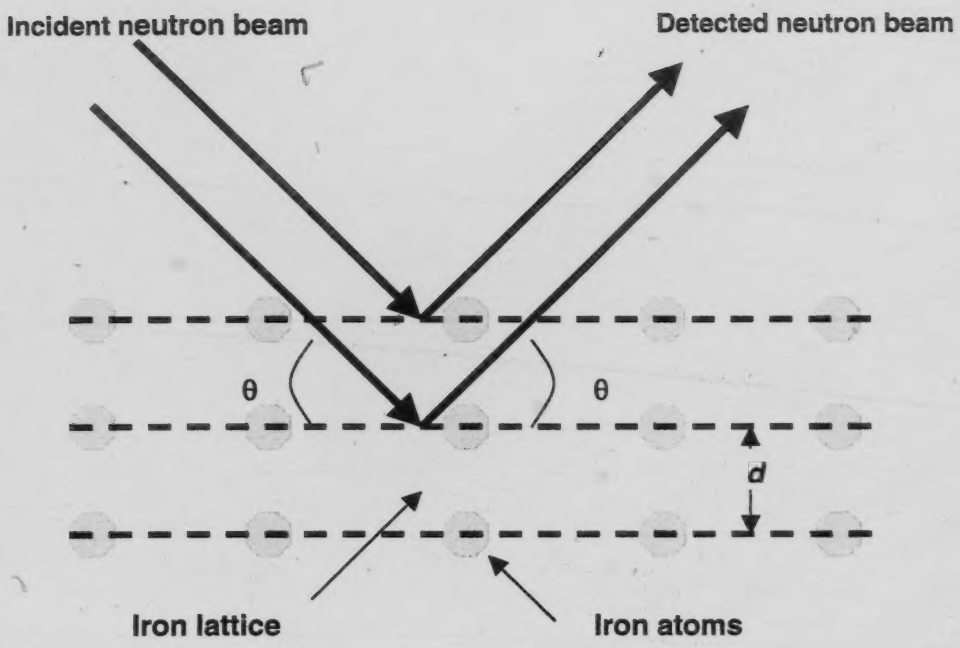

$$d \text{ (interplanar spacing)} = \frac{n\lambda}{2\sin\theta}$$

Measured (110) plane

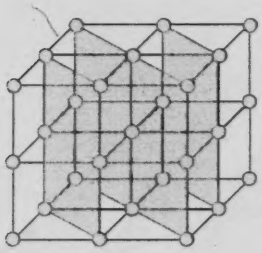

Figure 12: Schematic of neutron scattering to measure interplanar distance.

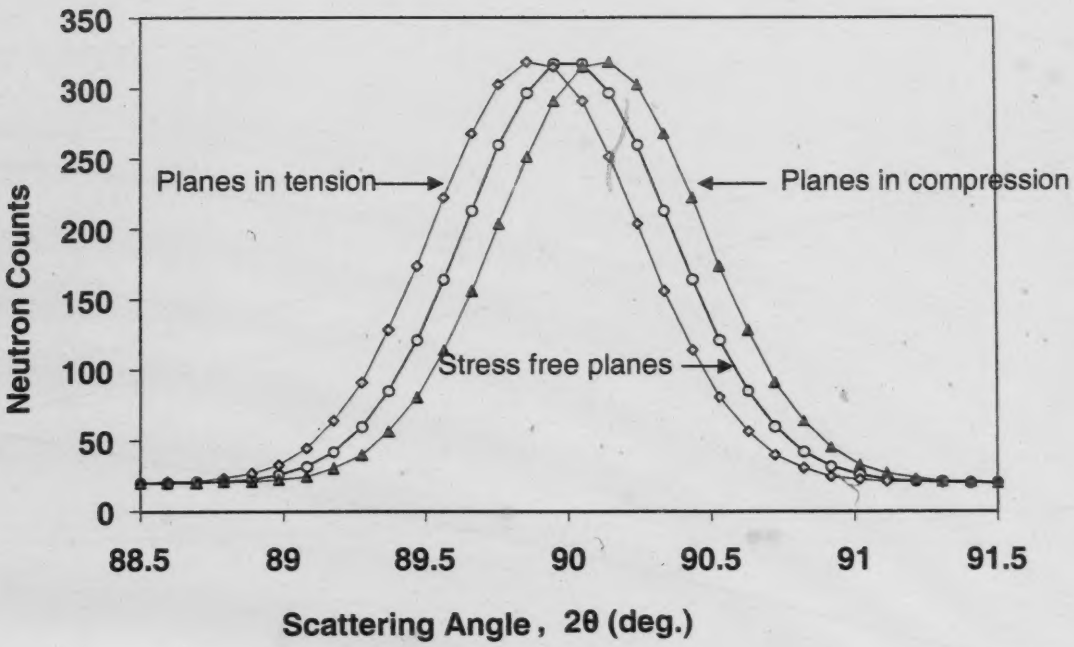

Figure 13: Illustration of a magnitude versus scattering angle Gaussian curve collected by the neutron spectrometer.

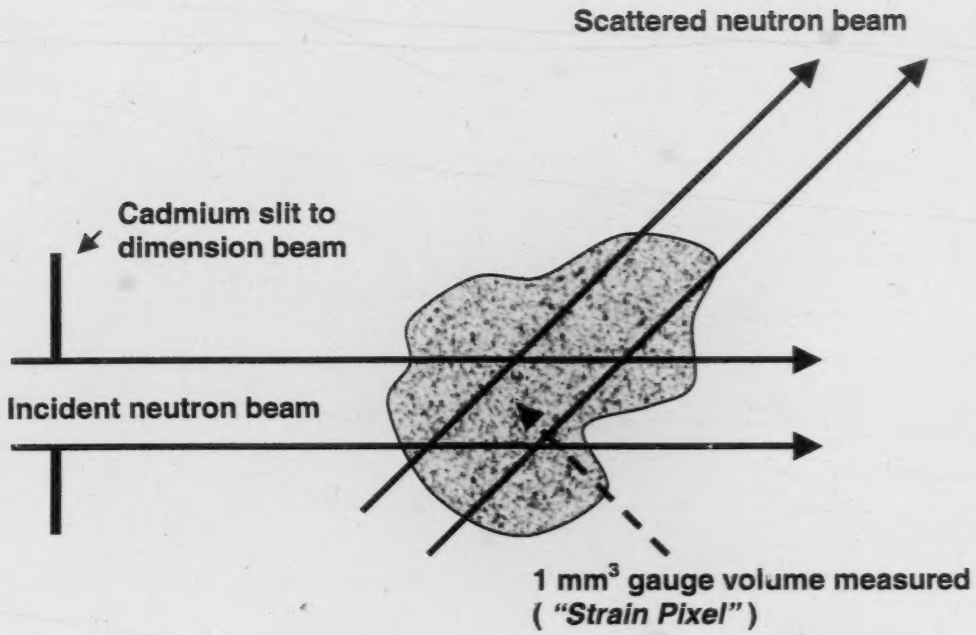

Figure 14: Gauge volume of material measured by neutron diffraction.

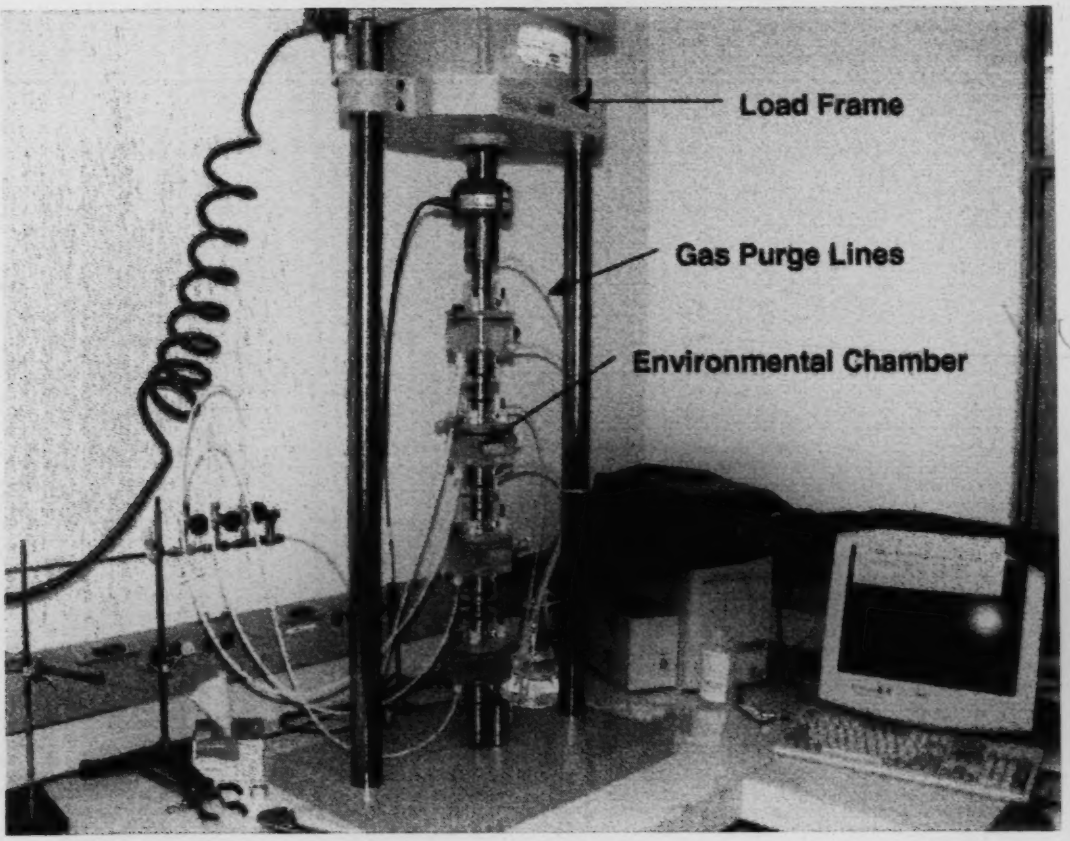

Figure15: Cyclic loading experiment for tSCC after test completion.

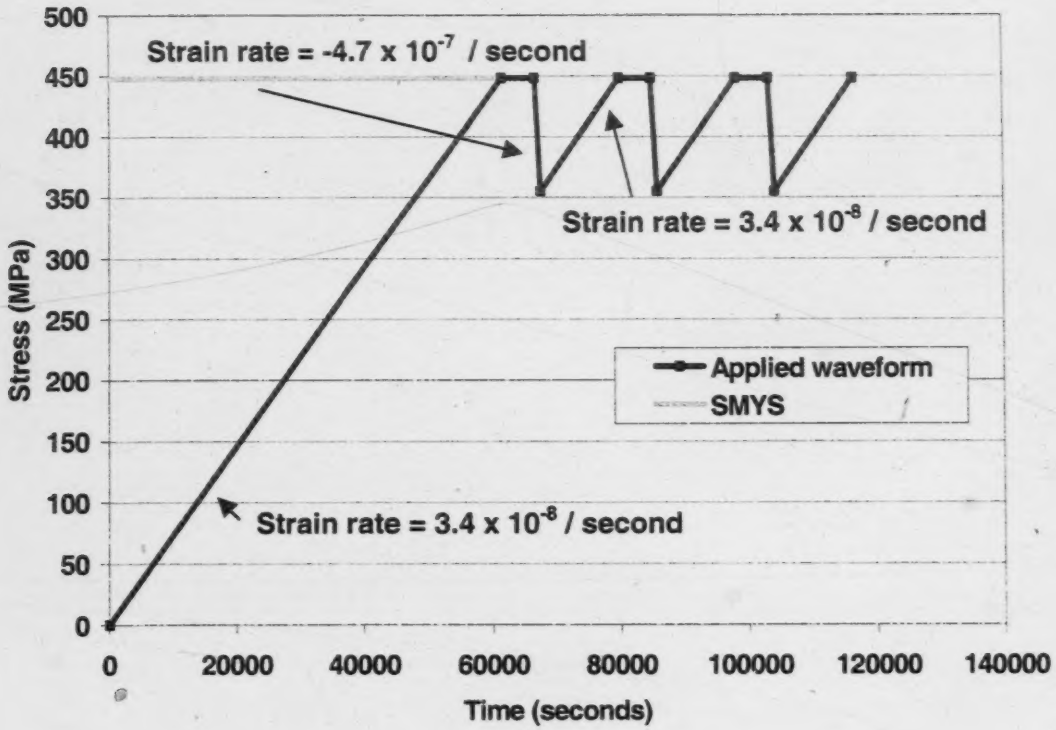

Figure 16: Load pattern used in cyclic loading experiment. (2631 hrs , 517 cycles).

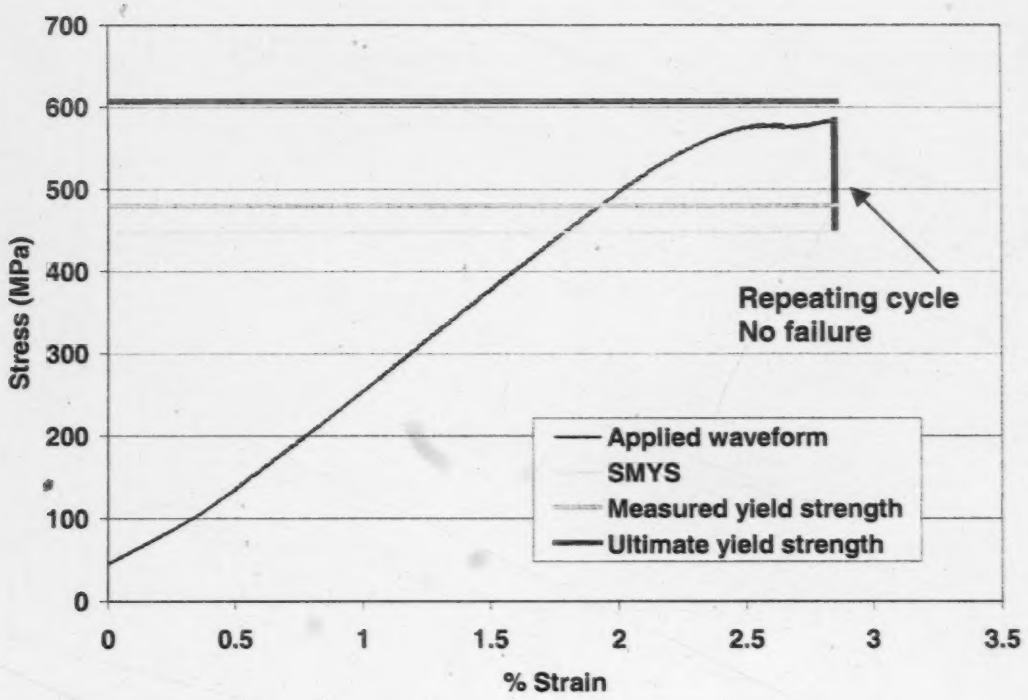

Figure 17: Stress – strain curve recorded during a modified slow strain rate experiment.

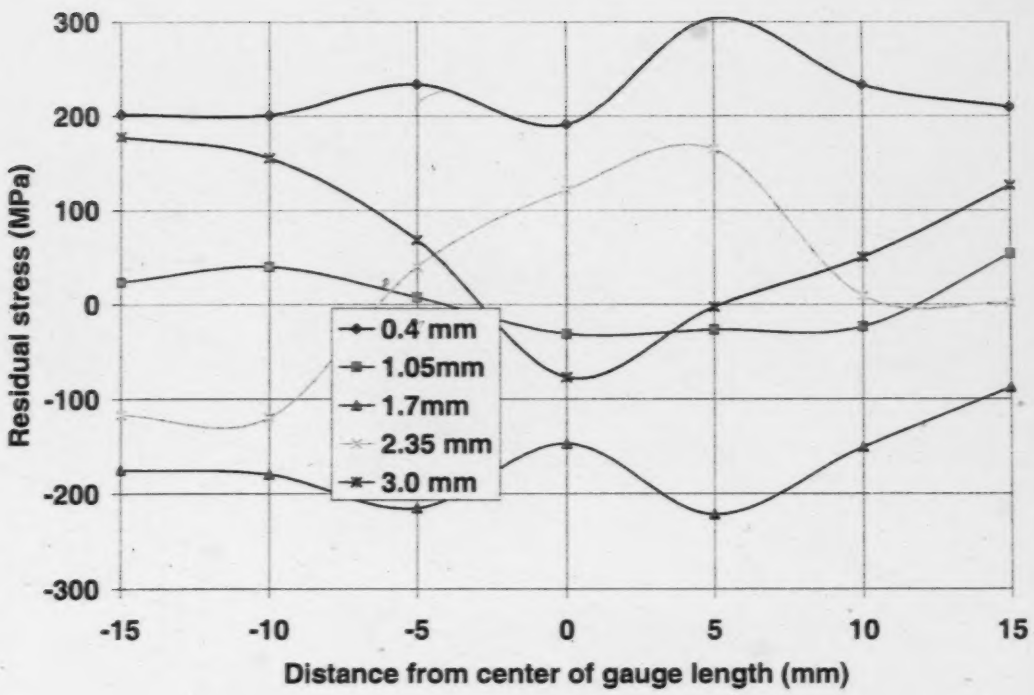

Figure 18: Axial (gauge length) residual stresses measured on tensile specimen 13.

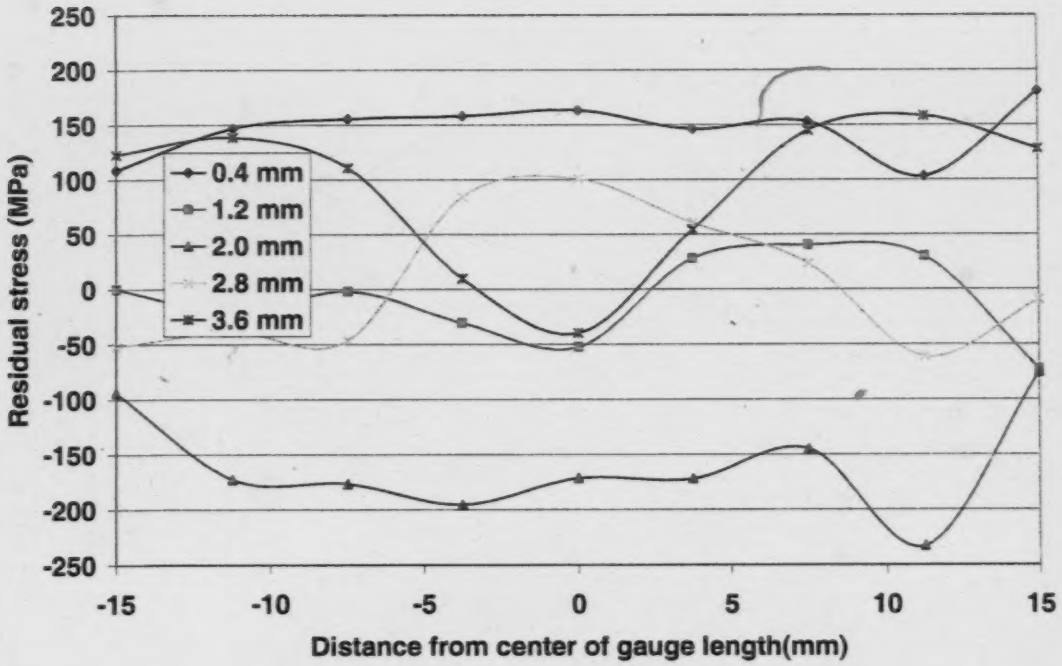

Figure 19: Axial (gauge length) residual stresses measured on tensile specimen 21.

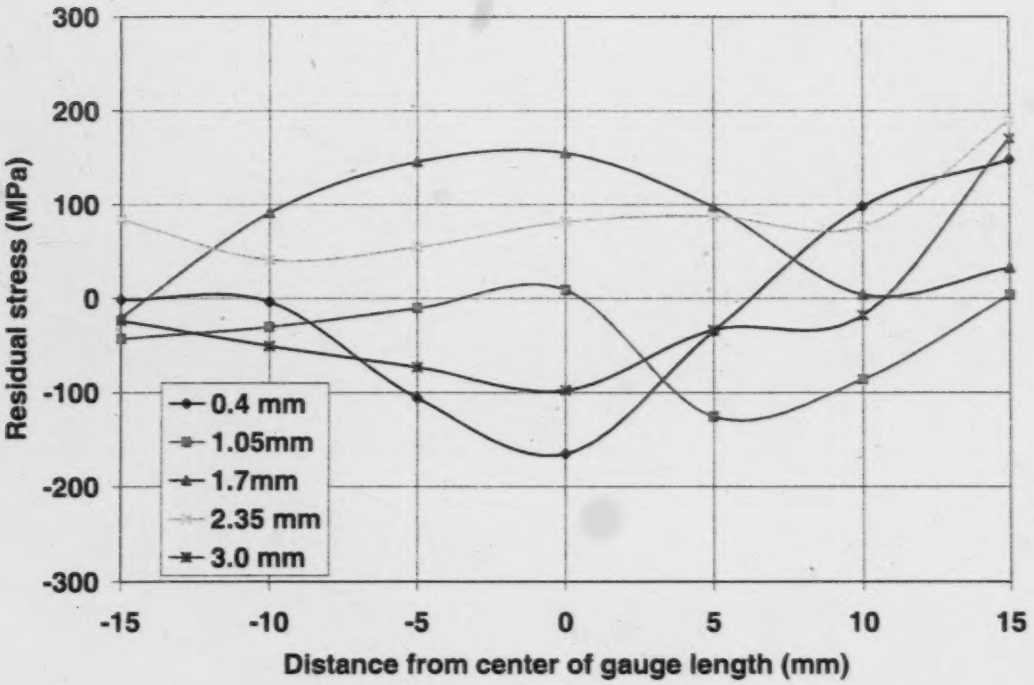

Figure 20: Axial (gauge length) residual stresses measured on the pre-conditioned tensile specimen 32.

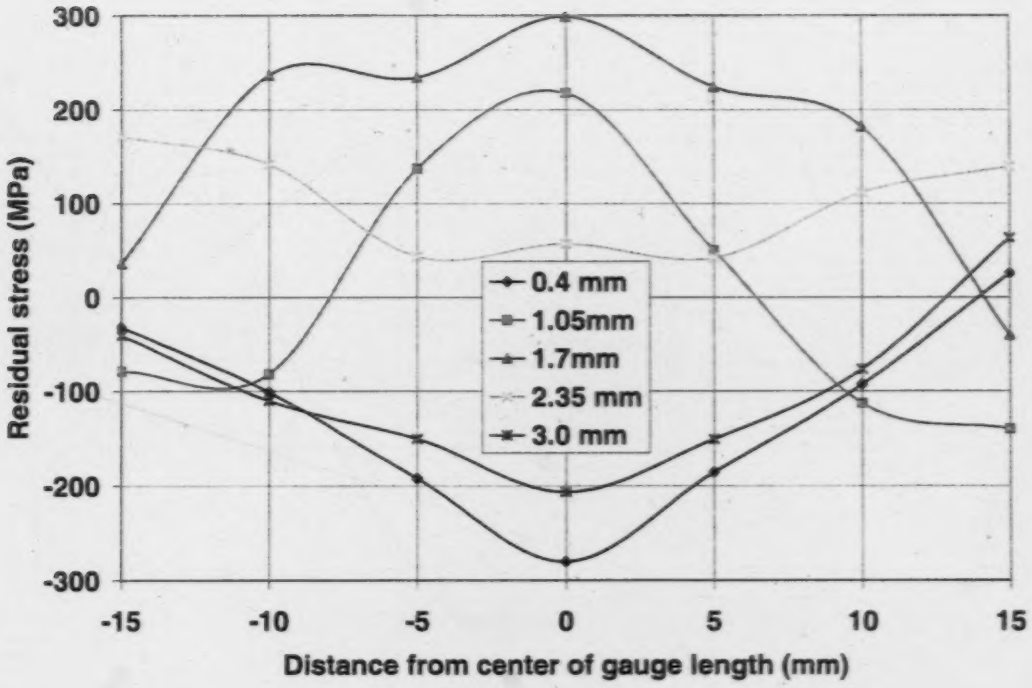

Figure 21: Axial (gauge length) residual stresses measured on tensile specimen 33.

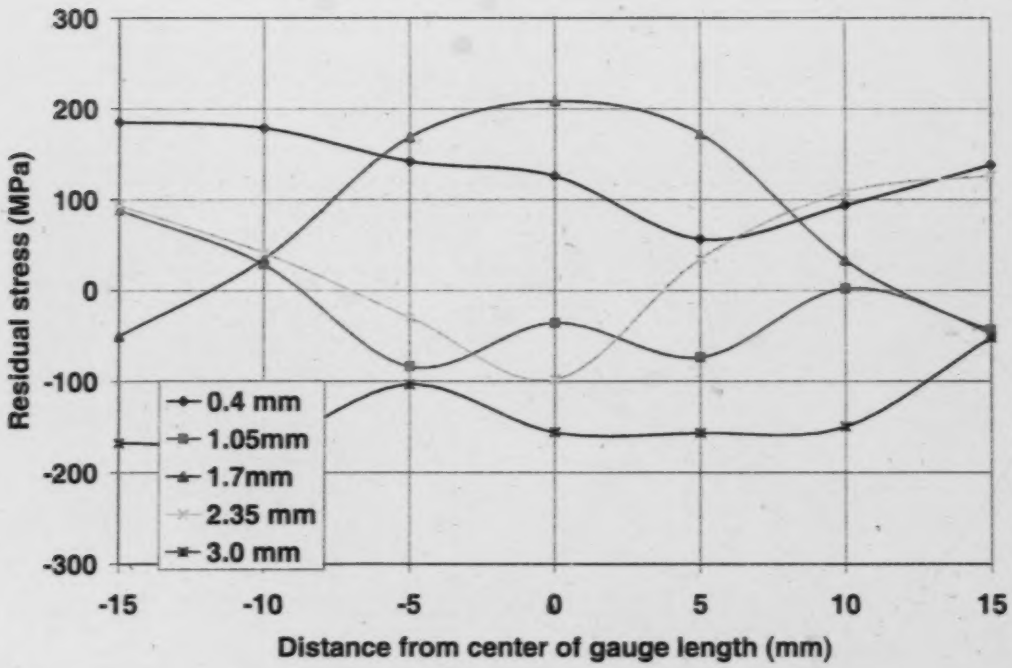

Figure 22: Axial (gauge length) residual stresses measured on tensile specimen 41.

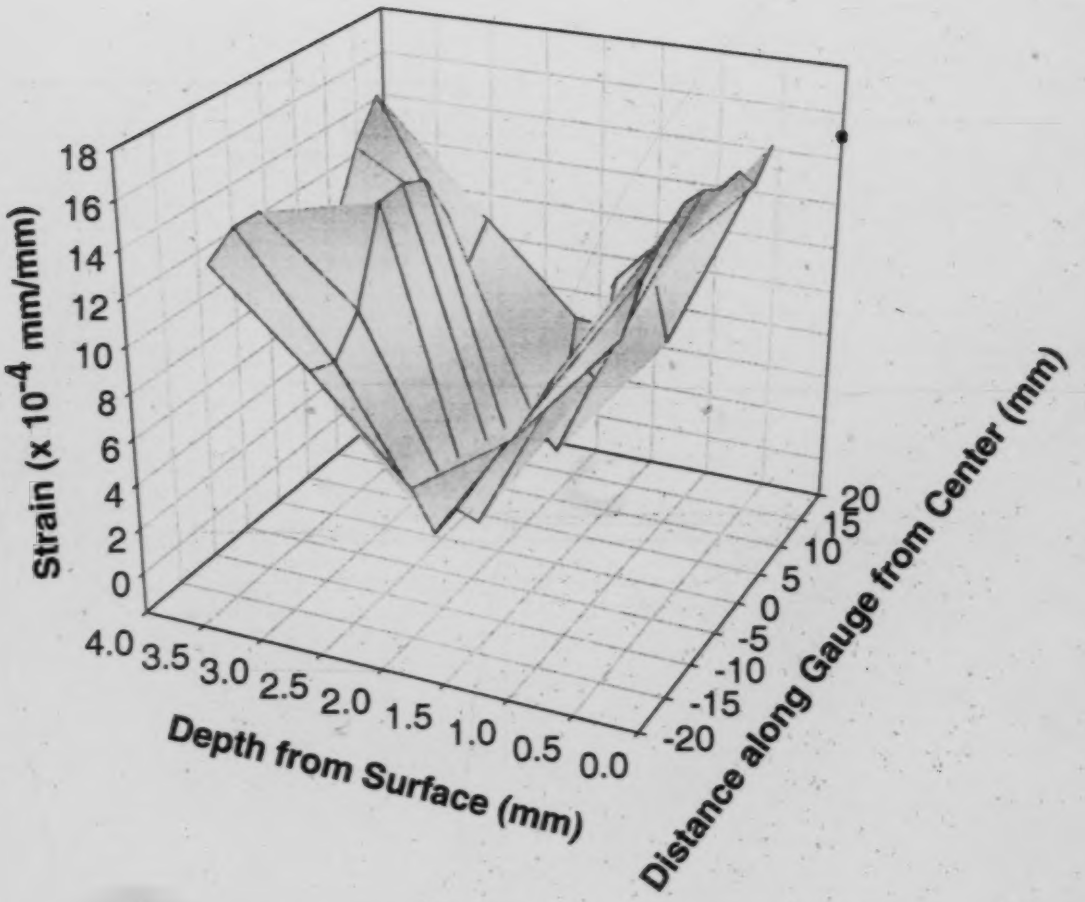

Figure 23: Axial (gauge length) strain measured on tensile specimen 21.

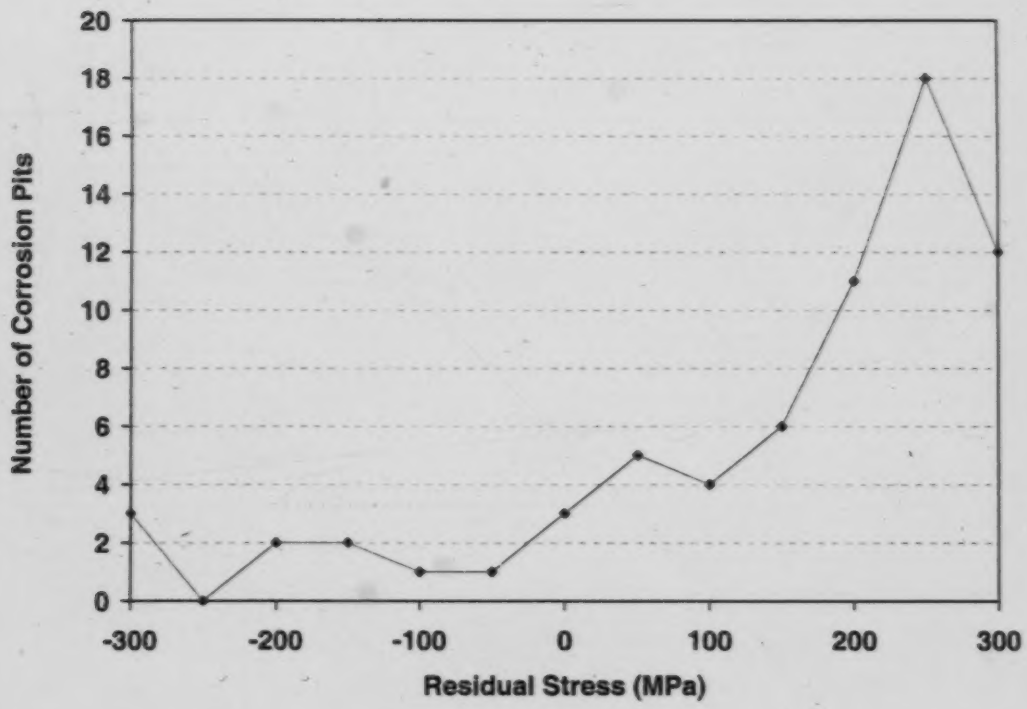

Figure 24: Number of corrosion pits versus residual stress level observed on the four tensile specimens after four months of testing in the cyclic loading experiment.

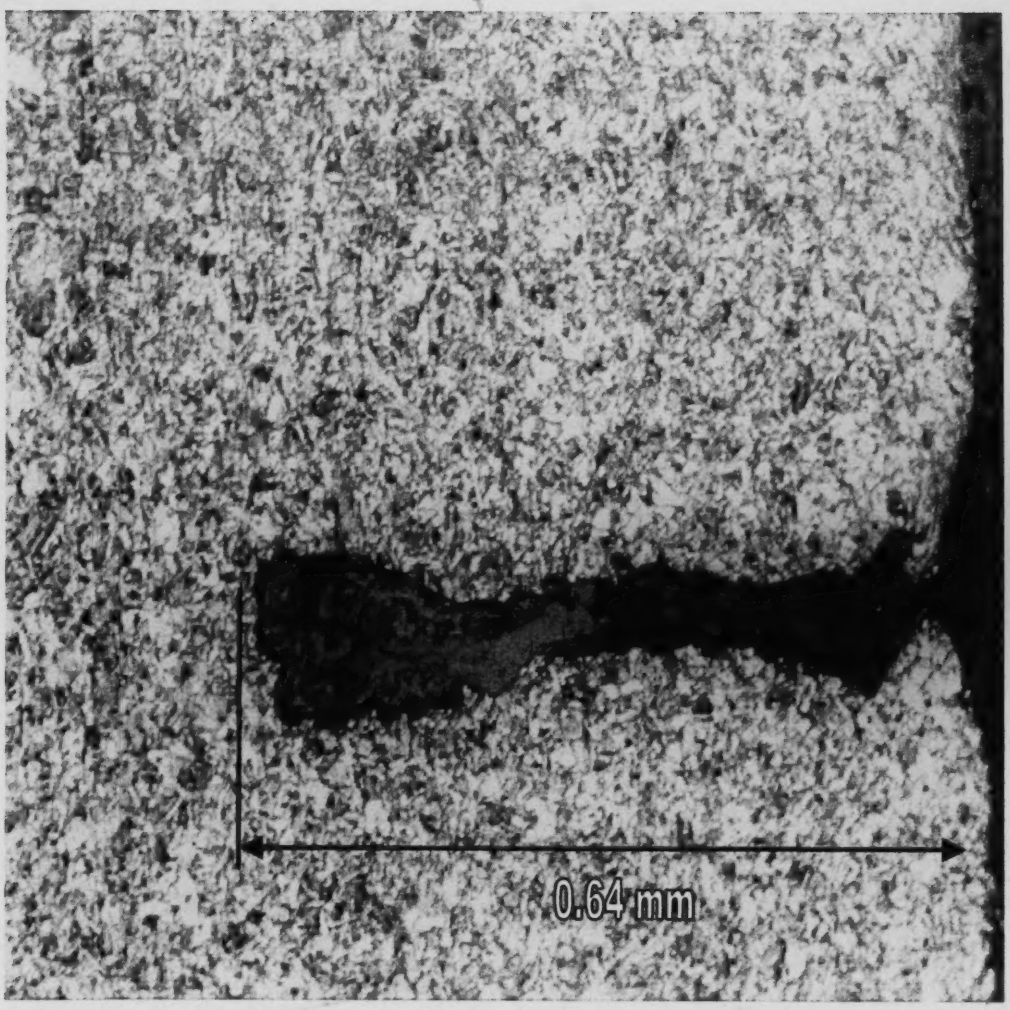

Figure 25: Crack formed in tensile specimen 13 during a four-month cyclic loading test in an aqueous environment. (2.1 mm from the gauge length center location).

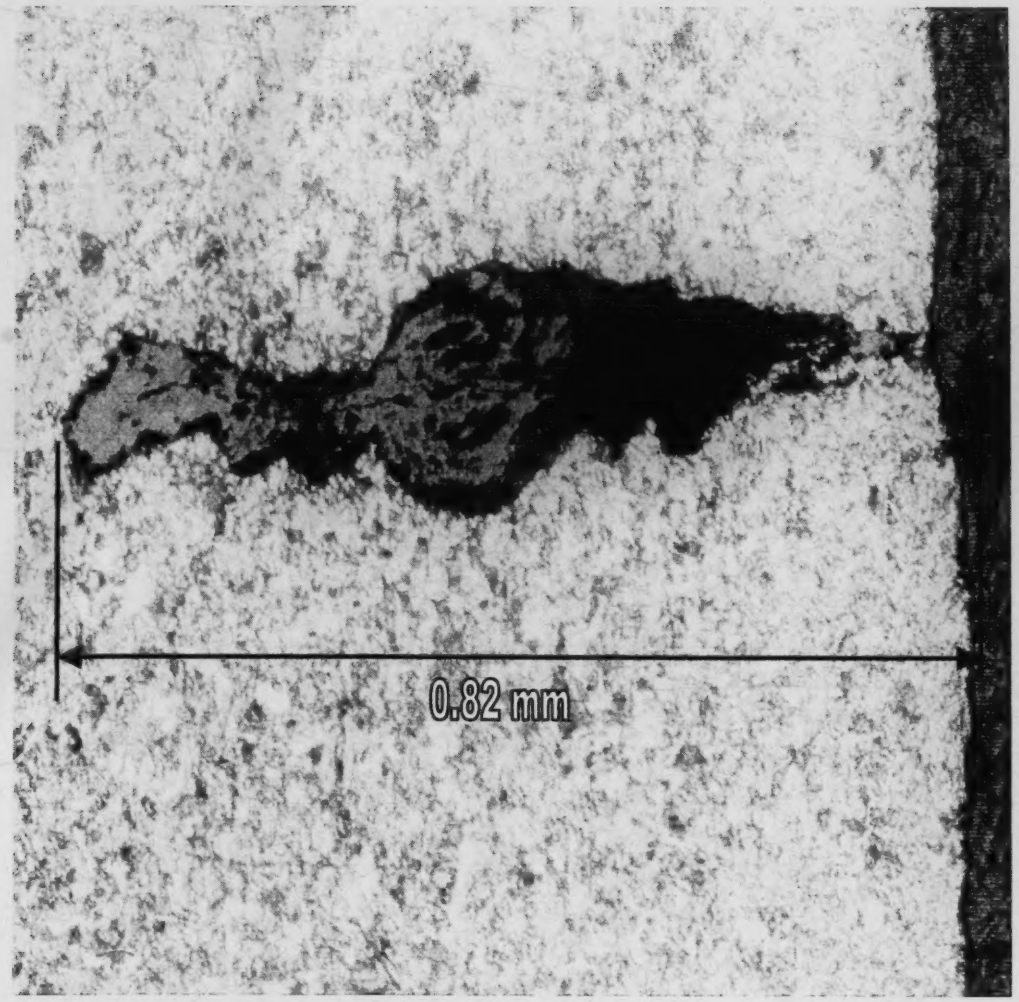

Figure 26: Crack formed in tensile specimen 13 during a four-month cyclic loading test in an aqueous environment. (2.0 mm from the gauge length center location).

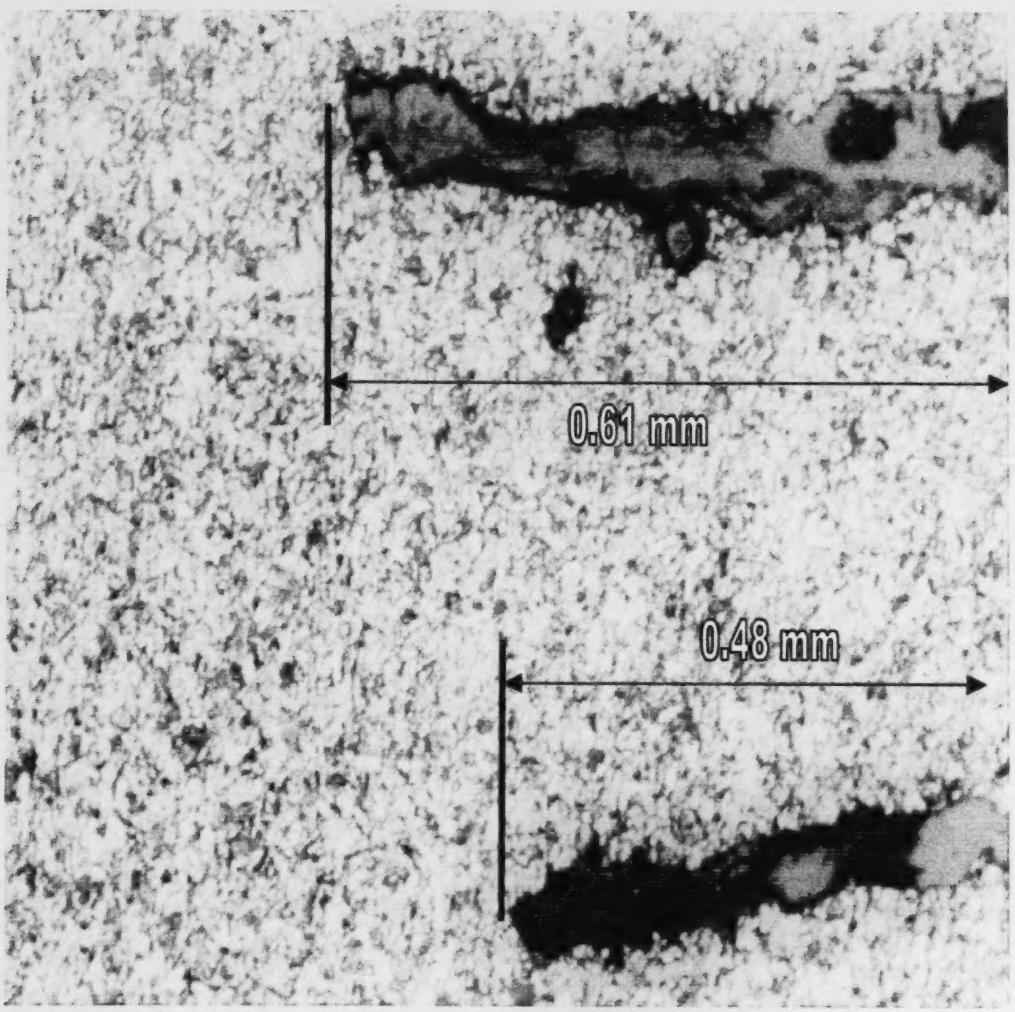

Figure 27: Two cracks formed in tensile specimen 13 during a four-month cyclic loading test in an aqueous environment. (-1.5 mm and – 3.7 mm from the gauge length center location)

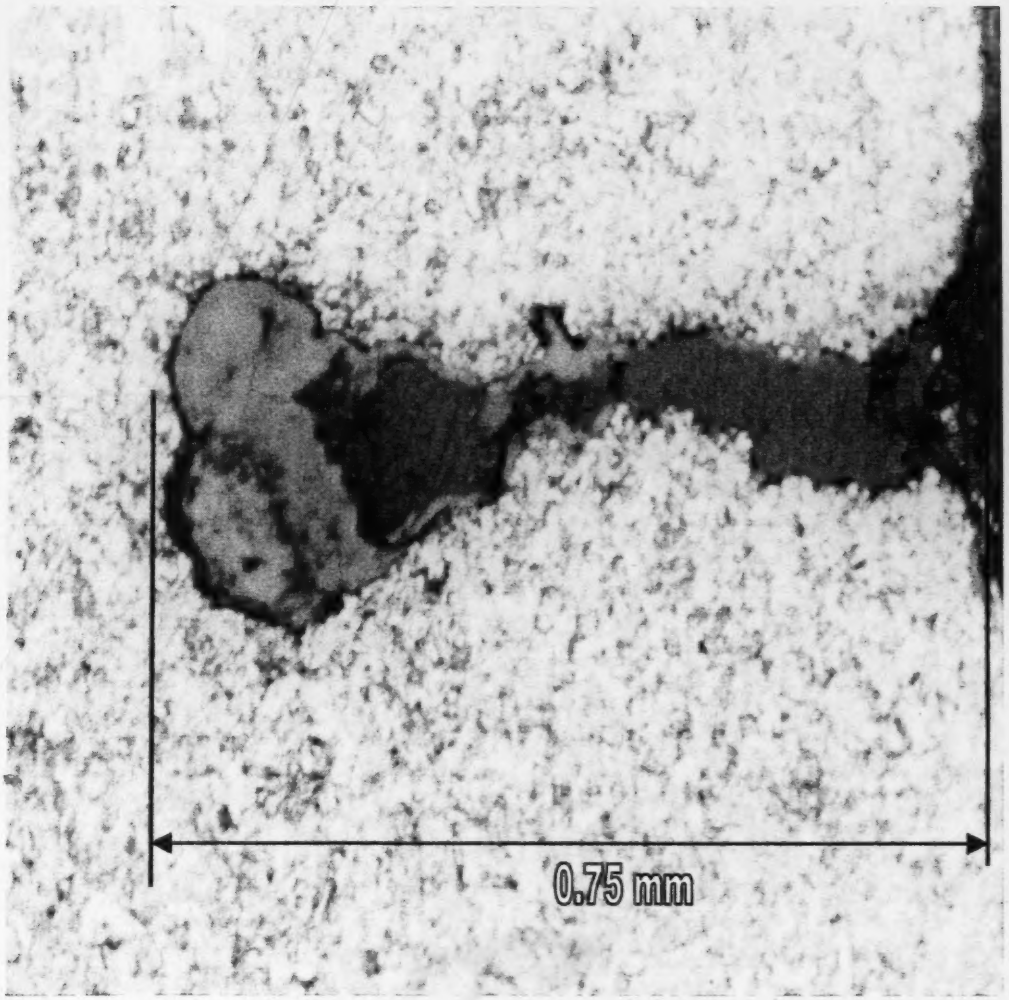

Figure 28: Crack formed in tensile specimen 13 during a four-month cyclic loading test in an aqueous environment. (-4.2 mm from the gauge length center location).

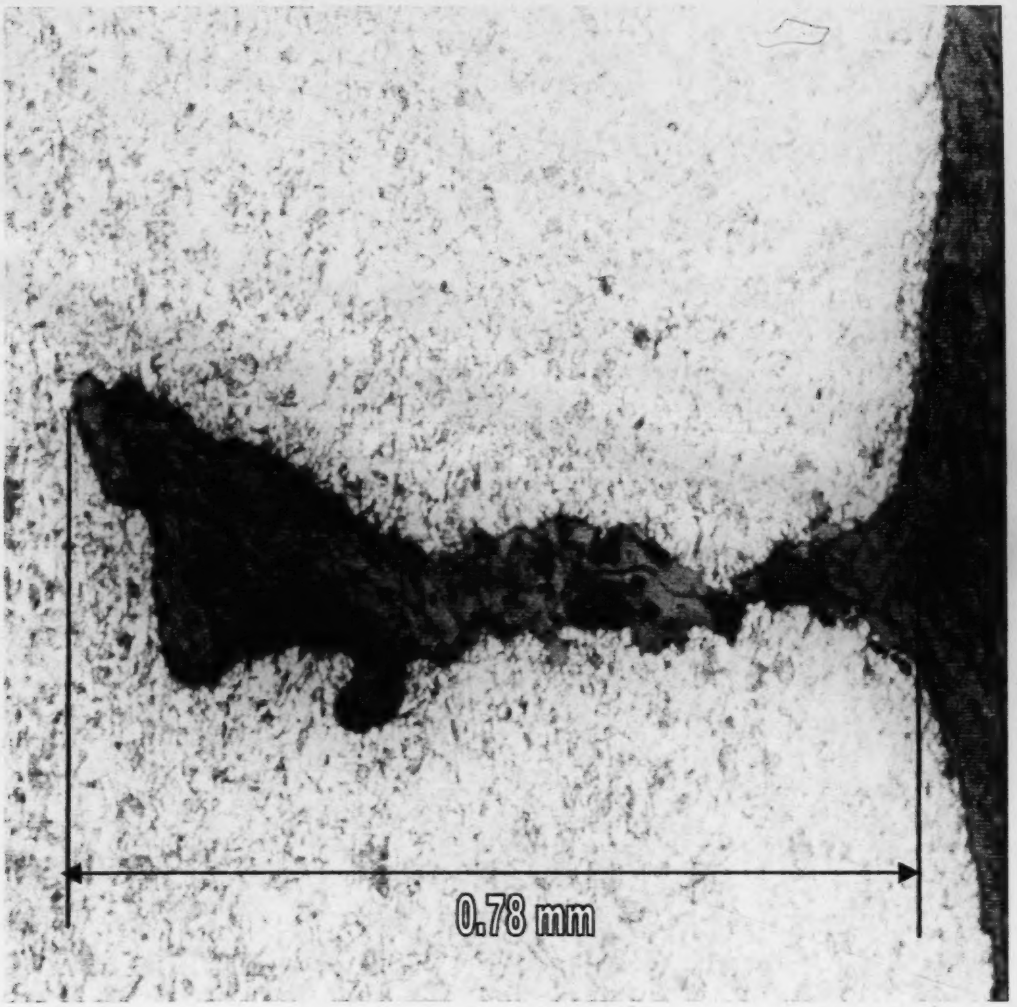

Figure 29: Crack formed in tensile specimen 13 during a four-month cyclic loading test in an aqueous environment. (-2.2 mm from the gauge length center location).

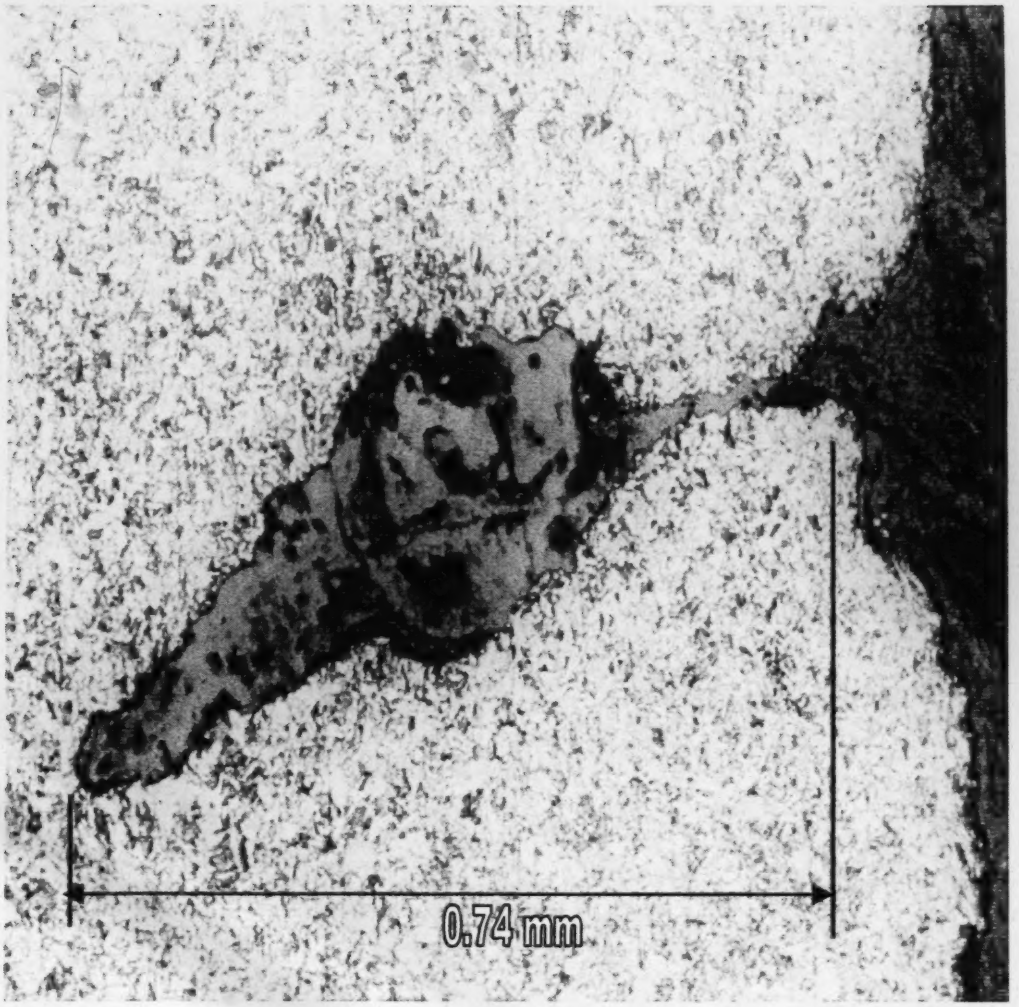

Figure 30: Crack formed in tensile specimen 21 during a four-month cyclic loading test in an aqueous environment. (-3.4 mm from the gauge length center location).

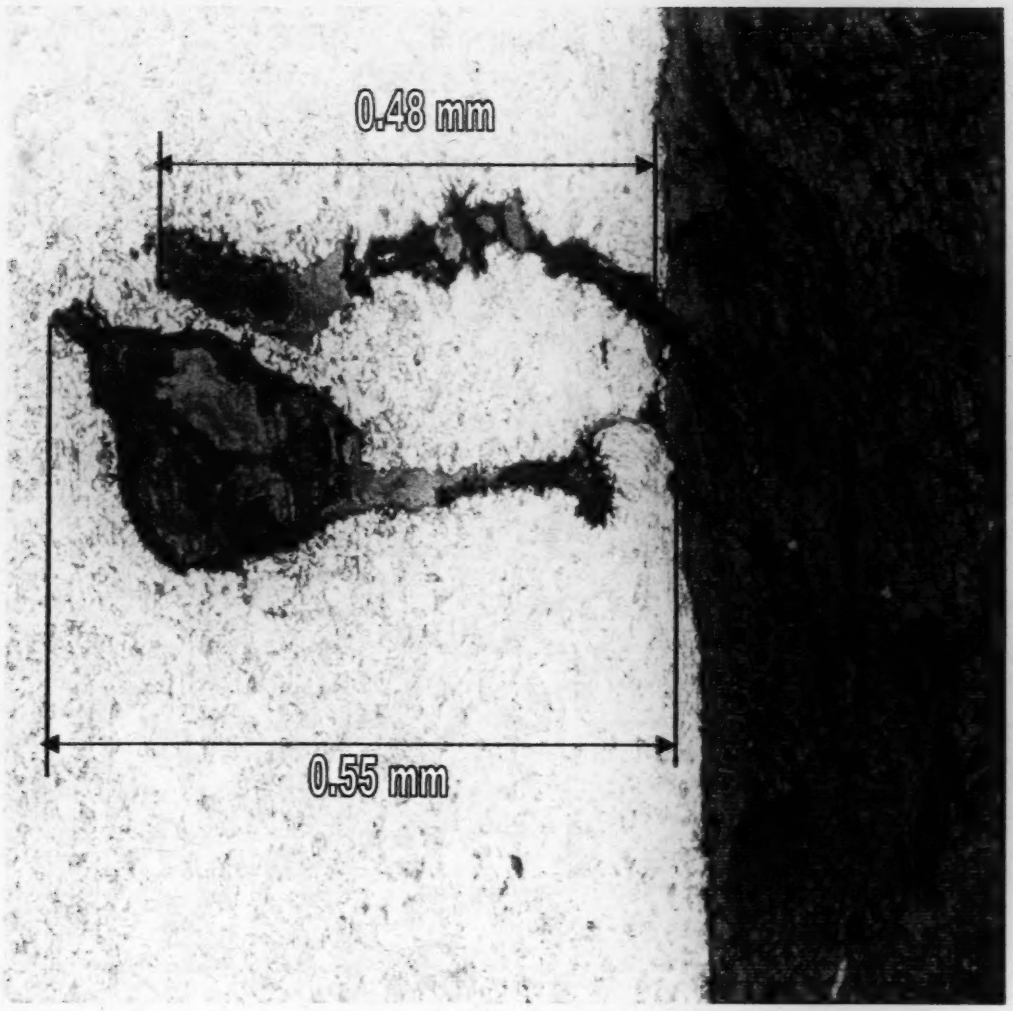

Figure 31: Two cracks formed in tensile specimen 21 during a four-month cyclic loading test in an aqueous environment. (-4.2 mm and –3.9 mm from the gauge length center location).

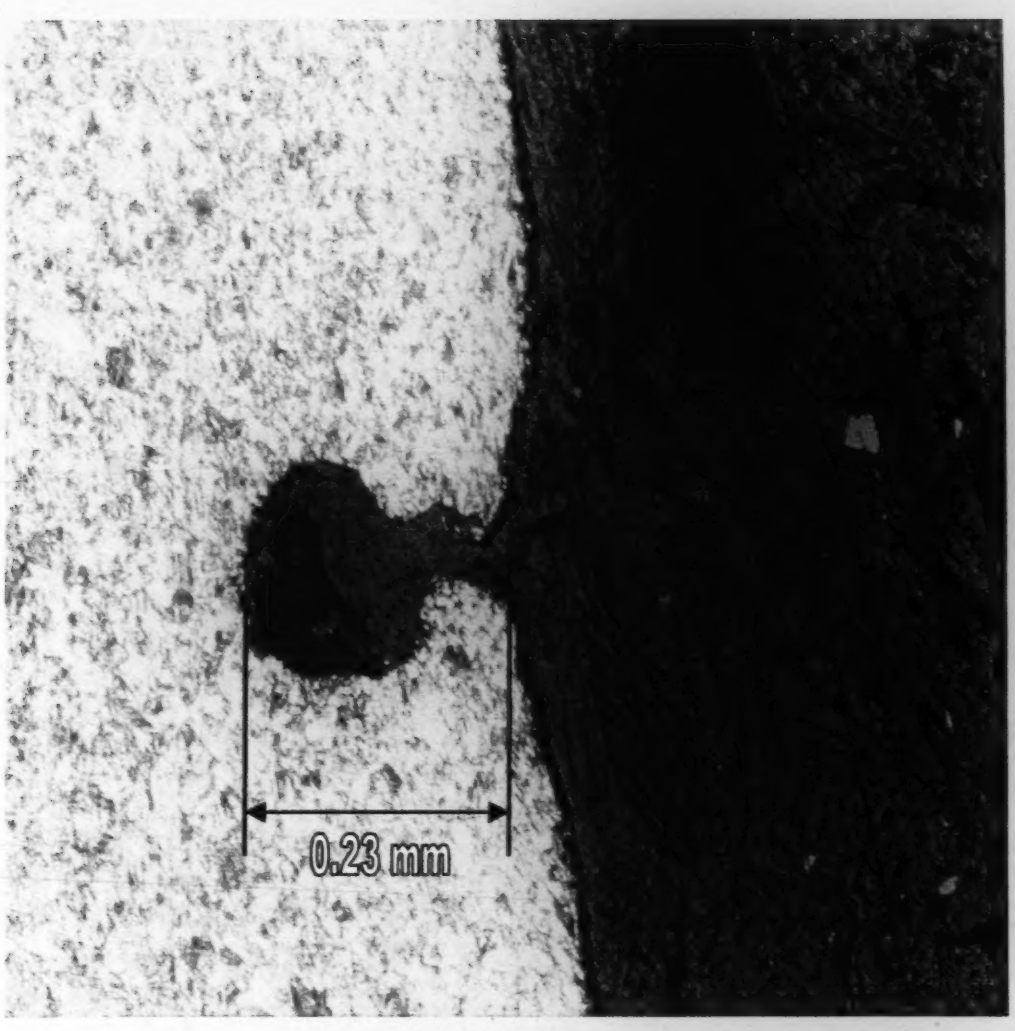

Figure 32: Crack formed in tensile specimen 21 during a four-month cyclic loading test in an aqueous environment. (-4.0 mm from the gauge length center location).

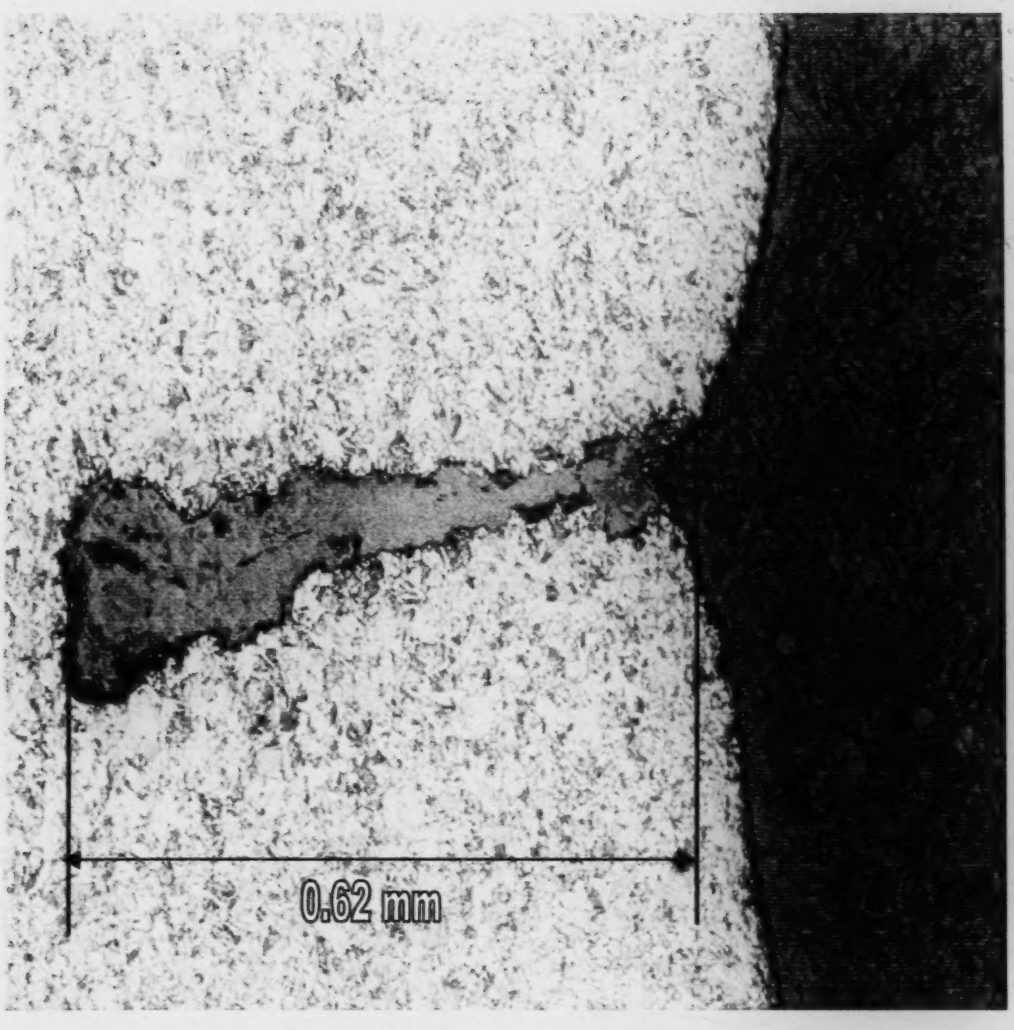

Figure 33: Crack formed in tensile specimen 21 during a four-month cyclic loading test in an aqueous environment. (4.3 mm from the gauge length center location).

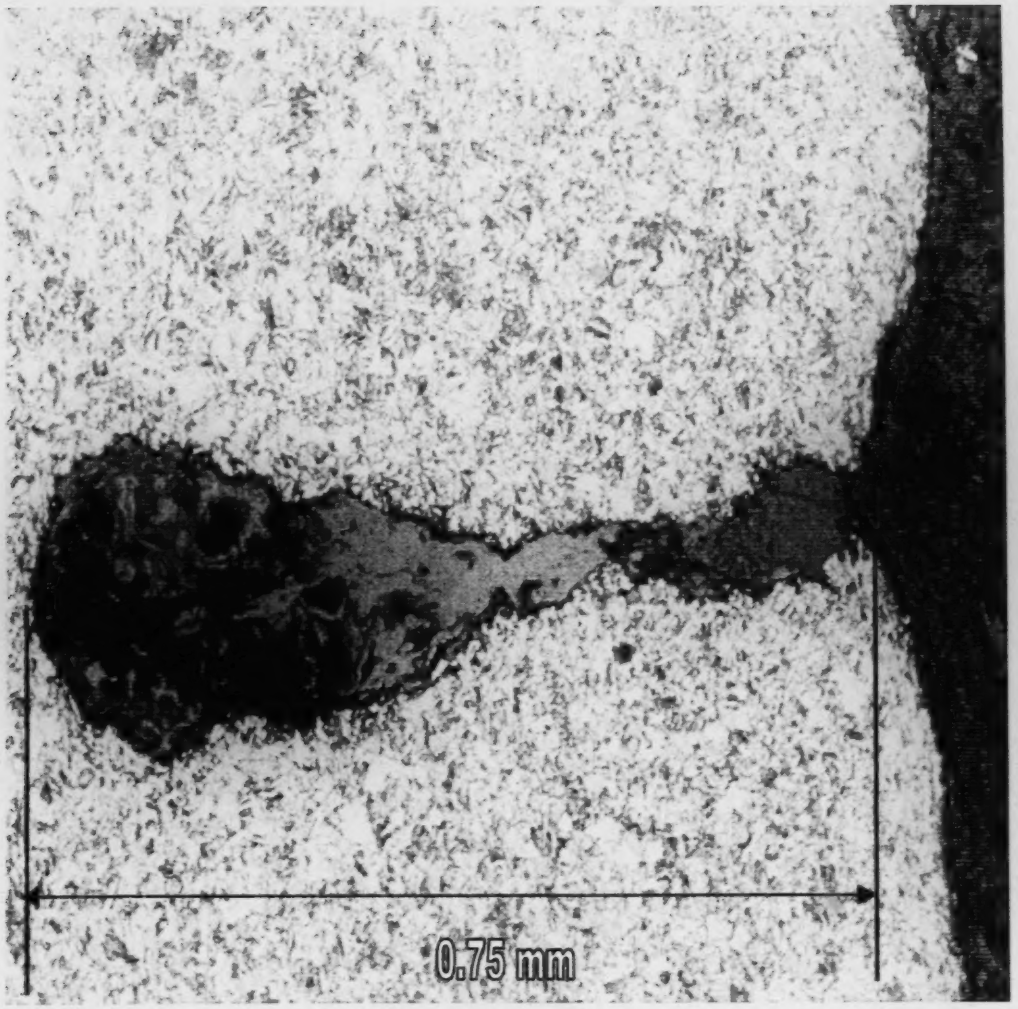

Figure 34: Crack formed in tensile specimen 22 during a four-month cyclic loading test in an aqueous environment. (4.8 mm from the gauge length center location).

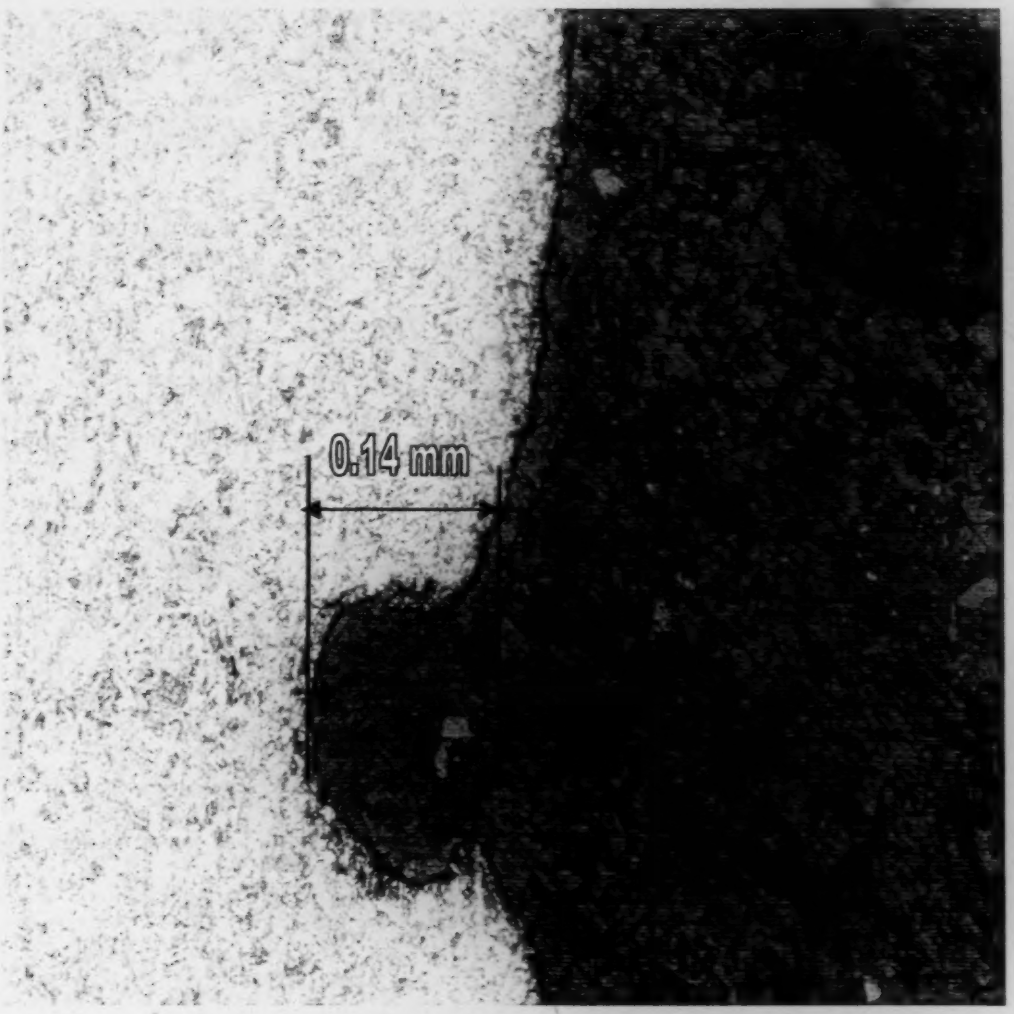

Figure 35: Crack formed in tensile specimen 31 during a four-month cyclic loading test in an aqueous environment. (14.1 mm from the gauge length center location).

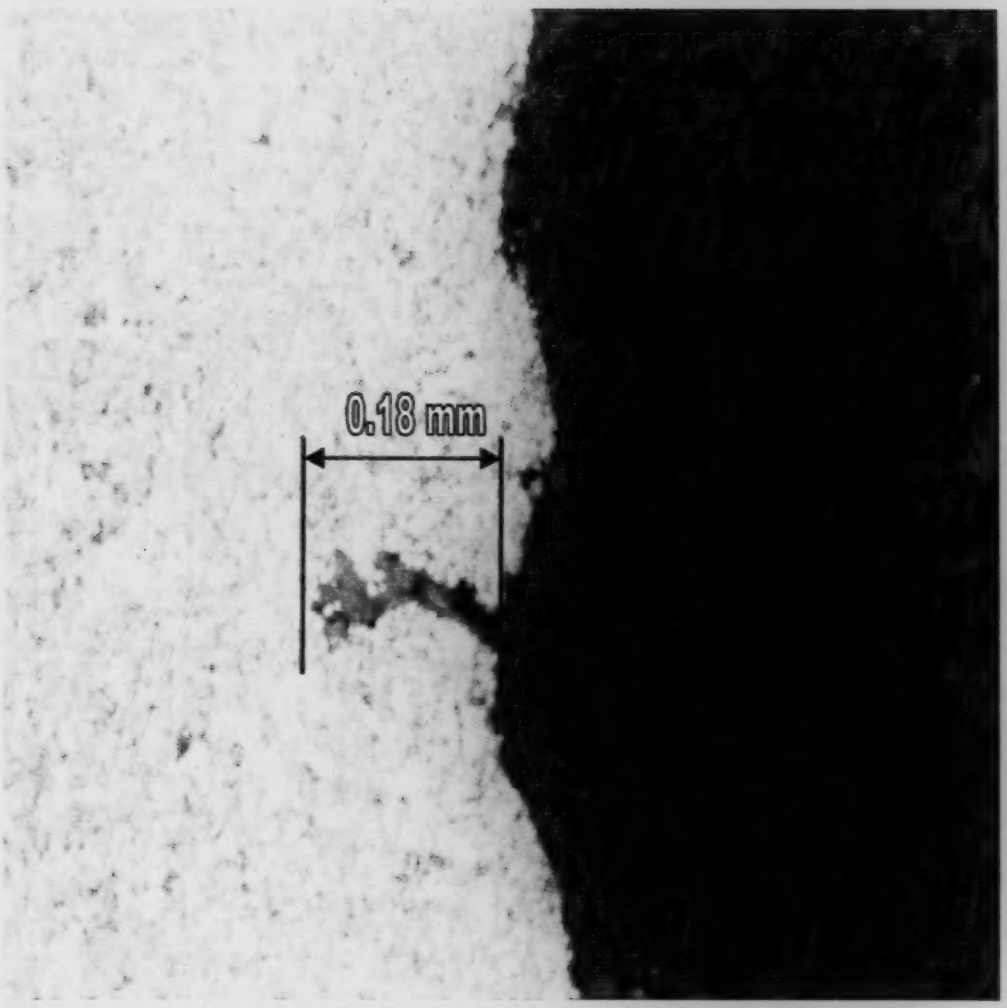

Figure 36: Crack formed in tensile specimen 31 during a four-month cyclic loading test in an aqueous environment. (14.2 mm from the gauge length center location).

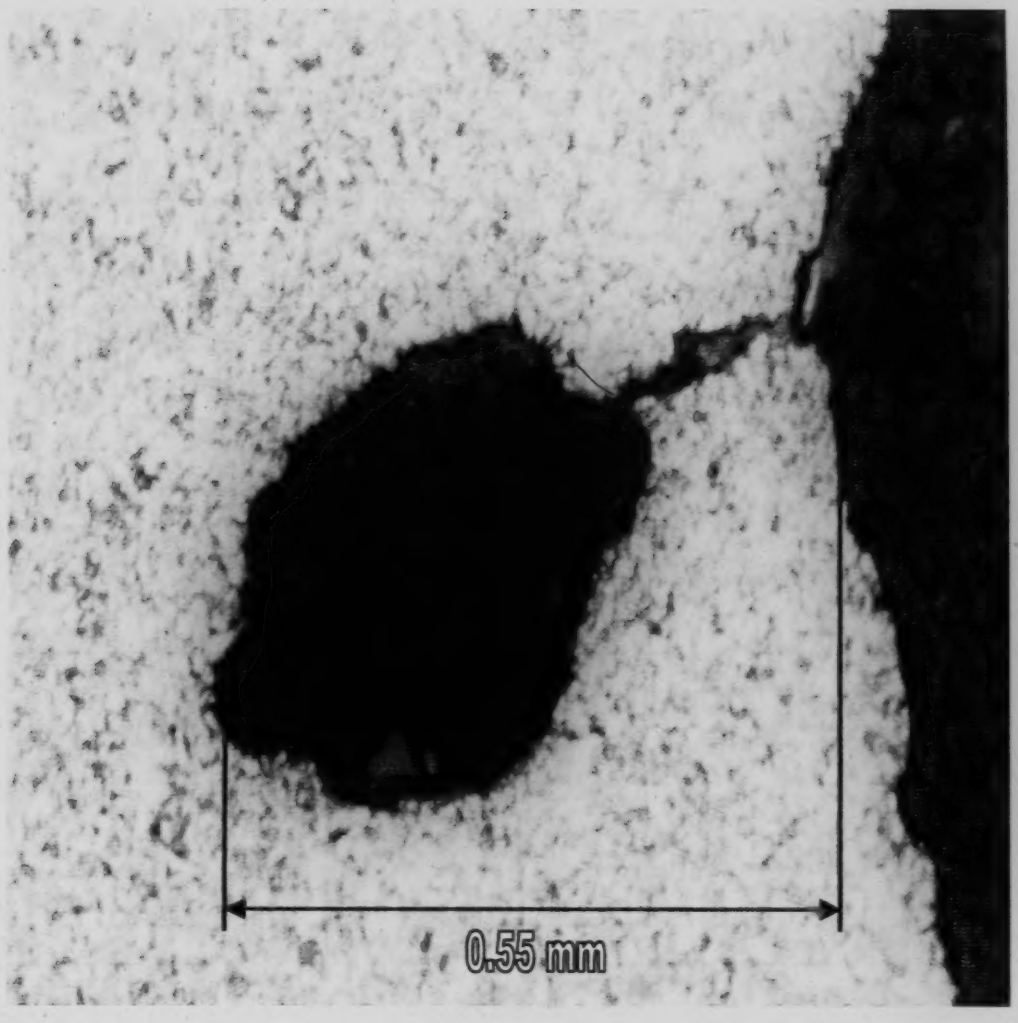

Figure 37: Crack formed in tensile specimen 22 during a four-month cyclic loading test in an aqueous environment. (5.0 mm from the gauge length center location).

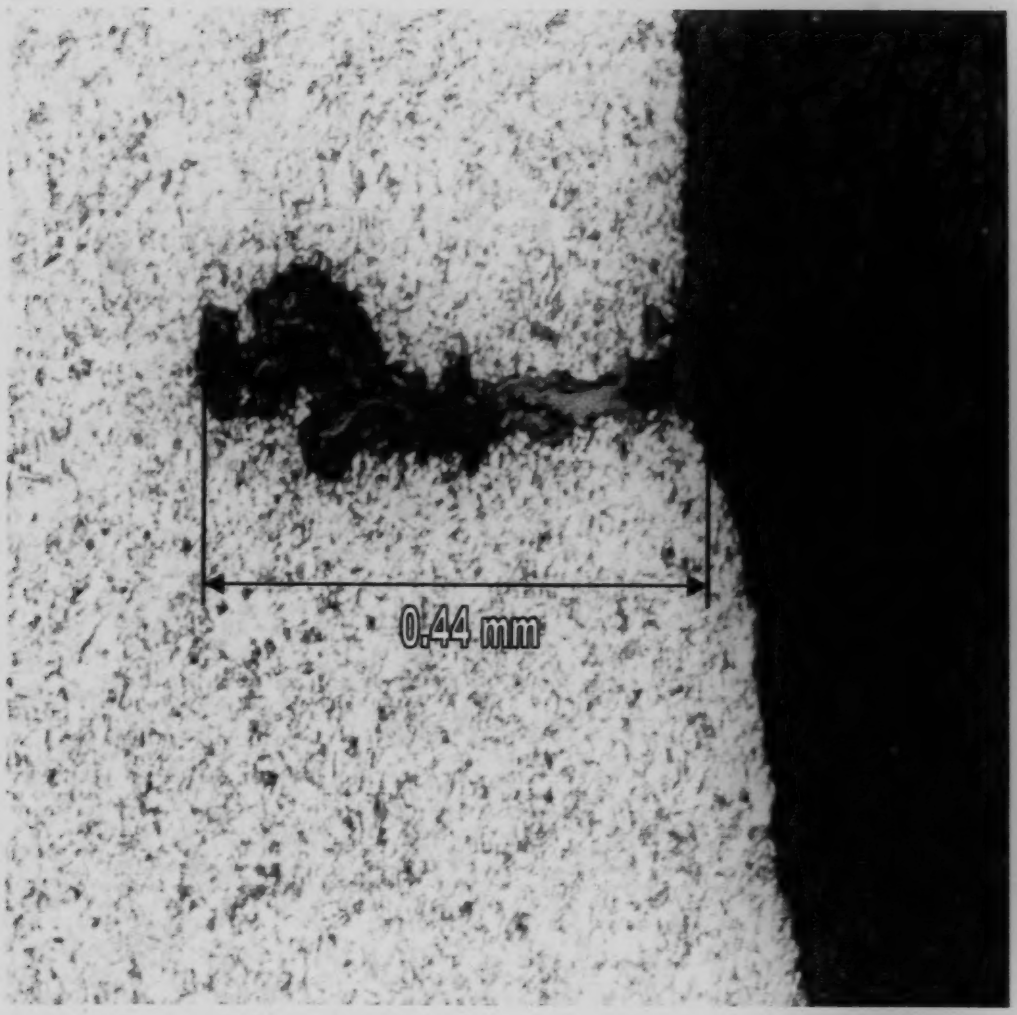

Figure 38: Crack formed in tensile specimen 22 during a four-month cyclic loading test in an aqueous environment. (0.9 mm from the gauge length center location).

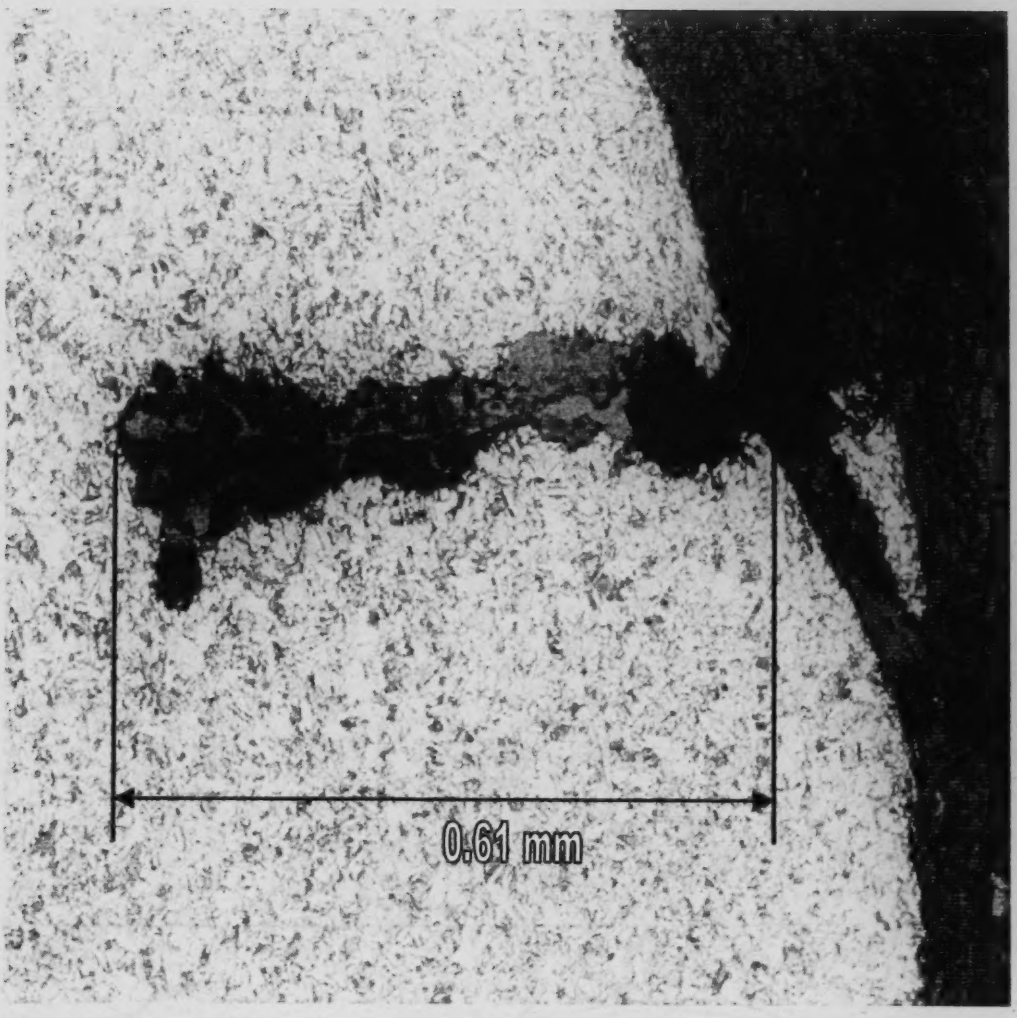

Figure 39: Crack formed in tensile specimen 22 during a four-month cyclic loading test in an aqueous environment. (6.8 mm from the gauge length center location).

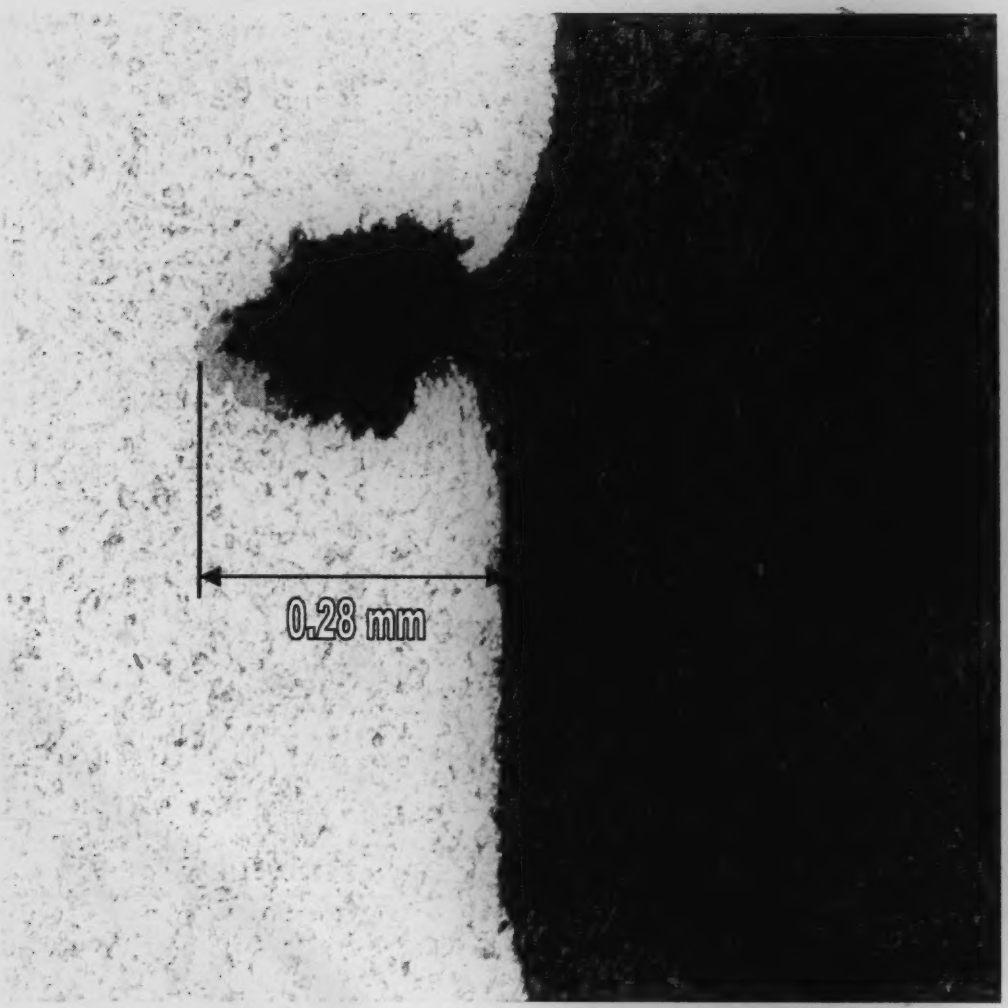

Figure 40: Crack formed in tensile specimen 22 during a four-month cyclic loading test in an aqueous environment. (6.7 mm from the gauge length center location).

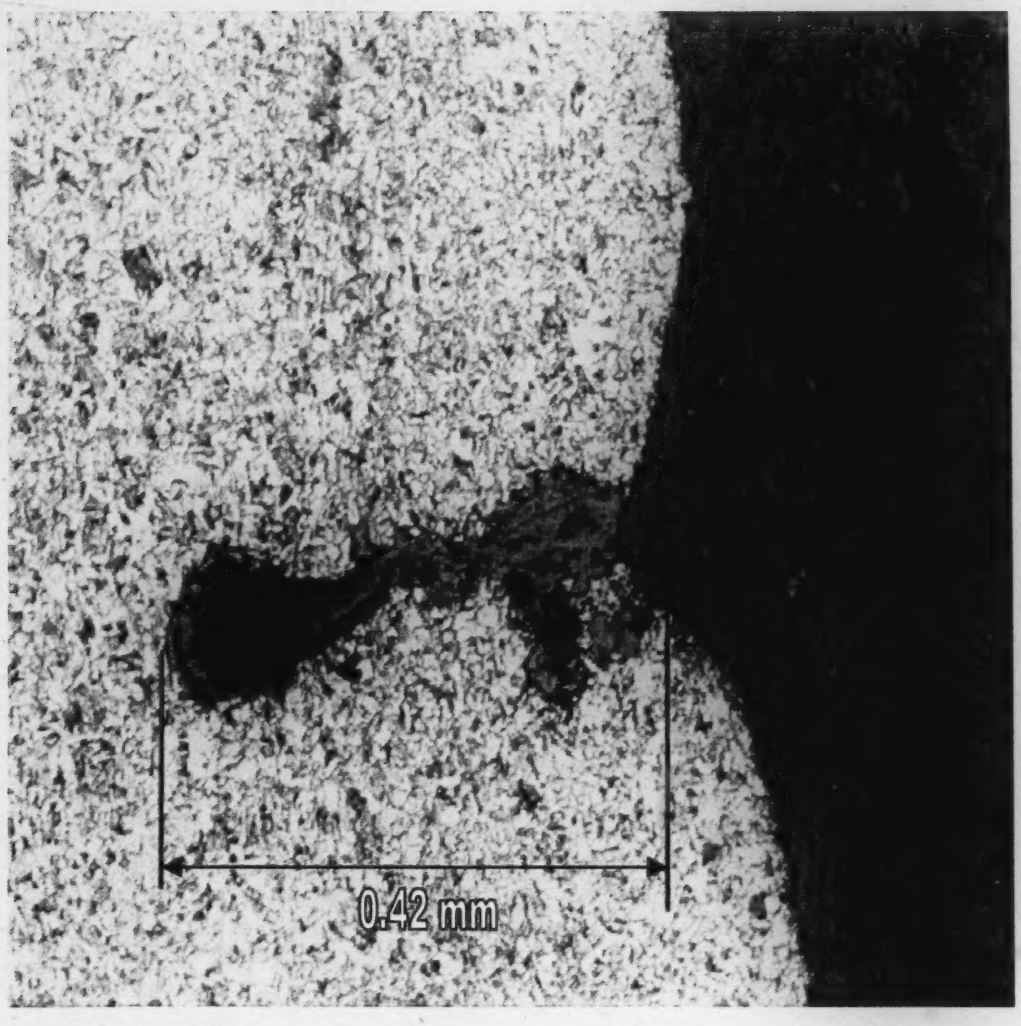

Figure 41: Crack formed in tensile specimen 22 during a four-month cyclic loading test in an aqueous environment. (-3.1 mm from the gauge length center location).

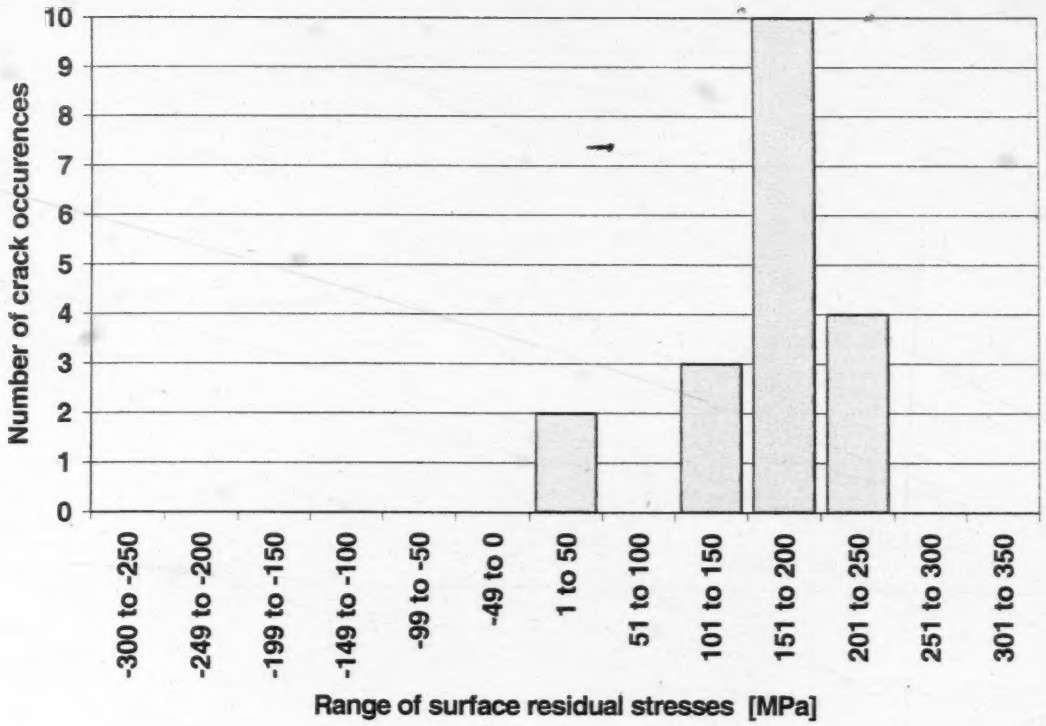

Figure 42: Measured surface residual stress versus frequency of cracking of four tensile specimens after a four-month cyclic loading experiment.

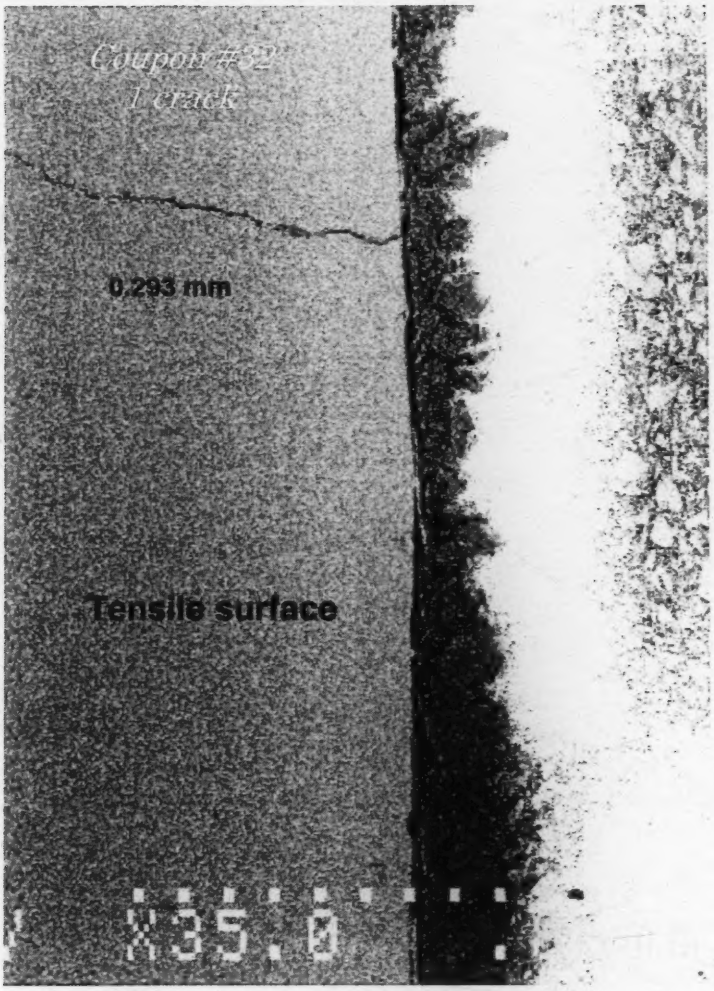

Figure 43: Electron micrograph of cracking in pre-conditioned tensile specimen 32.

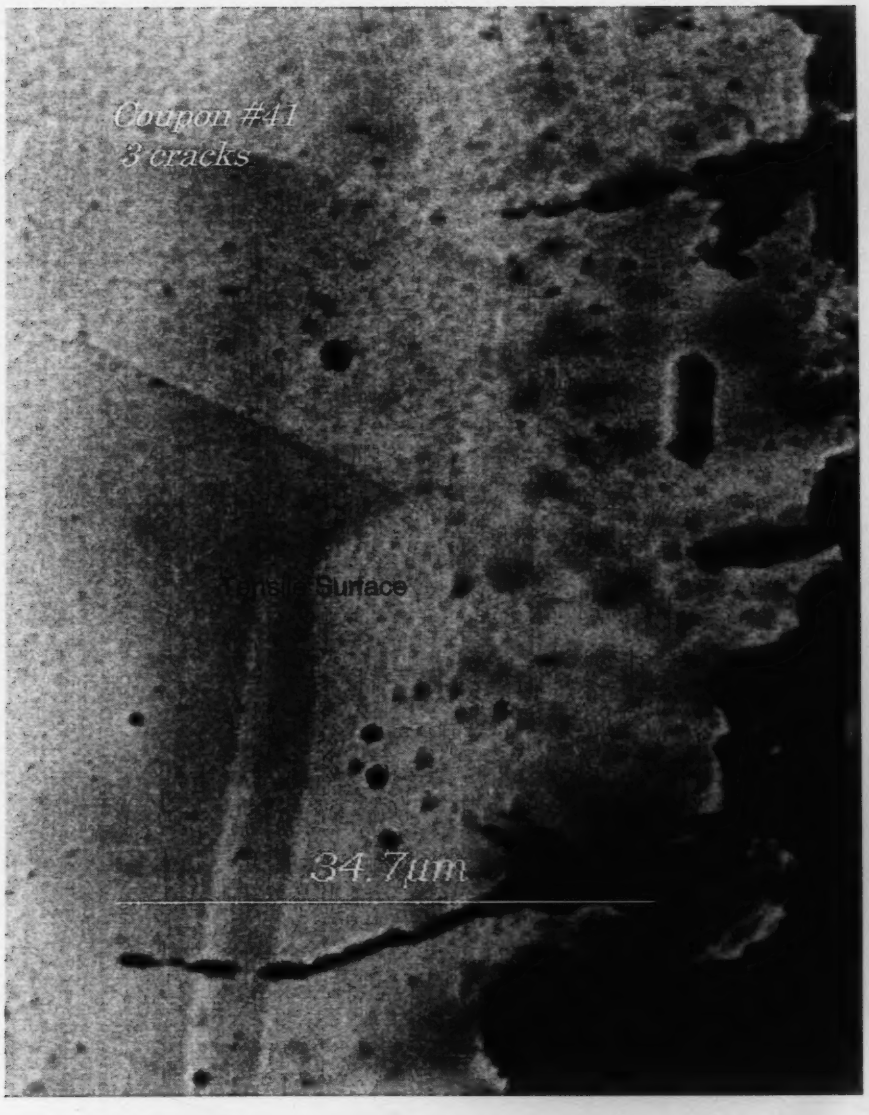

Figure 44: Electron micrograph of cracking in tensile specimen 41.

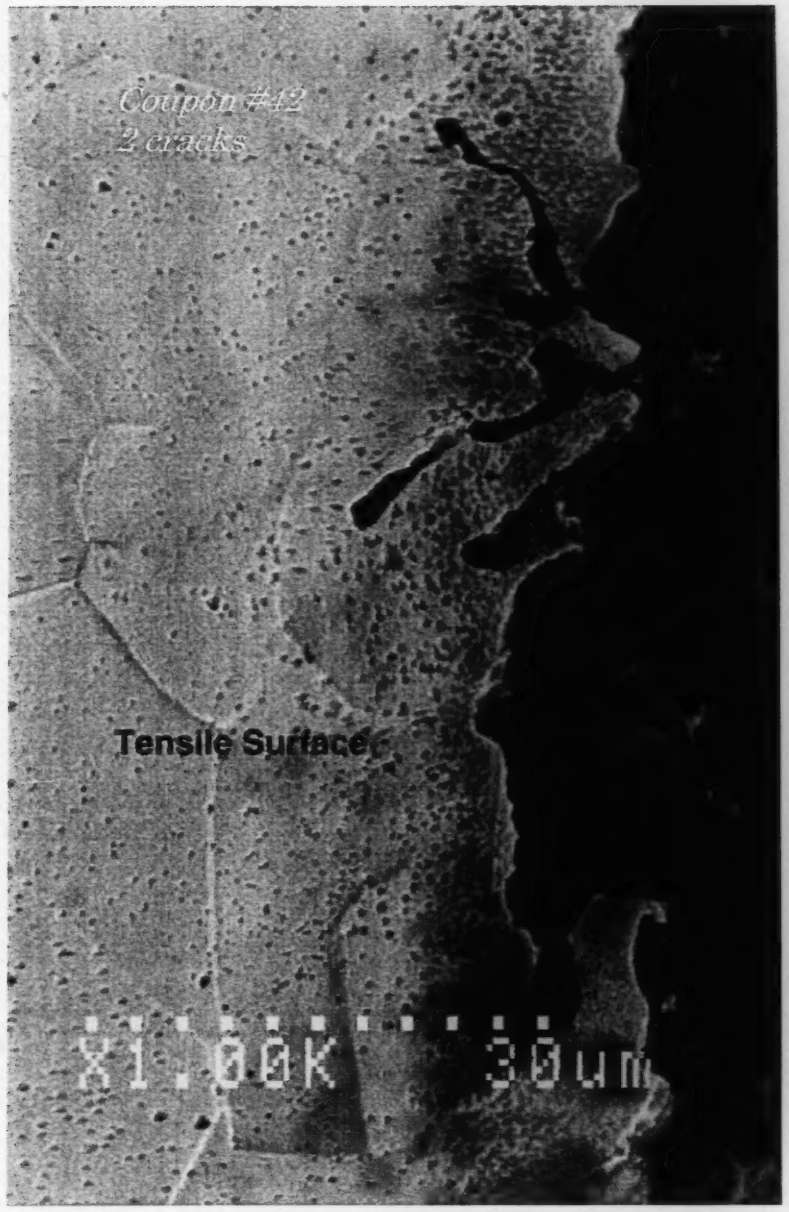

Figure 45: Electron micrograph of cracking in tensile specimen 42.

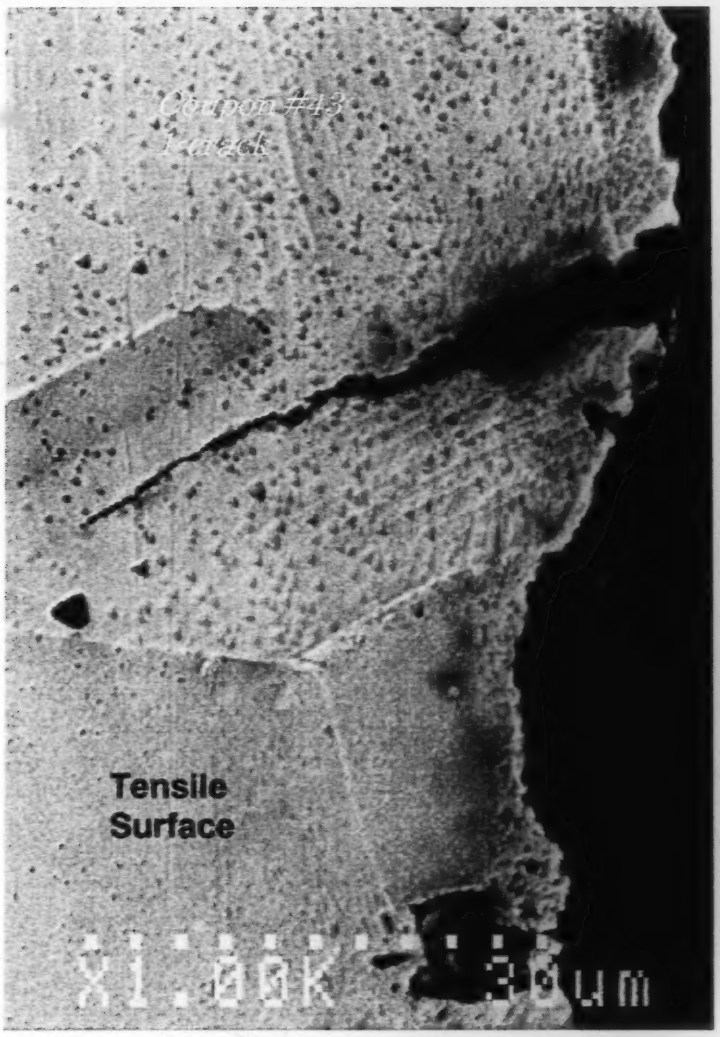

Figure 46: Electron micrograph of cracking in tensile specimen 43.

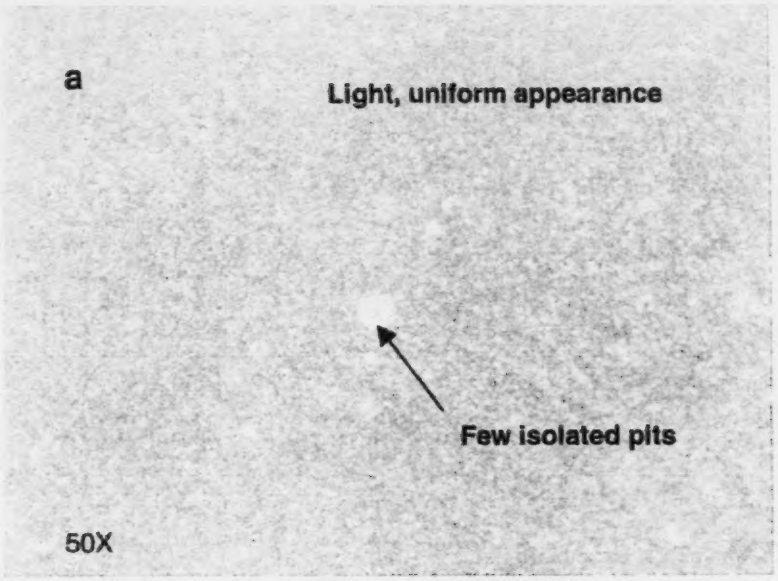

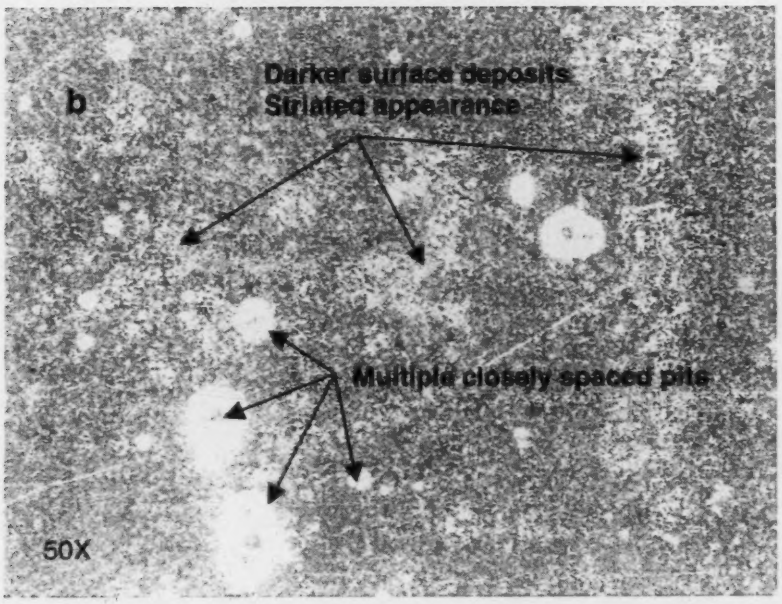

Figure 47: Optical micrograph of compressive residual stress surface area (**a**) and tensile residual stress surface area (**b**) after a twelve day exposure in a modified SSRT experiment.

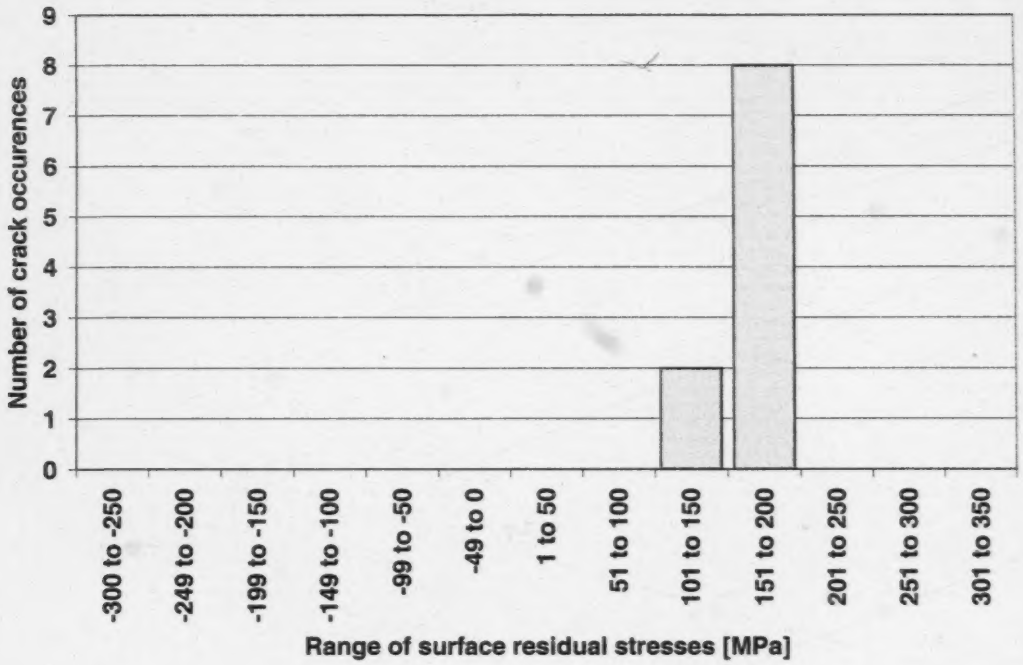

Figure 48: Measured surface residual stress versus frequency of cracking on six tensile specimens tested in the twelve day modified slow strain rate experiment.

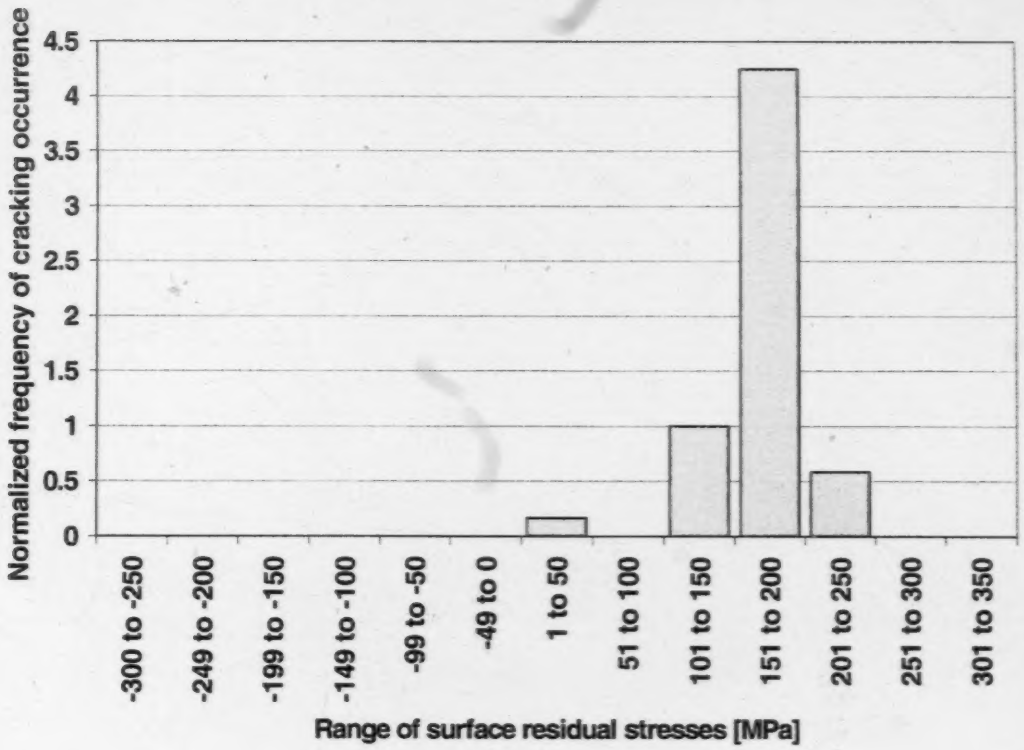

Figure 49: Measured surface residual stress versus normalized frequency of cracking for all cracks detected.

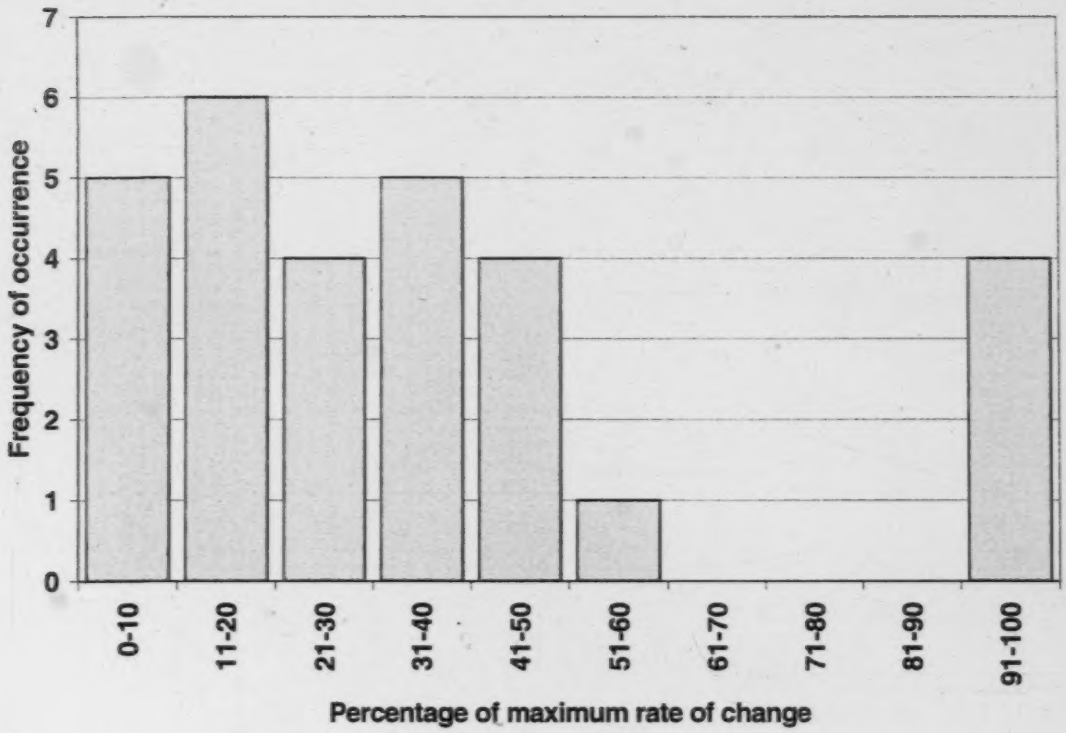

Figure 50: Frequency of the absolute rate of change of residual stress at each cracking location as a percentage of the maximum rate of change of residual stress measured for each tensile specimen.

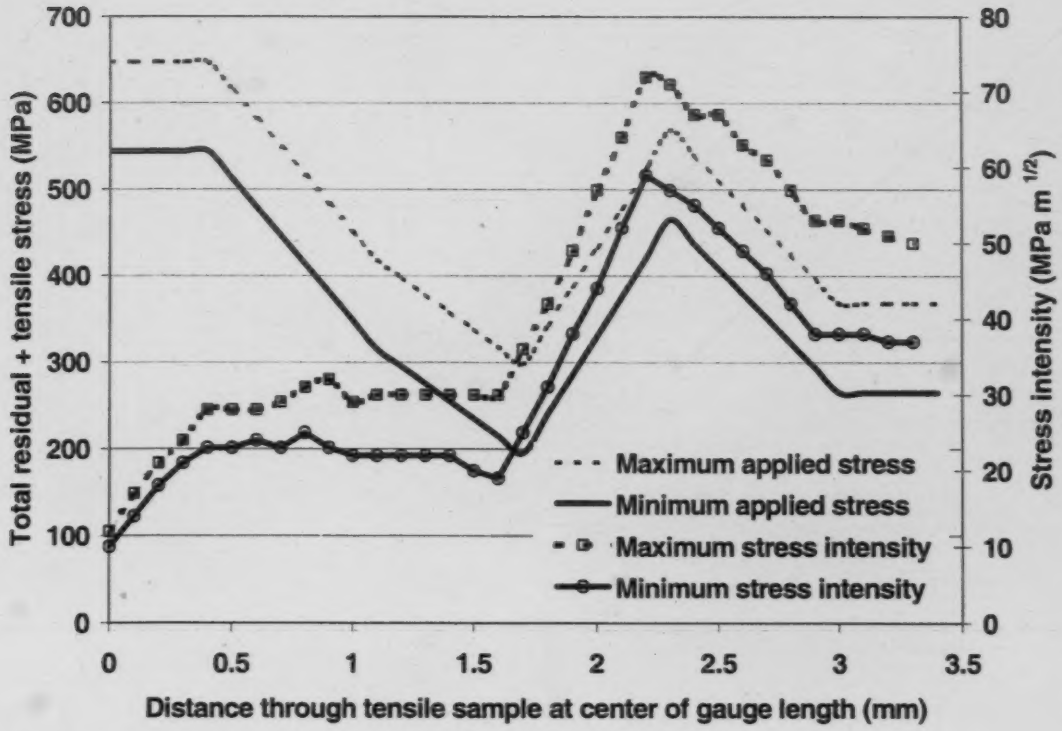

Figure 51: Stress and stress intensity for a theoretical crack propagating though the center of the gauge section on tensile specimen 13.

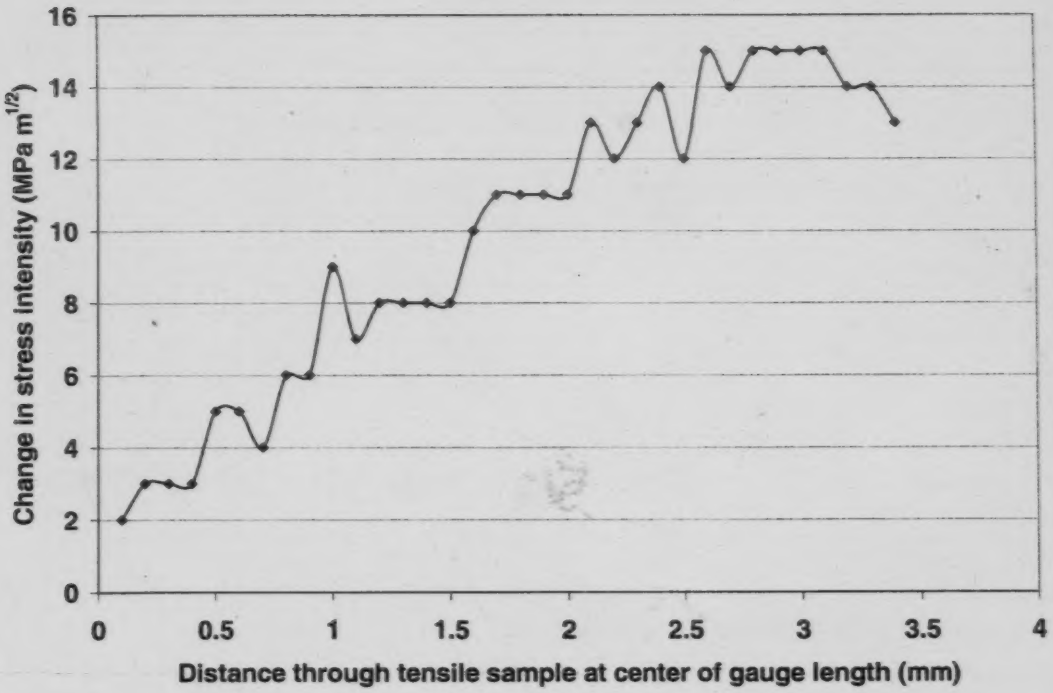

Figure 52: The change in stress intensity (ΔK) experienced by a crack propagating through the center of the gauge section on tensile specimen 13 when calculated from the experimental cyclic stress and measured residual stress.

10.0 APPENDICES

APPENDIX A

Tensile specimen schematic

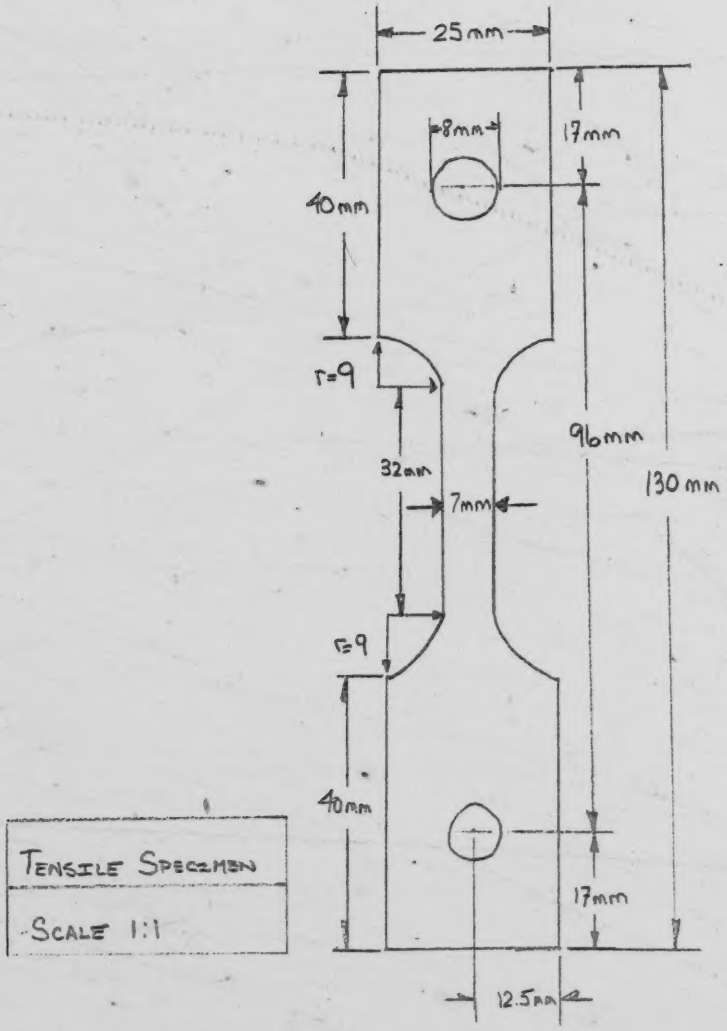

APPENDIX B

Environmental cell schematic: Top view and bottom view.

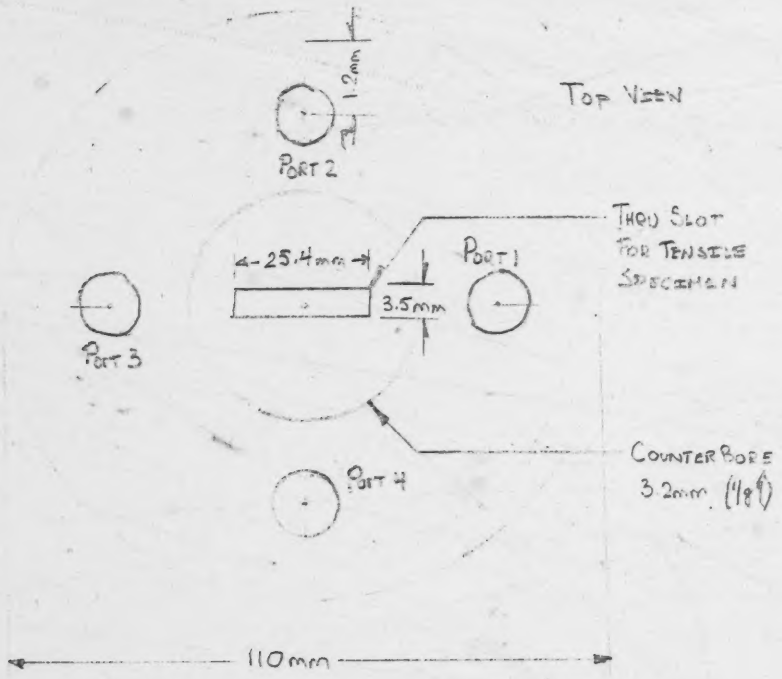

Ports Tap NPT 1/8"

#1 - Reference Electrode

#2 - Purge Gas Out

#3 - Counter Electrode

#4 - Solution Fill

#5 - Purge Gas In

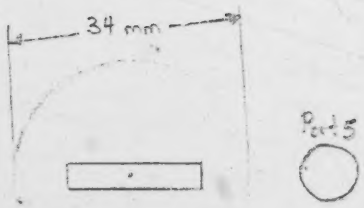

Plexiglass Cell
Scale 4:5

APPENDIX B (Continued)

Environmental cell schematic: Side view.

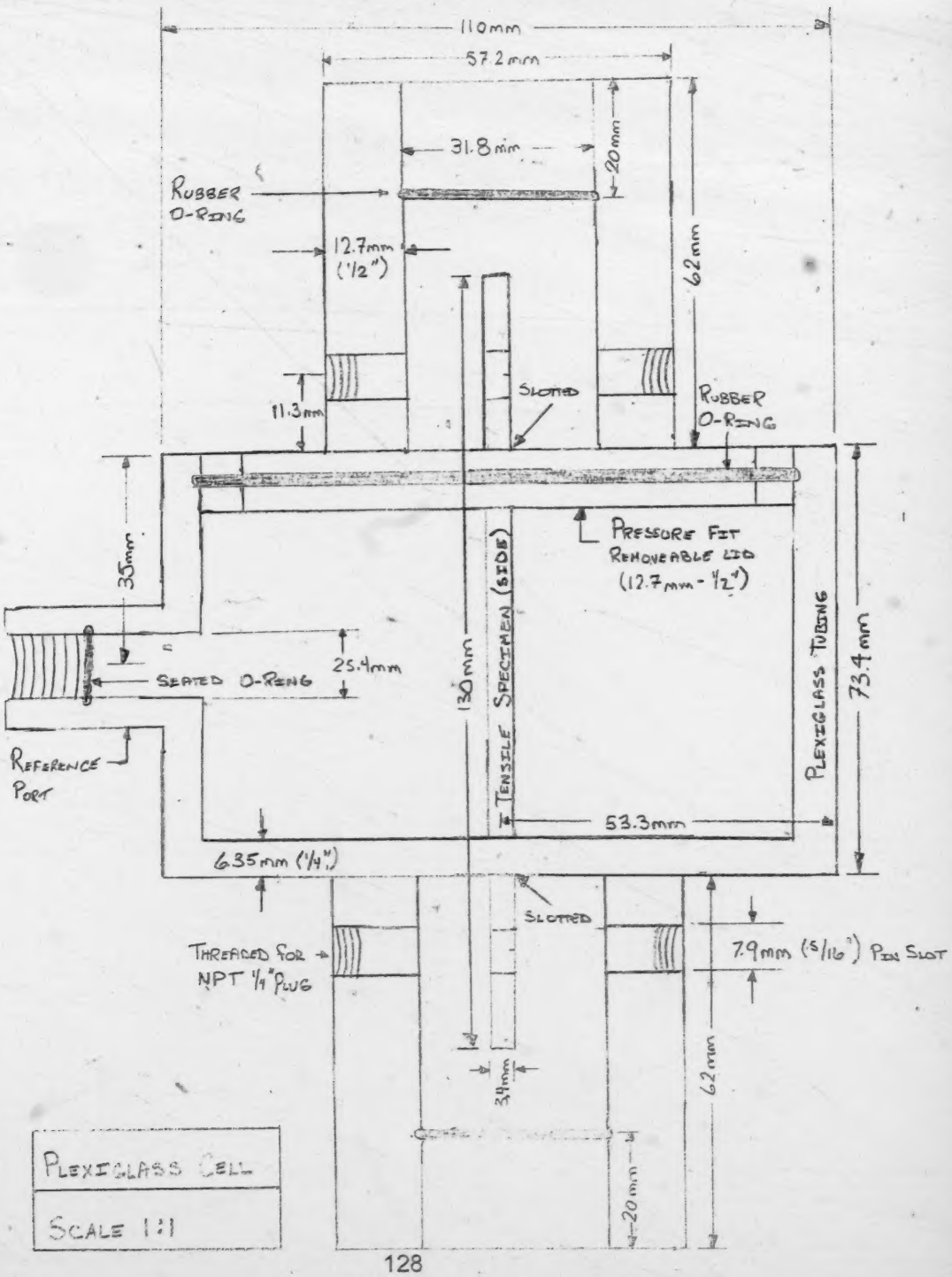

APPENDIX C

Tensile grip schematic.

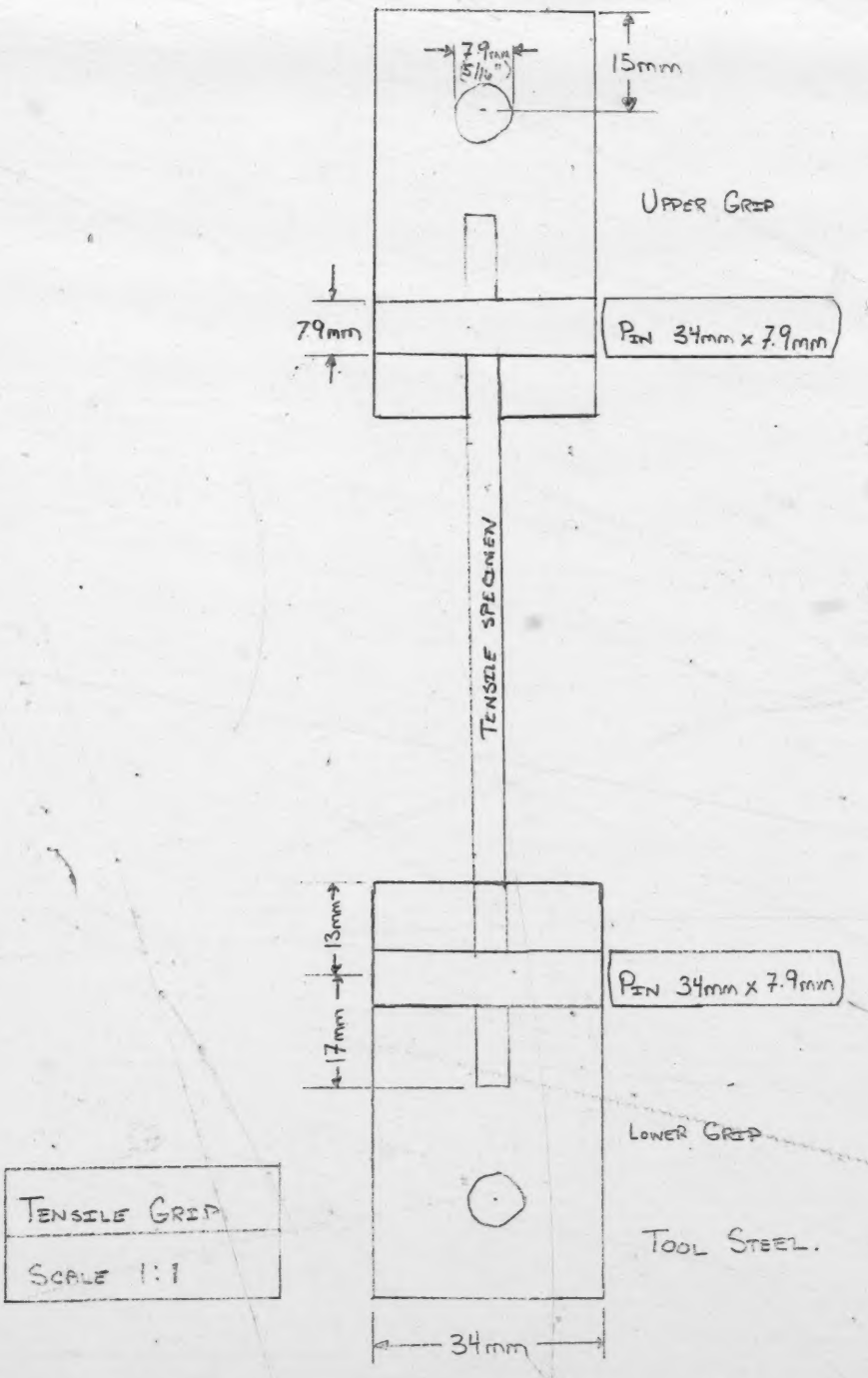

APPENDIX D
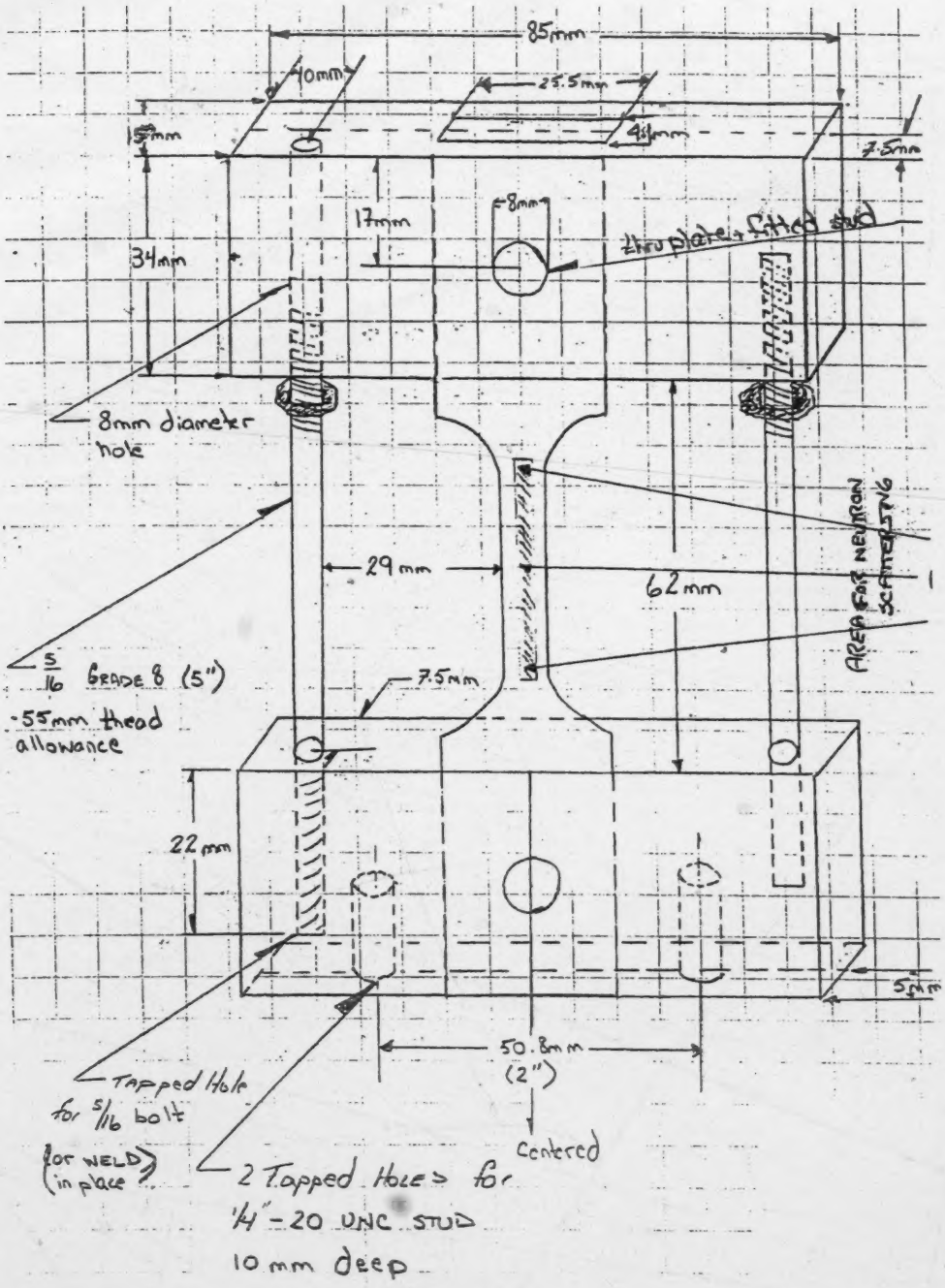
Tensile specimen mounting jig schematic.